# Nonproportionality of inorganic scintillators

**Proefschrift**

ter verkrijging van de graad van doctor
aan de Technische Universiteit Delft,
op gezag van de Rector Magnificus prof. ir. K.C.A.M. Luyben,
voorzitter van College voor Promoties,
in het openbaar te verdedigen op dinsdag 15 januari 2013 om 10.00 uur
door Ivan Vyacheslavovich KHODYUK
Master of Science in Experimental Nuclear Physics,
Saint Petersburg State Politechnical University
Geboren te Leningrad, Sovjet-Unie

Dit proefschrift is goedgekeurd door de promotor:
Prof. dr. P. Dorenbos

Samenstelling promotiecommissie:

| | |
|---|---|
| Rector Magnificus, | vorzitter |
| Prof. dr. P. Dorenbos | Technische Universiteit Delft, promotor |
| Prof.dr. P.A. Rodnyi | St. Petersburg State Politechnical University, Rusland |
| Prof. dr. C. R. Ronda | Universiteit Utrecht |
| Prof. Dr. E. H. Bruck | Technische Universiteit Delft |
| Prof. Dr. B. Dam | Technische Universiteit Delft |
| Prof.dr.ir. C.W.E. van Eijk | Technische Universiteit Delft |
| Dr. V. Ouspenski | Saint-Gobain Recherche, Frankrijk |

The research leading to these results has received funding from the Dutch Technology Foundation STW (project 07644 "The ultimate scintillator").
The Work was carried out at the Luminescence Materials research group, part of the Radiation Detection & Medical imaging (RD&M) section of the department of Radiation, Radionuclides & Reactors ($R^3$), Faculty of Applied Sciences, Delft University of Technology, The Netherlands.

Cover design: Proefschriftmaken.nl || Uitgeverij BOXPress
Printed & Lay Out by: Proefschriftmaken.nl || Uitgeverij BOXPress
Published by: Uitgeverij BOXPress, Oisterwijk

ISBN: 978-90-8891-553-6

# Table of contents


**Chapter 1** **Introduction to nonproportionality** ..... 1

1.1 Physics of the scintillation event ..... 2
1.2 Energy resolution and nonproportionality ..... 3
1.2.1 Pulse height spectra ..... 4
1.2.2 Energy Resolution ..... 5
1.2.3 Methods for measuring the nonproportionality ..... 6
1.3 Historic overview of nonproportionality studies ..... 9
1.4 Thesis research objectives ..... 12
1.5 Thesis outline ..... 13

**Chapter 2** **Nonproportionality of NaI:Tl** ..... 19

2.1 Introduction ..... 19
2.2 Experimental methods ..... 21
2.3 Results and discussion ..... 23
2.3.1 Data analysis ..... 23
2.3.2 Photopeak nonproportional response ..... 25
2.3.3 Escape nonproportional response ..... 29
2.3.4 K-electron nonproportional response ..... 33
2.3.5 Comparison of the experimental data with simulations ..... 35
2.4 Conclusion ..... 36

**Chapter 3** **Nonproportionality of LSO:Ce, LuAG:Pr, LPS:Ce, and GSO:Ce** ..... 41

3.1 Introduction ..... 41
3.2 Materials and experiment ..... 42
3.3 Results and discussion ..... 44
3.3.1 Nonproportionality ..... 44
3.3.2 Energy resolution ..... 45
3.3.3 Information derived from escape peaks ..... 47
3.3.4 K-dip spectroscopy ..... 48
3.3.5 Comparison of the three methods ..... 52
3.4 Conclusion ..... 52

**Chapter 4** **Nonproportionality of $LaBr_3$:Ce and $LaCl_3$:Ce** ..... 55

4.1 Introduction ..... 55
4.2 Experimental methods ..... 58
4.3 Results ..... 58
4.4 Discussion ..... 65
4.5 Conclusion ..... 68

**Chapter 5** **Trends and patterns of scintillator nonproportionality** ..... 73

5.1 Introduction ..... 73
5.2 Experimental methods ..... 74
5.3 Results ..... 76
5.4 Oxide scintillators ..... 76
5.4.1 Influence of chemical composition ..... 76
5.4.2 Influence of dopant ..... 78
5.4.3 Cation substitution effect ..... 81
5.4.4 Other oxides ..... 84
5.4.5 Semiconductor scintillators ..... 84
5.5 Halide scintillators ..... 85
5.5.1 Anion effect (F – Cl – Br – I) ..... 85
5.5.2 Fluorides ..... 86
5.5.3 Chlorides ..... 87
5.5.4 Bromides ..... 88
5.5.5 Iodides ..... 89
5.6 Discussion ..... 90
5.7 Conclusion ..... 94

**Chapter 6** **Charge carrier mobility and nonproportionality of $LaBr_3$:Ce scintillators** ..... 103

6.1 Introduction ..... 103
6.2 Experimental methods ..... 104
6.3 Photon response ..... 105
6.4 Energy resolution ..... 107
6.4.1 Energy resolution as a function of energy at different temperatures ..... 107
6.4.2 Energy resolution as a function of temperature at 662 keV ..... 108
6.5 Electron response ..... 110
6.6 Discussion ..... 112
6.6.1 Charge carrier diffusion and quenching ..... 113
6.6.2 Theory of electrical transport ..... 114
6.6.3 Onsager mechanism ..... 117
6.7 Conclusion ..... 118

**Summary** ..... 123

**Samenvatting** ..... 127

**Acknowledgements** ..... 131

**Curriculum Vitae** ..... 133

**List of publications** ..... 135

# Chapter 1 Introduction to nonproportionality

A scintillator is a transparent material with a size that ranges from few cubic millimeters to hundreds and thousands of cubic centimeters, and that emits a flash of light when it absorbs a γ-ray photon or an energetic particle. The flash must be intense and with a short duration. Scintillation crystals are widely used as spectroscopic detectors of ionizing radiation in nuclear science, space exploration, medical imaging, homeland security, etc. The important parameters for X- or γ-ray spectrometry are the total light output by the scintillator expressed in photons emitted per MeV of absorbed ionizing energy, decay time of the scintillation light flash, energy resolution for the detection of the ionizing particle and the detection efficiency. Taking into account all parameters one of the best inorganic scintillator commercially available today is $LaBr_3$:Ce. Concerning high light output and good energy resolution the rediscovered [1-3] $SrI_2$:Eu and recently discovered [4] $CsBa_2I_2$:Eu scintillators are very promising. Despite the new materials mentioned lots of research and routine measurements are still done with NaI:Tl and CsI:Tl scintillators which were discovered in the 1950's.

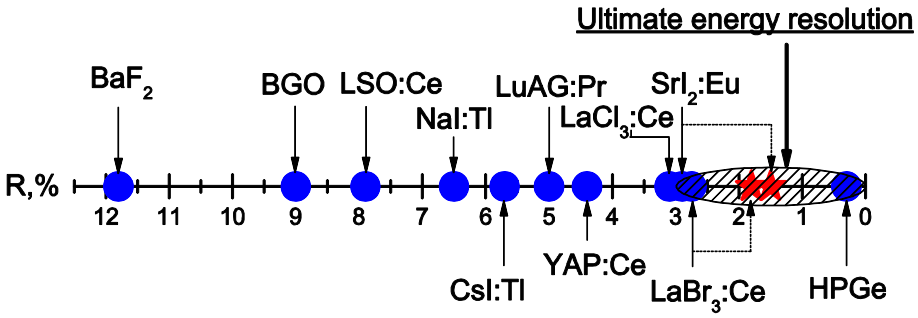


**Fig. 1.1** Energy resolution of inorganic scintillators and HPGe detector for the detection of 662 keV gamma photons. The energy resolution is defined as the full width at half maximum of the photoabsorption peak divided by the energy of the centroid of the peak.

In spite of all efforts by the scintillation community the energy resolution of inorganic scintillators is still far below the fundamental limit dictated by photon statistics [5]. Figure 1.1 shows the energy resolution achieved by well-known scintillators for the detection of 662 keV gamma ray photons. The best resolution is for $LaBr_3$:Ce followed by $SrI_2$:Eu. The red star symbols are the fundamental limit as dictated by photon statistics [6] for these two scintillators which demonstrates that there is still very

significant improvement possible to well below 2%. For a solid state detector like high purity germanium (HPGe) photon statistics does not contribute and much better resolution down to 0.3% can be obtained. To decrease the energy resolution by almost a factor of two to 1.8% for $LaBr_3$ and to 1.5% for $SrI_2$ it is necessary to minimize all contributions other than photon statistics that influence energy resolution. The most essential contribution to be minimized is the contribution determined by nonproportionality [7].

## 1.1 Physics of the scintillation event

Scintillation is one of the different luminescence processes, and luminescence is one of the four basic phenomena giving light emission. These phenomena are: thermal radiation, bremsstrahlung, Cherenkov radiation and luminescence. Luminescence can be excited in many different ways by UV-photons, ionizing radiation (X-, γ-, α-, β-rays, etc.), electron beam, or electric fields. Luminescence can be subdivided in fluorescence – luminescence during excitation and phosphorescence – luminescence after excitation. The scintillation process is fluorescence due to ionizing radiation.

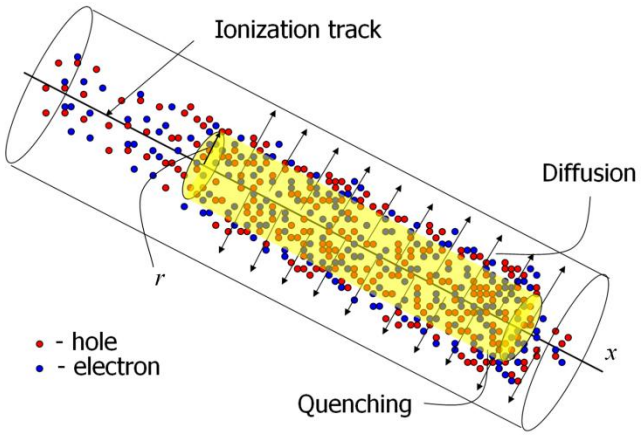


**Fig. 1.2** Sketch of an ionization track formed by a primary electron starting from the left creating free electrons and holes that diffuse radially away from the track. Radiationless carrier recombination occurs at the dense carrier concentration regions.

The core of the scintillation process is the transformation of an X-, γ-, α-, β-ray, etc. energy into a variety of optical photons. After the interaction of ionizing radiation with

atoms of a single crystal or a ceramic, hot charge carriers are created that are in a nonequilibrium state. Return to the equilibrium state is called the relaxation process.

The whole scintillation process can be subdivided into five main steps:

1. Interaction of ionizing radiation with the atoms of the crystal. Creation of primary (Compton, photo-, etc.) high energy electrons.
2. Interaction of the primary electrons with the bulk of the crystal. Formation of secondary (Auger, delta-rays, etc.) high energy electrons. Production of hot carriers (electrons, holes, excitons) within the ionization track.
3. Diffusion of the hot carriers from the point of creation to low ionization density regions and their thermalization. Creation of electron-hole pairs with energy roughly equal to the band gap.
4. Energy transfer from the thermalized electron-hole pairs to or direct caption of the thermalized carriers by the luminescence centers.
5. Emission of the luminescence centers.

The dynamics of hot charge carriers created in the ionization track of ionizing particles is of interest in various disciplines of science. In a small cylindrical volume with radius $r \sim 5$ nm around the ionization track [8] schematically shown in Fig. 1.2 on the ps time scale [9] a very high ionization density $n > 10^{20}$ e-h/cm$^3$ of free electrons and holes are created [10] that can cause secondary effects. The energy density available can be sufficient to displace atoms from their normal lattice positions thus creating radiation damage [11]. In tissue radiation damage may have severe health risks, and in personnel dosimetry it can lead to underestimation of the dose. Currently there are many investigations in utilizing carrier multiplication to develop better efficiency photo-voltaic cells. In inorganic scintillators, that is the topic of this thesis, the created free charge carriers need to escape the volume of high ionization density or to be trapped by a luminescence center to avoid quenching and finally recombine under emission of an optical photon [12].

## 1.2 Energy resolution and nonproportionality

Nonproportionality is the nonlinear dependence of the total light output of the scintillator on the detected amount of ionization energy, i.e., the emitted number of photons/MeV at 10 keV is not necessarily the same as at 100 keV or at 1000 keV. This dependence is due to a scintillation efficiency that depends on the density of the ionization track. The production of secondary electrons during slowing down of the primary electron inside the scintillator is a probabilistic process and may occur in different ways for the same absorbed energy. The dependence of the absolute light

yield on the energy of secondary electrons and the probabilistic mechanism of their creation result in variability of the total number of photons produced inside the scintillator [13]. This process leads to broadening of the photoabsorption peak in the pulse height spectrum measured by a scintillation detector.

### *1.2.1 Pulse height spectra*

To determine the absolute light output and energy resolution of the scintillation crystal under investigation the so-called pulse height spectrum is usually measured. Figure 1.3 shows pulse height spectra of a $^{137}$Cs γ-ray source as measured by a NaI:Tl and a $LaBr_3$:Ce scintillators optically coupled to a photomultiplier tube.

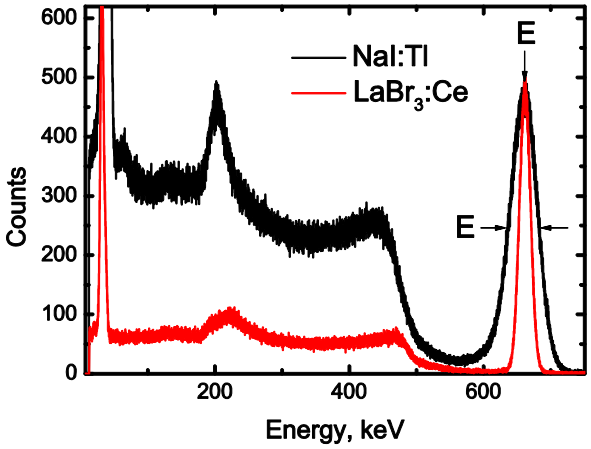


**Fig. 1.3** Pulse height spectra of 662 keV γ-ray excitation from $^{137}$Cs measured with NaI:Tl and $LaBr_3$:Ce scintillators.

The absolute light output is determined by comparing the position of the total absorption peak maximum in the $^{137}$Cs spectrum at 662 keV to the position of the center of gravity of the single photoelectron spectrum of the photomultiplier tube [14]. The energy resolution is defined as the full width at half maximum of the total absorption peak $\Delta E$ divided by the energy of the centroid of the peak $E$. The energy resolution is expressed as a percentage value. Shown in Fig. 1.3 the energy resolution of NaI:Tl at 662 keV is 7.6%. Under the same experimental conditions the energy resolution of $LaBr_3$:Ce is almost 3 times better 2.9%. To understand the difference it is necessary to analyze which parameters determine total energy resolution $\Delta E/E$ of a scintillation crystal.

### *1.2.2 Energy Resolution*

The energy resolution $\Delta E/E$ of a scintillator is determined [6] by three basic parameters: the intrinsic resolution of the scintillation crystal $R_{\text{int}}$, transport resolution $R_{\text{tr}}$, and the resolution of the photodetector $R_{\text{M}}$. The intrinsic resolution of the scintillation crystal $R_{\text{int}}$ depends on two parameters: nonproportionality $R_{\text{nPR}}$ and inhomogeneity of the scintillation crystal $R_{\text{inh}}$. Therefore, the energy resolution of the detector is defined by the formula:

$$\left(\frac{\Delta E}{E}\right)^2 = R_{nPR}^2 + R_{inh}^2 + R_{tr}^2 + R_M^2 . \qquad (1.1)$$

The inhomogeneity of the scintillator can be caused by the irregular distribution of the luminescence centers inside the crystal or by the presence of various defects, which makes the light yield dependent on the interaction point and contributes to the broadening of the total absorption peak. The $R_{\text{nPR}}$ value is determined by nonproportionality. There are many factors that determine the efficiency of photon transport and conversion and thereby affect the energy resolution. Contributions to transport resolution $R_{\text{tr}}$ can also be made by the sensitivity of the photomultiplier tube (PMT) photocathode at a certain wavelength of the scintillation light, the self-absorption in the bulk of the scintillator, the efficiency of light collection, the efficiency of photoelectron collection on the first dynode, and others [6, 15].

The contribution of the PMT $R_{\text{M}}$ to the total energy resolution of the scintillation detector depends on the light output according to the formula[6]

$$R_M(T) = 2.35\sqrt{\frac{1+v(M)}{N_{phe}^{PMT}(T)}}, \qquad (1.2)$$

where $v(M)$ is the variance of the gain during multiplication of photoelectrons in the PMT, and $N_{phe}^{PMT}$ is the number of photoelectrons that are produced by the interaction of scintillation photons with the PMT photocathode and are multiplied on the first dynode [16, 17].

The effect exerted by energy resolution of the PMT $R_{\text{M}}$ on the total energy resolution of the detector decreases with an increase in the light yield in the scintillator and a decrease in the dispersion caused by the PMT. Today, the researchers have approached the maximum of the light yield in the majority of the known scintillators [5]. The maximum of the light yield is primarily determined by the emission wavelength and scintillator's width of the band gap $E_g$ [11, 18]:

$$\frac{N_{ph}\langle h\nu\rangle}{E_\gamma} = Y\frac{h\nu_{\max}}{E_g}SQ, \qquad (1.3)$$

where $N_{ph}\langle h\nu\rangle$ is the number of scintillation photons with the averaged radiation energy, $E_\gamma$ is the energy of primary radiation (in units of 1 MeV), $Y = E_g / E_{eh} = 1/\beta$ is the efficiency of the ionization process (for most scintillators, β is in the range of 1.5–3.5 [18-20]), $h\nu_{\max}$ is the energy of scintillation photons in the maximum of the luminescence peak, *S* is the efficiency of the electron-hole transfer from the scintillator matrix to the luminescence centers, and *Q* is the quantum efficiency of the luminescence process.

### *1.2.3 Methods for measuring the nonproportionality*

The nonlinear dependence of the relative light output on the energy of incident radiation – the nonproportionality – is a significant factor determining the energy resolution [6, 18, 21]. This phenomenon is the key obstacle in developing scintillation detectors of ionizing radiation with improved characteristics. By the nonproportionality of the relative light output is meant the nonlinear dependence of the number of light photons produced in the scintillator, on the absorbed radiation energy.

Serious attempts have recently been made to reveal the mechanism of the nonproportionality and develop the theoretical model capable of predicting both the nonproportionality scale and a energy resolution of scintillation materials [9, 22-26]. However, most of the models existing today can only describe available experimental data, but are incapable of predicting the behavior of new scintillators.

For understanding the physical processes resulting in a partial loss of the scintillator efficiency and, hence, in the nonproportionality of the relative light output, it is essential to have an adequate amount of experimental data. Today, there are two main approaches to measuring the nonproportionality. The first is based on measuring the light output of the scintillator as a function of γ or X-ray photon energy. This method requires the use of radioactive sources, e.g., $^{137}$Cs, $^{241}$Am, $^{22}$Na, $^{55}$Fe, etc. The main drawbacks of this method are the limited number of available radioactive sources and the signal overlapping if a source emits several quanta with close energy values. For limited energy range synchrotron irradiation is available and can be used as an alternative to radioactive sources. Figure 1.4 shows data measured with radioactive sources from [27] and with synchrotron radiation in this thesis work that is in detail discussed in Chapter 2. Historically this type of data is presented normalized at 662 keV and shown as a percentage value.

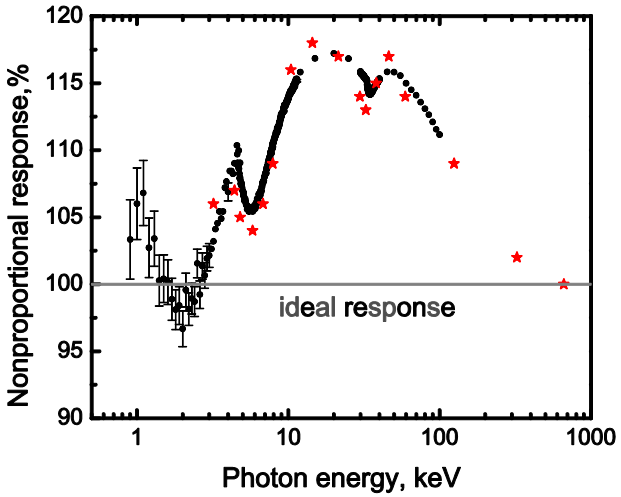


**Fig. 1.4** Nonproportional response NaI:Tl crystals measured with radioactive sources (stars) [27] and synchrotron radiation (dots). For more details see Chapter 2.

A substantial limitation is imposed by the small absorption length of X-ray quanta at energies below few keV. It makes the results susceptible to the surface properties. Although the effects on the characteristics of inorganic scintillation materials has not yet been systematically investigated, observations of this kind have been reported [22, 28]. Usually, in the low energy range (<10 keV) the largest deviation of the relative light output from the ideal response is observed. So, it is very important to develop a new method for measuring the nonproportionality that is not influenced by the surface effects.

Utilization of low energy electrons seems to be even more problematic than X-ray photons. Simulation results of 10 keV and 1 keV monoenergetic electrons interacting with a $Lu_2SiO_5$ scintillator are shown in Fig. 1.5. Casino v2.42 Monte-Carlo (MC) software was used to simulate trajectories and energy dissipation of the electrons in the $Lu_2SiO_5$ crystal. Figure 1.5 shows that for 10 keV electrons 95% of their initial energy is released within the first 250 nm. For 1 keV electrons 95% of their energy is released already within first the 10 nm. Short absorption length makes light output of scintillators at low electron energies extremely sensitive to the quality of the surface.

To overcome influence of the surface and to study bulk properties of the scintillator an alternative method for measuring the nonproportionality, named Compton coincidence technique, was introduced by B.D. Rooney and J.D. Valentine in the early 1990's [29]. Later this method was improved by W.S. Choong et al., in 2008 [30, 31].

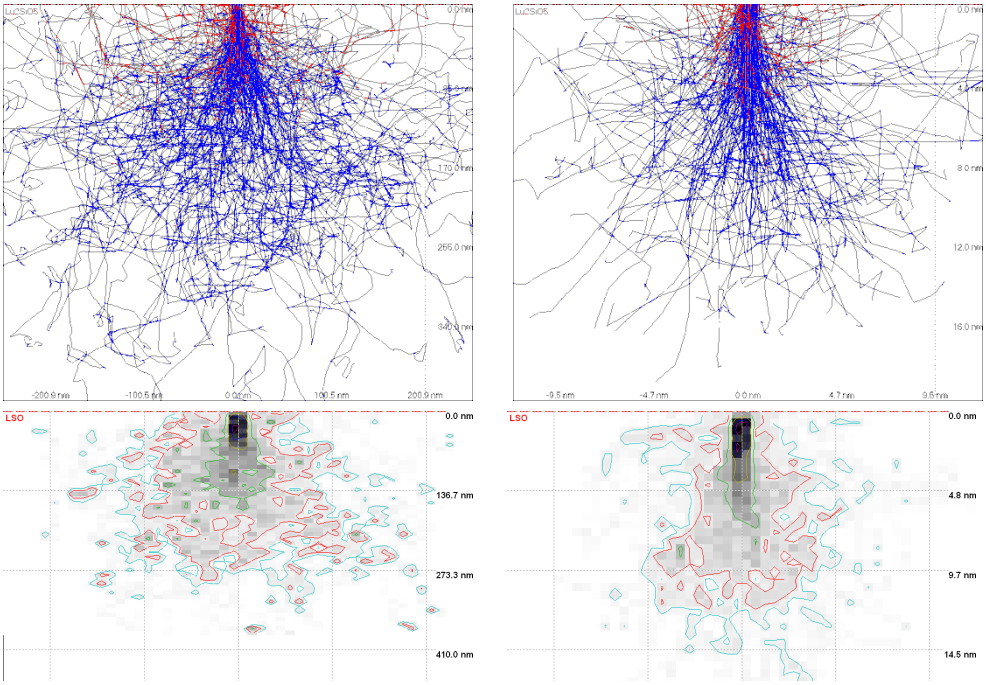


**Fig. 1.5** Monte-Carlo simulations of energetic electron trajectories (top) and energy dissipation (bottom) in $Lu_2SiO_5$ crystal using Casino v2.42 software. Left – 10 keV electrons; right – 1 keV electrons.

The technique is based on detecting Compton scattered electrons created by incident γ-photons in the scintillator material. After Compton scattering, a γ-photon escapes from the scintillator and is detected by a high-purity germanium detector. The energy resolution of the high-purity germanium detector, which is ~0.3 keV [32], allows the energy of the scattered γ-ray photon to be measured with a high degree of accuracy. Knowing the initial and final energies of the γ-ray photon, one can evaluate the energy transferred to the Compton scattered electron inside the scintillator. Simultaneously measuring the light output of the scintillator in a coincidence mode using a PMT, one can establish the scintillation yield at the Compton electron energy. Therefore, one can determine the relative scintillation light output as a function of electron energy. As an xample the NaI:Tl nonproportionality curve measured by Rooney and Valentine [33] using the Compton coincidence technique is presented in Fig. 1.6. This method is applicable in a wide energy range, 3–466 keV [30]. The Compton coincidence technique is very difficult to use below 3 keV, since the PMT noise starts to predominate over the signal arriving from the scintillator.

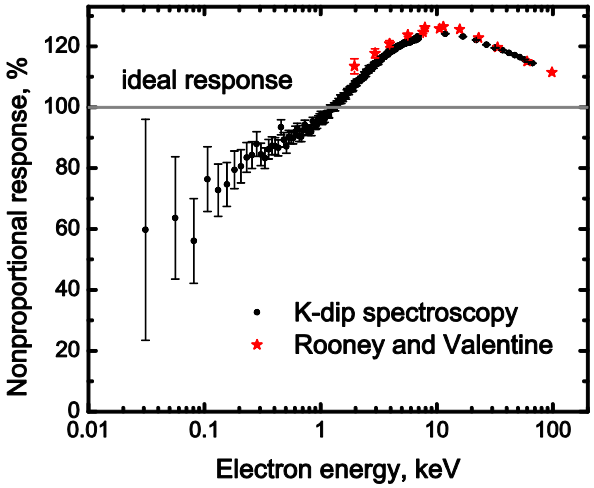


**Fig. 1.6** Nonproportional response of NaI:Tl measured by Compton coincidence technique [33] and K-dip spectroscopy.

In this thesis a new method that was developed based on the so-called Collinson and Hill algorithm [34] will be presented. This method allows us to derive the electron response curve of various scintillators down to energies as low as tens of eV as shown in Fig. 1.6. This method uses highly monochromatic synchrotron radiation instead of radioactive sources. Special attention is paid to the X-ray escape peaks, which provide us additional information about photon response in the low energy range. Also a dense sampling of data can be performed around the K-shell electron binding energy and that data can be used to apply a method, which we named K-dip spectroscopy [35]. This method will be discussed in detail in Chapter 2.

## 1.3 Historic overview of nonproportionality studies

Despite a long history of nonproportionality studies, the number of publications with systematic studies trying to identify trends is fairly small. One of the first comprehensive studies was done by Aitken, *et al.*, in 1967 [27]. They investigated the photon-nPRs of NaI:Tl, CsI:Tl, CsI:Na and $CaF_2$:Eu. The three iodides show qualitatively similar photon-nPRs down to photon energy of about 20 keV. The shape of the calcium fluoride photon-nPR curve differs significantly. The only common feature noted was a dip in the photon-nPR near K-shell and L-shell absorption edges of iodine or calcium.

With an increasing number of available scintillators, the amount of data on nonproportionality also increased. In 1995 an overview paper by Dorenbos, *et al.*, was published [6]. It describes the photon-nPRs of "classic" (NaI:Tl, CsI:Tl, CsI:Na, $CaF_2$:Eu, $Bi_4Ge_3O_{12}$ (BGO), and $CdWO_4$ (CWO)), and "modern" ($BaF_2$, $Gd_2SiO_5$:Ce (GSO:Ce), $YAlO_3$:Ce (YAP:Ce), $Lu_2SiO_5$:Ce (LSO:Ce), $Lu_3Al_5O_{12}$:Sc (LuAG:Sc), and $K_2LaCl_5$:Ce) scintillators. The photon-nPR curves of LSO:Ce samples with different light output and energy resolution were measured. Based on these results it was shown that the photon-nPR of LSO:Ce does not depend or very weakly on the parameters that determine scintillator's quality, such as: impurities, defects, synthesis parameters, self-absorption, concentration of vacancies, presence of the afterglow, etc. A similar study to establish a relationship between the energy resolution, light output and afterglow of LSO:Ce with photon-nPR was carried out by Kapusta, *et al.*, in 2005 [36]. The authors suggested a correlation between presence of traps, photon-nPR and intrinsic energy resolution. Nevertheless, a direct relationship was not established, and the most proportional response at room temperature was shown by the LSO:Ce crystal with the lowest light yield and energy resolution of about 16.7% at 662keV.

The next important step in the systematization of nonproportionality was done by Rooney, Valentine and co-workers [29, 33, 37, 38]. Using the Compton Coincidence Technique, the electron-nPR curves of the most common scintillators at that time were studied as a function of Compton electron energy. The major trend was that iodide compounds show a different shape of the electron-nPR curve than other types of scintillators, mostly oxides. High proportionality of YAP:Ce electron-nPR was also highlighted.

Balcerzyk, *et al.*, [39] studied the oxides YSO:Ce, GSO:Ce, LSO:Ce, and $Lu_{1.8}Gd_{0.2}SiO_5$:Ce (LGSO:Ce). They concluded that the shape of the photon-nPR is mainly determined by the crystal structure, but not by the type of rare earth cation. The photon-nPR of the LGSO:Ce crystal, in which 10% of the Lu atoms, were substituted by Gd atoms demonstrated a stronger nonproportionality in comparison with LSO:Ce and GSO:Ce.

In 2002, Dorenbos continued to systematize data on the photon-nPR [40] and introduced a new quantity, the so-called degree of nonproportionality. A clear correlation between the degree of nonproportionality and the deviation from the fundamental limit of energy resolution was noted.

Jaffe, *et al.*, [25, 41] compared the response of semiconductors, scintillators and gas detectors. They noted that there are significant differences in the shape of the photon-nPR with energy among various scintillators. Chemically distinct groups of materials display different photon-nPR curve shapes. Despite this observation, the grouping was

based solely on the shape of the photon-nPR. It was noted that the group of alkali monohalides like NaI:Tl and CsI:Tl is characterized by an increase of the photon-nPR with a decrease in detected gamma or X-ray photon energy with a maximum at 10-100 keV and the presence of dips just above the K-edges. The second group includes:1) the alkaline earth dihalides $CaF_2$:Eu and $BaF_2$, 2) the oxides CWO, GSO:Ce, LuAG:Sc, LSO:Ce, YSO:Ce, and BGO, 3) the ternary halide $RbGd_2Br_7$:Ce and 4) the semiconductor scintillator ZnSe:Te. When energy increases from 20 to 100 keV, the photon-nPR of these materials increases by about 20-30%. The last group is formed by the "proportional scintillators" and includes the lanthanide trihalides $LaCl_3$:Ce, $LaBr_3$:Ce, $LuI_3$:Ce, $LuCl_3$:Ce, $LuBr_3$:Ce and aluminum perovskite YAP:Ce.

Cutler, *et al.*, [42] studied the dependence of photon-nPR of lutetium- and yttrium-based silicates and aluminates (LSO:Ce; LSO:Ce,Ca; $Lu_2Si_2O_7$:Ce (LPS:Ce), LuAG:Pr; YSO:Ce and YSO:Ce,Ca) on crystal structure, crystal growth atmosphere, activator concentration and type of co-doping. They established that the photon-nPR of Lu- and Y-based scintillators is not significantly affected by activator concentration or substitution of crystal matrix rare earth (Lu by Y and vice versa). In addition, the authors observed that the photon-nPR depends on the composition; LSO:Ce appears more proportional than LPS:Ce, and aluminates are generally more proportional than silicates, except for LuAP:Ce. They also observed that the synthesis conditions and type of co-doping did not significantly influence the shape and degree of the photon-nPR. The usage of $Ca^{2+}$ co-doping did not have any significant effect on the photon-nPR of LSO:Ce.

In 2009, Swiderski, *et al.*, [43] explored the photon-nPR of LuAG:Pr, LuAG:Ce, LSO:Ce and $LaBr_3$:Ce scintillators versus crystal structure and composition properties and dopant type. It was shown that LuAG:Pr is more proportional than LuAG:Ce, and LuAG:Ce in turn is more proportional than LSO:Ce.

Another example of independence of the photon-nPR shape from the type of the cation in the scintillator material composition is presented by Chewpraditkul, *et al.*, [44]. The authors compared the photon-nPR of $Y_3Al_5O_{12}$:Ce (YAG:Ce) and LuAG:Ce and no significant difference was observed. The photon-nPR of $Lu_{1.8}Y_{0.2}SiO_5$:Ce (LYSO:Ce) was also studied in this paper and a significant deviation from linearity was observed. These results confirm that the response depends strongly on the chemical composition of the compound.

A large contribution was made by Payne, *et al.*, [45, 46]. Using SLYNCI (Scintillator Light Yield Nonproportionality Compton Instrument), the electron-nPRs of 29 scintillators were measured in the energy range from 3 to 460 keV. The data obtained by the authors were compared with the results of calculations using a model they

proposed. The model is based on theories by Onsager, Birks, Bethe-Bloch, and Landau and by appropriate choice of parameters it can accurately reproduce the experimental data. Seven groups of scintillator materials were distinguished: "alkali halides, simple oxides, silicates, fluorides, organics, multivalent halides and Gd-based compounds".
In addition, papers with a more theoretical approach to the problem appeared: Murray, *et al.*, [47], Lempicki, *et al.*, [20], Rodnyi, *et al.*, [11, 18], Bizarri, *et al.*, [23], Keresit, *et al.*, [26], Setyawan, *et al.*, [48], Vasil'ev [8], Kirkin , *et al.*, [49], Singh [50], Li, *et al.*, [12], Williams, *et al.*, [9], Kozorezov, *et al.*, [51].

## 1.4 Thesis research objectives

The widespread use of inorganic scintillators for applications in science and society is the driving force behind the search for new high performance compounds. Both novel and known phosphors are constantly suggested as promising scintillators. One of the most important requirements imposed on new scintillators is a high energy resolution for gamma ray detection. Apart from the statistical contribution $R_M$ to the energy resolution, see Eq. (1.2), the essential contribution to be minimized is the contribution determined by nonproportionality $R_{nPR}$.
Nonproportionality means that the total light output of a scintillator is not precisely proportional to the energy of the absorbed gamma-ray photon. This has a deteriorating effect on energy resolution [6]. Because the light yield and the PMT performance is already close to optimal we need to reduce nonproportionality in order to improve the energy resolution, and for that we wish to understand the physical causes of the phenomenon.
Nonproportionality is due to electron-hole recombination losses during the scintillation process. It is currently believed that those losses occur inside parts of the ionization track where the ionization density is high. That density increases when the gamma-ray energy decreases. The scintillation yield per energy unit in $LaBr_3$:Ce scintillator at 10 keV energy is for example 15% smaller than at 662 keV. The origin of this decrease in efficiency, i.e., the true cause of electron-hole recombination losses, and the related deterioration in energy resolution is not known. It is a mystery to the scintillation community why some scintillators reveal poor proportionality while others appear reasonably good. Two main research objectives of this thesis are to develop a method that allows to measure nonproportional response at low energies and to elucidate the true origin of nonproportionality.

## 1.5 Thesis outline

This thesis addresses both research objectives mentioned in the previous section and can be divided in two main parts. Chapters 2, 3 and 4 form the first part and are devoted to the development of new experimental methods (nonproportionality studies using synchrotron irradiation, escape peak analysis, and K-dip spectroscopy) and data collection using these methods. In the 2nd chapter a description of the experimental setup used to obtain data is presented. The method, which we called K-dip spectroscopy, will be described and used to reconstruct the electron nonproportional response curve of NaI:Tl down to electron energies as low as 30 eV. In the 3rd chapter we will start from the nonproportionality response curves determined using direct observation of photo peaks from total absorption of highly monochromatic X-ray synchrotron irradiation in the 9 – 100 keV energy range. The nonproportionality curves as function of deposited energy for LSO:Ce, LuAG:Pr, LPS:Ce and GSO:Ce will be presented. Using K-dip spectroscopy makes it possible to reconstruct the electron response curve that starts already at energies as low as 100 eV. Finally, a comparison of all three methods will be performed for LSO:Ce and LuAG:Pr. The limitations of the methods and differences will be discussed. In the 4th chapter the nonproportional scintillation response of $LaBr_3$ doped with 5% $Ce^{3+}$ and of $LaCl_3$ doped with 10% $Ce^{3+}$ that was measured using highly monochromatic synchrotron irradiation will be presented. Special attention will be paid to the X-ray fluorescence escape peaks as they provide us with additional information about photon response in the range 1.2 - 14.5 keV for $LaBr_3$:Ce and 2.0 - 11.6 keV for $LaCl_3$:Ce. A rapid variation of the photon response curve that was observed near the Lanthanum K- electron binding energy for both scintillators will be explained. K-dip spectroscopy will allow us to derive the electron response curves of $LaBr_3$:Ce and $LaCl_3$:Ce down to energies as low as 100 eV. Chapters 5 and 6 are focused on the physical origin of nonproportionality. The aim of the 5th chapter is to overview, systematize, analyze and interpret the data on the photon-nPR of inorganic scintillation materials. The main trends and patterns of the photon-nPR typical for the different groups of scintillators, especially for complex oxides and halides, will be highlighted. The dependence of the shape of the photon-nPR curve and the degree of the photon-nPR will be studied as a function of chemical composition, dopant type, refractive index and other fundamental properties of the materials. In chapter 6 the dependence of $LaBr_3$ nonproportionality on temperature and $Ce^{3+}$ concentration will be studied. The nonproportional response as a function of photon and electron energy will be analyzed at 80K, 300K and 450K for $LaBr_3$ with 0.2%, 5% and 30% of $Ce^{3+}$. A model will be presented to reproduce the nonproportional response, and the degree of nonproportionality will be introduced and

determined. Its dependence on temperature and concentration will be compared with our model estimate of the mobility for thermalized carriers in wide band gap semiconductors.

## References


[1] N. J. Cherepy, G. Hull, A. D. Drobshoff, S. A. Payne, E. van Loef, C. M. Wilson, K. Shah, U. N. Roy, A. Burger, L. A. Boatner, W. S. Choong, and W. W. Moses, "Strontium and barium iodide high light yield scintillators," *Appl. Phys. Lett,* vol. 92, p. 083508, 2008.

[2] M. S. Alekhin, J. T. M. de Haas, K. W. Kramer, and P. Dorenbos, "Scintillation Properties of and Self Absorption in $SrI_2$: $Eu^{2+}$," *Nuclear Science, IEEE Transactions on,* vol. 58, pp. 2519-2527, 2011.

[3] M. S. Alekhin, I. V. Khodyuk, J. T. M. De Haas, and P. Dorenbos, "Non-proportional response and energy resolution of pure $SrI_2$ and $SrI_2$:5%Eu scintillators," *IEEE Trans. Nucl. Sci.,* vol. 59, pp. 665-670, 2012.

[4] G. Bizarri, E. D. Bourret-Courchesne, Z. Yan, and S. E. Derenzo, "Scintillation and Optical Properties of BaBrI:$Eu^{2+}$ and $CsBa_2I_2$:$Eu^{2+}$," *IEEE Trans. Nucl. Sci.,* vol. 58, pp. 3403-3410, 2011.

[5] P. Dorenbos, "Fundamental Limitations in the Performance of $Ce^{3+}$–, $Pr^{3+}$–, and $Eu^{2+}$– Activated Scintillators," *IEEE Trans. Nucl. Sci.,* vol. 57, pp. 1162-1167, 2010.

[6] P. Dorenbos, J. T. M. de Haas, and C. W. E. van Eijk, "Non-Proportionality in the Scintillation Response and the Energy Resolution Obtainable with Scintillation Crystals," *IEEE Trans. Nucl. Sci.,* vol. 42, pp. 2190-2202, 1995.

[7] I. V. Khodyuk and P. Dorenbos, "Trends and patterns of scintillator nonproportionality," *IEEE Trans. Nucl. Sci.,* 2012.

[8] A. N. Vasil'ev, "From luminescence non-linearity to scintillation non-proportionality," *IEEE Trans. Nucl. Sci.,* vol. 55, pp. 1054-1061, Jun 2008.

[9] R. T. Williams, J. Q. Grim, Q. Li, K. B. Ucer, and W. W. Moses, "Excitation density, diffusion-drift, and proportionality in scintillators," *Phys. Status Solidi B,* vol. 248, pp. 426-438, 2011.

[10] M. Kirm, V. Nagirnyi, E. Feldbach, M. De Grazia, B. Carre, H. Merdji, S. Guizard, G. Geoffroy, J. Gaudin, N. Fedorov, P. Martin, A. Vasil'ev, and A. Belsky, "Exciton-exciton interactions in $CdWO_4$ irradiated by intense femtosecond vacuum ultraviolet pulses," *Physical Review B,* vol. 79, p. 4, Jun 2009.

[11] P. A. Rodnyi, *Physical Processes in Inorganic Scintillators*. NY: CRC Press, 1997.

[12] Q. Li, J. Q. Grim, R. T. Williams, G. Bizarri, and W. W. Moses, "A transport-based model of material trends in nonproportionality of scintillators," *J. Appl. Phys.,* vol. 109, p. 123716, 2011.

[13] W. W. Moses, S. A. Payne, W. S. Choong, G. Hull, and B. W. Reutter, "Scintillator non-proportionality: Present understanding and future challenges," *IEEE Trans. Nucl. Sci.*, vol. 55, pp. 1049-1053, Jun 2008.

[14] M. Bertolaccini, S. Cova, and C. Bussolati, "A technique for absolute measurement of the effective photoelectron per keV yield in scintillation counters," *presented at the Nucl. Electr. Symp., Versailles, France*, 1968.

[15] J. T. M. de Haas and P. Dorenbos, "Advances in Yield Calibration of Scintillators," *IEEE Trans. Nucl. Sci.*, vol. 55, pp. 1086-1092, 2008.

[16] J. T. M. de Haas and P. Dorenbos, "Methods for accurate measurement of the response of photomultiplier tubes and intensity of light pulses," *IEEE Trans. Nucl. Sci.*, vol. 58, pp. 1290-1296, 2011.

[17] J. T. M. de Haas, P. Dorenbos, and C. W. E. van Eijk, "Measuring the absolute light yield of scintillators," *Nucl. Instr. and Meth. A*, vol. 537, pp. 97-100, Jan 2005.

[18] P. A. Rodnyi, P. Dorenbos, and C. W. E. van Eijk, "Energy Loss in Inorganic ScintiNators," *Phys. Statatus Solidi B*, vol. 187, pp. 15-29, 1995.

[19] P. A. Rodnyi, "Efficiency and yield spectra of inorganic scintillates," *Radiation Measurements*, vol. 29, pp. 235-242, Jun-Aug 1998.

[20] A. Lempicki, A. J. Wojtowicz, and E. Berman, "Fundamental limits of scintillator performance," *Nucl. Instr. and Meth. A*, vol. 333, pp. 304-311, 1993.

[21] V. K. Lyapidevskii and M. I. Ryazanov, "On the influence of ionization density in a fast charged particle track on the light output of scintillations," *Technical Physics*, vol. 45, pp. 948-949, 2000.

[22] A. M. Kudin, B. V. Grinyov, V. Y. Gres', and A. I. Mitichkin, "A possible reason for non-proportionality of response in NaI:Tl and CsI:Tl scintillation crystals," *Functional Materials*, vol. 13, pp. 54-58, 2006.

[23] G. Bizarri, W. W. Moses, J. Singh, A. N. Vasil'ev, and R. T. Williams, "An analytical model of nonproportional scintillator light yield in terms of recombination rates," *J. Appl. Phys.*, vol. 105, p. 044507, 2009.

[24] I. V. Khodyuk and P. Dorenbos, "Nonproportional response of $LaBr_3$:Ce and $LaCl_3$:Ce scintillators to synchrotron x-ray irradiation," *J. Phys. Condens. Matter*, vol. 22, p. 485402, Dec 2010.

[25] J. E. Jaffe, D. V. Jordan, and A. J. Peurrung, "Energy nonlinearity in radiation detection materials: Causes and consequences," *Nucl. Instr. and Meth. A*, vol. 570, pp. 72-83, 2007.

[26] S. Kerisit, K. M. Rosso, B. D. Cannon, F. Gao, and Y. Xie, "Computer simulation of the light yield nonlinearity of inorganic scintillators," *J. Appl. Phys.*, vol. 105, p. 114915, 2009.

[27] D. W. Aitken, B. L. Beron, G. Yenicay, and H. R. Zulliger, "The Fluorescent Response of NaI(Tl), CsI(Tl), CsI(Na) and $CaF_2$(Eu) to X-Rays and Low Energy Gamma Rays," *IEEE Trans. Nucl. Sci.*, vol. 14, pp. 468-477, 1967.

[28] G. C. Meggitt, "The effect of the crystal surface on the derived electron scintillation response of NaI(Tl)," *Nucl.Instr.and Meth.*, vol. 83, pp. 313-316, 1970.
[29] B. D. Rooney and J. D. Valentine, "Benchmarking the Compton Coincidence Technique for Measuring Electron Response Non-Proportionality in Inorganic Scintillators," *IEEE Trans. Nucl. Sci.*, vol. 43, pp. 1271-1276, 1996.
[30] W.-S. Choong, G. Hull, W. W. Moses, K. M. Vetter, S. A. Payne, N. J. Cherepy, and J. D. Valentine, "Performance of a Facility for Measuring Scintillator Non-Proportionality," *IEEE Trans. Nucl. Sci.*, vol. 55, pp. 1073-1078, 2008.
[31] W.-S. Choong, K. M. Vetter, W. W. Moses, G. Hull, S. A. Payne, N. J. Cherepy, and J. D. Valentine, "Design of a Facility for Measuring Scintillator Non-Proportionality," *IEEE Trans. Nucl. Sci.*, vol. 55, pp. 1753-1758, 2008.
[32] A. Owens, "Scintillators on Interplanetary Space Missions," *IEEE Trans. Nucl. Sci.*, vol. 55, pp. 1430-1436, 2008.
[33] B. D. Rooney and J. D. Valentine, "Scintillator light yield nonproportionality: calculating photon response using measured electron response," *IEEE Trans. Nucl. Sci.*, vol. 44, pp. 509-516, 1997.
[34] A. J. L. Collinson and R. Hill, "The Fluorescence Response of NaI(Tl) and CsI(Tl) to X Rays and g Rays," *Proc. Phys. Soc.*, vol. 81, pp. 883-892, 1963.
[35] I. V. Khodyuk, J. T. M. de Haas, and P. Dorenbos, "Nonproportional Response Between 0.1-100 keV Energy by Means of Highly Monochromatic Synchrotron X-Rays," *IEEE Trans. Nucl. Sci.*, vol. 57, pp. 1175-1181, Jun 2010.
[36] M. Kapusta, P. Szupryczynski, C. L. Melcher, M. Moszynski, M. Balcerzyk, A. A. Carey, W. Czarnacki, M. A. Spurrier, and A. Syntfeld, "Non-Proportionality and Thermoluminescence of LSO:Ce," *Nuclear Science, IEEE Transactions on*, vol. 52, pp. 1098-1104, 2005.
[37] W. Mengesha, T. D. Taulbee, B. D. Rooney, and J. D. Valentine, "Light yield nonproportionality of CsI(Tl), CsI(Na), and YAP," *IEEE Trans. Nucl. Sci.*, vol. 45, pp. 456-461, 1998.
[38] J. D. Valentine, B. D. Rooney, and J. Li, "The light yield nonproportionality component of scintillator energy resolution," *IEEE Trans. Nucl. Sci.*, vol. 45, pp. 512-517, 1998.
[39] M. Balcerzyk, M. Moszynski, M. Kapusta, D. Wolski, J. Pawelke, and C. L. Melcher, "YSO, LSO, GSO and LGSO. A Study of Energy Resolution and Nonproportionality," *IEEE Trans. Nucl. Sci.*, vol. 47, pp. 1319-1323, 2000.
[40] P. Dorenbos, "Light output and energy resolution of $Ce^{3+}$-doped scintillators," *Nucl. Instr. and Meth. A*, vol. 486, pp. 208-213, 2002.
[41] J. E. Jaffe, "Energy and length scales in scintillator nonproportionality," *Nucl.Instr.and Meth. A*, vol. 580, pp. 1378-1382, 2007.
[42] P. A. Cutler, C. L. Melcher, M. A. Spurrier, P. Szupryczynski, and L. A. A. Eriksson, "Scintillation Non-Proportionality of Lutetiumand Yttrium-Based Silicates and Aluminates," *IEEE Trans. Nucl. Sci.*, vol. 56, pp. 915-919, 2009.

[43] L. Swiderski, M. Moszynski, A. Nassalski, A. Syntfeld-Kazuch, T. Szczesniak, K. Kamada, K. Tsutsumi, Y. Usuki, T. Yanagida, A. Yoshikawa, W. Chewpraditkul, and M. Pomorski, "Scintillation Properties of Praseodymium Doped LuAG Scintillator Compared to Cerium Doped LuAG, LSO and $LaBr_3$," *IEEE Trans. Nucl. Sci.*, vol. 56, pp. 2499-2505, 2009.

[44] W. Chewpraditkul, L. Swiderski, M. Moszynski, T. Szczesniak, A. Syntfeld-Kazuch, C. Wanarak, and P. Limsuwan, "Scintillation Properties of LuAG:Ce, YAG:Ce and LYSO:Ce Crystals for Gamma-Ray Detection," *IEEE Trans. Nucl. Sci.*, vol. 56, pp. 3800-3805, 2009.

[45] S. A. Payne, N. J. Cherepy, G. Hull, J. D. Valentine, W. W. Moses, and C. Woon-Seng, "Nonproportionality of Scintillator Detectors: Theory and Experiment," *IEEE Trans. Nucl. Sci.*, vol. 56, pp. 2506-2512, 2009.

[46] S. A. Payne, W. W. Moses, S. Sheets, L. Ahle, N. J. Cherepy, B. Sturm, S. Dazeley, G. Bizarri, and C. Woon-Seng, "Nonproportionality of Scintillator Detectors: Theory and Experiment. II," *IEEE Trans. Nucl. Sci.*, vol. 58, pp. 3392-3402, 2011.

[47] R. B. Murray and A. Meyer, "Scintillation Response of Activated Inorganic Crystals to Various Charged Particles," *Physical Review*, vol. 122, pp. 815-826, 1961.

[48] W. Setyawan, R. M. Gaume, R. S. Feigelson, and S. Curtarolo, "Comparative Study of Nonproportionality and Electronic Band Structures Features in Scintillator Materials," *IEEE Trans. Nucl. Sci.*, vol. 56, pp. 2989-2996, 2009.

[49] R. Kirkin, V. V. Mikhailin, and A. N. Vasil'ev, "Recombination of Correlated Electron-Hole Pairs With Account of Hot Capture With Emission of Optical Phonons," *Nuclear Science, IEEE Transactions on*, vol. PP, pp. 1-1, 2012.

[50] J. Singh, "Study of nonproportionality in the light yield of inorganic scintillators," *J. Appl. Phys.*, vol. 110, pp. 024503-8, 2011.

[51] A. Kozorezov, J. K. Wigmore, and A. Owens, "Picosecond dynamics of hot carriers and phonons and scintillator non-proportionality," *J. Appl. Phys.*, vol. 112, p. 053709, 2012.

# Chapter 2 Nonproportionality of NaI:Tl

*Slightly modified version of this chapter has been published as: I.V. Khodyuk, P.A. Rodnyi, and P. Dorenbos, "Nonproportional scintillation response of NaI:Tl to low energy x-ray photons and electrons," Journal of Applied Physics, vol. 107, art. 113513, June 2010.*

Nonproportional response of the scintillation yield of NaI:Tl was measured using highly monochromatic synchrotron irradiation ranging from 9 to 100 keV. Special attention is paid to the X-ray escape peaks. They provide us additional information about photon response in the range 0.9 to 12 keV. A rapid variation of the photon response curve is observed near the Iodine K-electron binding energy. A dense sampling of data is performed around this energy and that data are used to apply a method, which we call K-dip spectroscopy. This method allows us to derive the electron response curve of NaI:Tl down to energies as low as 30 eV. A comparison of our data with data of others employing different methods is made. Advantages, limitations and peculiarities of presented techniques and methods are discussed.

## 2.1 Introduction

NaI:Tl inorganic scintillation crystals were discovered in 1948 [1] and are still today the best known and most widely used scintillators. Despite the large number of scintillating compounds only few of them [2, 3] can compete with NaI:Tl in terms of light output and energy resolution. Large amount of research has been done to unravel and to understand the scintillation mechanism in NaI:Tl, but many aspects are still not fully understood. For example, in 1956 Engelkemeir found [4] that the amount of photons emitted in the scintillation spark caused by absorption of an X-ray, a γ-quantum, or a particle in NaI:Tl is not precisely proportional to its energy. This finding appears important because it causes the energy resolution achievable with scintillation material to be worse than what might be expected on purely statistical grounds [5]. Although the phenomenon of non-proportional response (nPR) and its relation with energy resolution (R) has been studied quite intensively [6-12] there are still many major gaps in our understanding of the underlying physics. Accurate data from dedicated experimental techniques are needed to reveal the true origin of nPR and energy losses inside the solid state. We aim to develop models on nonproportionality

that may help us in improving the scintillation properties of existing materials and that helps us in our search for new highly effective and low energy resolution scintillators.
Since gamma radiation produce fast electrons in the solid state, photon-nPR as function of gamma energy is a direct consequence of the more fundamental electron-nPR as a function of primary electron energy. A method to study the electron response of a scintillator is the Compton Coincidence Technique (CCT) introduced by Valentine and Rooney [13] and further developed by Choong *et al.* [14, 15]. In a Compton scattering event the scattered gamma ray escapes the scintillator and the photon yield produced by the Compton electron alone is determined with the CCT as function of its energy. The main advantages of this method are the wide Compton electron energy range, usually from 3 to 450 keV, that is covered, and that the results are not affected by the surface of the scintillator. However, using CCT, it is not possible to obtain reliable data on the electron response at energies below 3 keV.
In this chapter we will demonstrate that by measuring the photon-nPR of the scintillator using highly monochromatic synchrotron X-rays, it is possible to obtain electron-nPR data starting from energy as low as 30 eV without a disturbing influence of the scintillator surface. Accurate experimental data is especially important in this low energy range because there the most dramatic change in scintillator efficiency and nPR is expected. We are not aware of any other experimental method that provides information on electron response down to that low energy.
We will start from a description of the experimental setup used to obtain data. The geometry of the sample and how it is packed will be described. In this work we will define and introduce different types of photon-nPR curves. The photon-nPR curve obtained using direct observation of photopeaks from total absorption of highly monochromatic X-ray synchrotron irradiation will be presented. We will call this the photopeak-nPR curve. Special attention is paid to the escape peaks and how to use them to get additional information about photon-nPR in the low energy range. So-called escape-nPR curves will be shown. The method to estimate electron-nPR analogous to the one used by Collinson and Hill [16] and later by Wayne *et al.* [17], which we called K-dip spectroscopy, is described in detail and used to reconstruct the so-called K- electron-nPR curve of NaI:Tl down to electron energies as low as 30 eV. A comparison of our data with the data of other authors is presented. Advantages, limitations and peculiarities of our techniques will be discussed. The aim of this work is to provide new data and methods to obtain those. It is not our aim to provide a complete explanation of the observed nPR curves.

## 2.2 Experimental methods

NaI:Tl is hygroscopic and to study its photon-nPR down to X-ray energies of 9 keV an X-ray assembly shown in Fig. 2.1 was manufactured by the company Saint-Gobain Crystals&Detectors [18]. Since we intended also to exploit X-ray escape peaks for our studies, a small 10 mm diameter and 2 mm thick NaI:Tl crystal was used to increase the probability of X-ray fluorescence escape. As entrance window for the X-rays, 220 μm thick Beryllium was used in order to avoid too much absorption at low energy X-ray irradiation. The crystal is sealed in an Al housing with 1 mm thick quartz window and its 2 mm edges were covered with a white reflector to maximize the photon collection at the photomultiplier tube (PMT) photocathode.

The number of photoelectrons $N_{phe}^{PMT}$ per MeV of absorbed energy produced in a Hamamatsu R6231-100 PMT by NaI:Tl was determined by comparing the position of the $^{137}$Cs 662 keV photopeak or of the $^{241}$Am 59.5 keV photopeak in recorded pulse

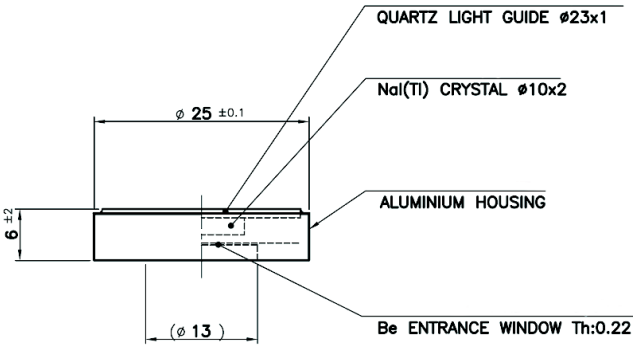


**Fig. 2.1** Cutaway view of NaI(Tl) X-ray assembly produced by Sain-Gobain Crystals&Detectors.

height spectra with the mean value of the so-called single photoelectron pulse height spectrum. The procedure has been described in detail by de Haas *et al.* [19]. To collect as much of the emitted light as possible, the NaI:Tl scintillator was optically coupled to the entrance window of the PMT and the shaping time of an Ortec 672 spectroscopic amplifier was set at 10 μs.

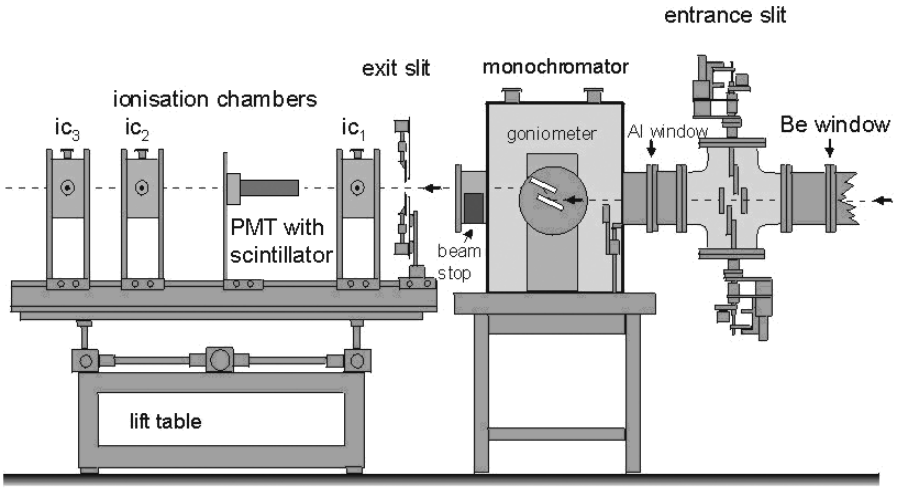


**Fig. 2.2** X-1 beamline experimental set-up at the Hamburger Synchrotronstrahlungslabor (HASYLAB) synchrotron radiation facility in Hamburg, Germany [20].

To measure the pulse height spectra at many finely spaced energy values between 9 keV and 100 keV, experiments at the X-1 beamline at the Hamburger Synchrotronstrahlungslabor (HASYLAB) synchrotron radiation facility in Hamburg, Germany were carried out. The scheme of the experimental set-up is presented in Fig. 2.2. A highly monochromatic pencil X-ray beam in the energy range 9 – 100 keV was used as excitation source. A tunable double Bragg reflection monochromator using a Si[511] and Si[311] set of silicon crystals providing an X-ray resolution of 1 eV at 9 keV rising to 20 eV at 100 keV was used to select the X-ray energies. The beam spot size was set by a pair of precision stepper-driven slits, positioned immediately in front of the sample coupled to the PMT. For all measurements, a slit size of $50 \times 50$ μm$^2$ was used. The PMT was mounted on an X-Y table capable of positioning with a precision of <1 μm in each direction. Prior to each measurement, the position of the PMT was adjusted to achieve as high count rate as possible. The intensity of the synchrotron beam was reduced in order to avoid pulse pileup. A lead shielding was used to protect the sample from receiving background irradiation which otherwise appeared as a broad background in our pulse height spectra.

To record synchrotron X-ray pulse height spectra of NaI:Tl, a Hamamatsu R6231-100 PMT connected to a homemade preamplifier, an Ortec 672 spectroscopic amplifier and an Amptek 8000A multichannel analyzer (MCA) were used. The quartz window of the NaI:Tl assembly was optically coupled to the window of the PMT with Viscasil 600000 cSt from General Electric. The NaI:Tl assembly plus PMT entrance window

was covered with several layers of ultraviolet reflecting Teflon tape (PFTE tape) forming an "umbrella" configuration [21]. Scintillation photons reflected from the photocathode are then reflected back by the umbrella thus enhancing detection efficiency. All measurements were carried out at room temperature and repeated several times.

Corrections were made for channel offsets in the pulse height measurement. The offset was measured by an Ortec 419 precision pulse generator with variable pulse height attenuation settings.

## 2.3 Results and discussion

### *2.3.1 Data analysis*

In Fig. 2.3 a typical pulse height spectrum recorded with NaI:Tl at 40 keV monochromatic X-ray irradiation is shown. The photopeak labeled "a" is fitted with a single Gaussian shaped curve from which the position of the maximum of the peak and its full width at half maximum (FWHM) intensity is obtained. This type of pulse height spectra was recorded for a large set of X-ray energies between 9 keV and 100 keV providing data on scintillation photon yield, from which the photon-nPR can be obtained, and data on scintillator resolution.

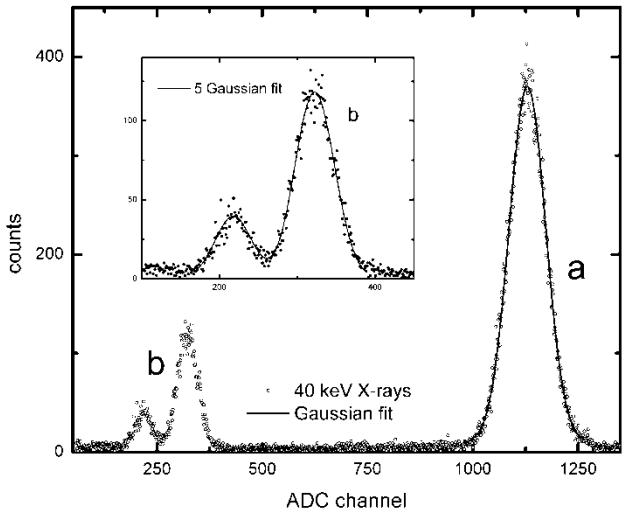


**Fig. 2.3** Pulse height spectrum measured with NaI:Tl at 40 keV monochromatic X-ray irradiation. a – photopeak, b – escape peaks. The inset shows the escape peaks on an expanded scale. The solid line in the inset is the result of a fit with five Gaussian peak.

To get additional information of the photon-nPR at low X-ray energies, escape peaks "b" in Fig. 2.3 were analyzed. X-ray photons of energy between the Iodine K-electron binding energy $E_{KI}$=33.169 keV [22] and 100 keV interact with matter almost exclusively by means of the photoelectric effect. After interaction the electron is ejected from the atom's K-shell, leaving a hole. As the atom returns to its stable lowest energy state, an electron from one of its outer shells jump to the hole in the K-shell, and in the process giving off a characteristic X-ray photon or Auger electrons. In the case that characteristic X-ray photons escape the bulk of the crystal we observe an escape peak like the peaks labeled "b" in Fig. 2.3. The ranges of Auger electrons are too short to escape the bulk of the material and we do not consider Auger electron escape here.

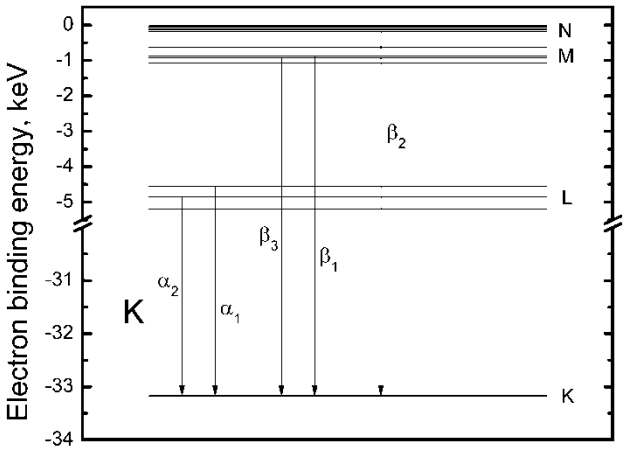


**Fig. 2.4** Most probable K X-ray fluorescence transitions in iodine atomic shells.

The deposited energy $E_d$ associated with events counted in the escape peak is then the energy of the X-ray photon $E_X$ from the synchrotron minus the energy $E_e$ of the escaped X-ray:

$$E_d = E_X - E_e . \qquad (2.1)$$

In fitting escape peaks we assumed 5 possible fluorescent transitions in Iodine. The scheme of Fig. 2.4 illustrates the $K_{\alpha 1}$, $K_{\alpha 2}$, $K_{\beta 1}$, $K_{\beta 2}$ and $K_{\beta 3}$ transitions between the shells of an Iodine atom. The energies and probabilities for the transitions used in the fitting of the escape peaks are listed in Table 2.1. Assuming that every type of escape results in a Gaussian shaped escape peak, we used a sum of five Gaussian peaks to fit

the observed escape peaks. The widths of the five Gaussian peaks were assumed all the same. Result of the fitting is shown in the inset of Fig. 2.3. After fitting, the experimental values of the maxima are known for the $K_{\alpha 1}$ $K_{\alpha 2}$ and $K_{\beta 1}$, $K_{\beta 2}$ and $K_{\beta 3}$ escape peaks.

***Table 2.1*** *Properties of Iodine X-ray fluorescence transitions. The type of transition (Line), the subshell and orbital where it originates from, its energy (in keV), and probability are given.*

| Line | Subshell | Orbital | Energy | Probability |
|---|---|---|---|---|
| $K_{\alpha 1}$ | $L_3$ | $2p_{3/2}$ | 28.612 | 0.5338 |
| $K_{\alpha 2}$ | $L_2$ | $2p_{1/2}$ | 28.317 | 0.2875 |
| $K_{\beta 1}$ | $M_3$ | $3p_{3/2}$ | 32.294 | 0.0947 |
| $K_{\beta 2}$ | $N_{2,3}$ | $4p_{1/2}$, $4p_{3/2}$ | 33.046 | 0.0326 |
| $K_{\beta 3}$ | $M_2$ | $3p_{1/2}$ | 32.238 | 0.0491 |

For this work we are interested in the weighted mean position of the two $K_\alpha$ peaks and the three $K_\beta$ peaks. For NaI:Tl it turns out that the position of the resulting $K_\alpha$ and $K_\beta$ maxima are located close to the values estimated by direct fitting of the two escape peaks with two Gaussians. Usage of two Gaussians instead of five would have simplified our fitting procedure, but for other scintillators $K_\alpha$ and $K_\beta$ escape peaks are not so well separated as in Fig. 2.3 and then fitting with five Gaussians is the preferred method.

Now we need to know what $E_d$ energies correspond to the found $K_\alpha$ and $K_\beta$ maxima. Based on the energies and probabilities taken from [22] and listed in Table 2.1 the mean values of the escape energies $E_{K_\alpha}$ and $E_{K_\beta}$ were calculated, and then Eq. (2.1) provides $E_d$. Repeating the same procedure for all $E_X$ above the $E_{KI}$ we obtain the photon yield curve as function of $E_d$.

### *2.3.2 Photopeak nonproportional response*

The number of photoelectrons $N_{phe}^{PMT}$, created in the PMT using synchrotron X-rays was determined at energies between 9 and 100 keV with a 5 keV step size. In the energy range 9 to 12 keV, a 1 keV step size was used. A much finer step size of 25 eV was used around $E_{KI}$ =33.169 keV, because interesting features are observed around that energy. Figure 2.5 shows $N_{phe}^{PMT}$, created in the PMT as derived from the

photopeak position in the pulse height spectra versus $E_X$. With this method of plotting data, the $N_{phe}^{PMT}$ appears to increase proportionally with $E_X$. In the inset of Fig. 2.5, the data near $E_{KI}$ has been plotted on an expanded scale. Now, a clear step can be seen in the $N_{phe}^{PMT}$ exactly at $E_{KI}$.

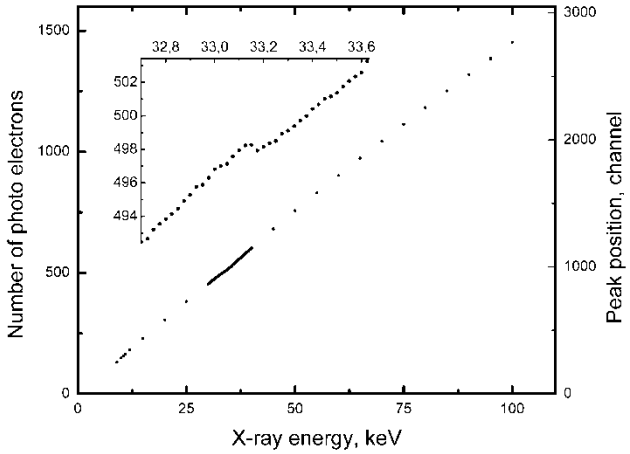


**Fig. 2.5** The scintillation yield of NaI:Tl measured with a Hamamatsu R6231-100 PMT versus X-ray energy. The right scale shows the peak position of the photopeak and the left scale corresponding number of the photoelectrons $N_{phe}^{PMT}$. Inset: expanded scale at energies near the Iodine K-electron binding energy.

We define the photopeak-nPR of NaI(Tl) at $E_X$ as the $N_{phe}^{PMT}/MeV$ observed at energy $E_X$ divided by the $N_{phe}^{PMT}/MeV$ observed at $E_X$ = 662 keV energy. The nPR will be expressed as a percentage value. Figure 2.6 shows the thus obtained photopeak-nPR curve as a function of $E_X$. Figure 2.7 shows the same photopeak-nPR curve but with a dense sampling at energies around $E_{KI}$. A clear dip is observed that we name the K-dip. As will be shown further in this paper we can derive valuable data on the electron response curve down to energies as low as 30 eV from a detailed analysis of the photopeak-nPR around such K-dip. We have named such analysis K-dip spectroscopy.

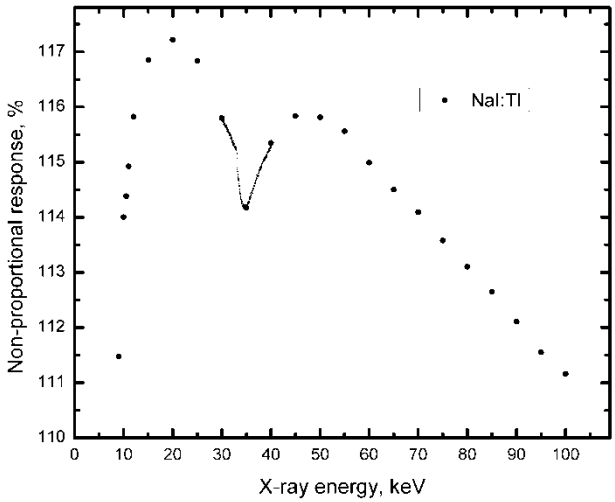


**Fig. 2.6** Photopeak non-proportional response of NaI:Tl as a function of X-ray energy at 5 keV intervals.

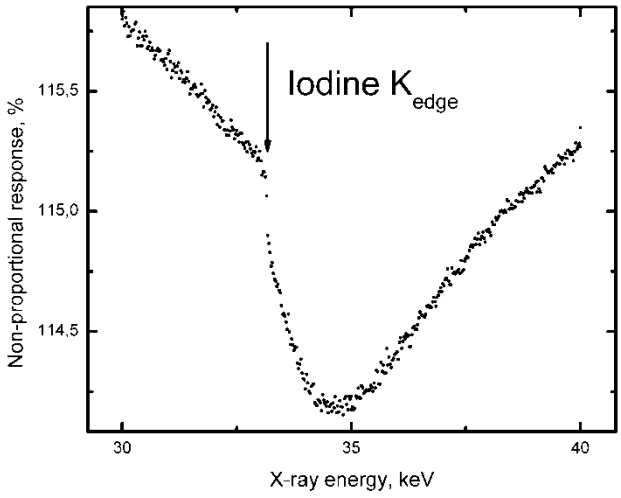


**Fig. 2.7** Photopeak non-proportional response of NaI:Tl as a function of X-ray energy near the Iodine K-electron binding energy at 25 eV intervals.

The shape of the photopeak-nPR curve is similar to results reported before [4, 8], i.e., a linear increase from 111.2% to 115.8% with decrease of $E_X$ from 100 keV to 50 keV followed by a drop in the range 30 – 45 keV with a local minimum of 114.1% at 34.5

keV. Next the photopeak-nPR increases up to 117.2% at 20 keV followed by a steep decrease of the response with further decrease of $E_X$. The nPR at 9 keV is 111.5% which is almost equal to the nPR at 100 keV. So there appears a drop of 5.7% in the photopeak-nPR is going from 20 keV to 9 keV which is of interest for further investigation.

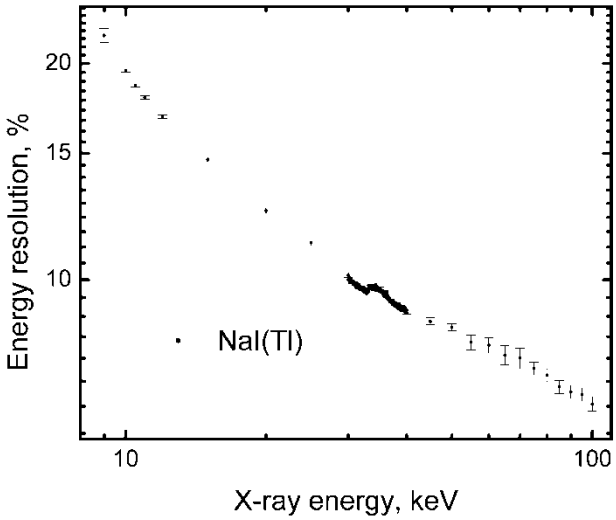


**Fig. 2.8** Energy resolution of the X-ray photopeak recorded with the NaI:Tl scintillator as a function of X-ray energy.

The energy resolution $R(E_X)$ of the X-ray photopeaks is plotted in Fig. 2.8 versus $E_X$. Starting from 9 keV to 100 keV $R$ decreases from 21.9% to 6.7%. A clear step-like change of almost 0.2% can be seen at $E_X$ around $E_{KI}$. *R(59.5 keV)* measured using the $^{241}$Am source, was 10.1 %. With 59.5 keV synchrotron X-ray irradiation a value of 8.1% is observed. We attribute the improvement to the fact that the synchrotron X-rays are collimated but the $^{241}$Am gamma rays are absorbed throughout the bulk of the crystal. In the latter case inhomogeneities in the crystal properties or light collection properties provide an additional contribution to the energy resolution.

In Fig. 2.9 the same data as in Fig. 2.8 are shown but now displayed versus $N_{phe}^{PMT}$. The solid curve represents the theoretical limiting resolution due to the always present Poisson statistics in the number of detected photons [8]:

$$R_M = 2.355\sqrt{\frac{1+\nu}{N_{phe}^{PMT}}}, \quad (2.2)$$

where $\nu = 0.25$ is the contribution from the variance in the gain of the Hamamatsu R6231-100 PMT.

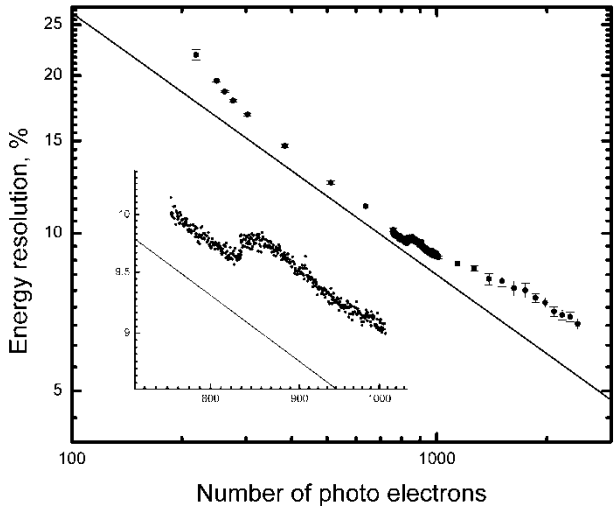


**Fig. 2.9** Energy resolution of NaI:Tl as function of the number of photoelectrons $N_{phe}^{PMT}$. Solid line – contribution due to Poisson statistics. The inset shows on an expanded scale the resolution near the Iodine K-electron binding energy.

Figure 2.9 shows that the $R(E_X)$ just below $E_{KI}$ is quite close to the theoretical limit. Besides the contribution from $R_M$ there are other contributions to $R$ [8]. The contribution from inhomogeneity in the scintillator light yield and light collection is regarded negligible because of the collimated X-ray beam geometry. What remains is an intrinsic contribution $R_{np}$ due to the nPR of NaI:Tl. This contribution can be calculated with:

$$R_{np} = \sqrt{R^2 - R_M^2} \,. \qquad (2.3)$$

### *2.3.3 Escape nonproportional response*

So far we only used information from the photopeaks in pulse height spectra as function of $E_X$ to obtain the photon-nPR curve. One may also use information derived from the escape peaks to obtain a photon-NPR curve. Using Eq. (2.1) and the procedure described after Eq. (2.1), we can construct a, what we call, an escape-nPR curve for NaI:Tl from the $K_\alpha$ and $K_\beta$ escape peaks data as a function of $E_d$. The results

are shown in Figs. 2.10 and 2.11. The $K_\alpha$ escape-nPR data from the $K_\alpha$ escape peak position analysis as function of $E_d$ match the data obtained from the photopeaks analysis as function of $E_X$ well in the energy interval 9 to 12 keV, as can be seen in Fig. 2.10. We explain this as follows. At $E_X$ below $E_{KI}$ = 33.169 keV, the by far most probable interaction of the incident X-ray with NaI is the photoelectric absorption by an L-shell electron of Iodine. The interaction creates a photoelectron with energy $E_{phe}^{L}$ equal to:

$$E_{phe}^{L} = E_X - E_{LI}^{i}, \qquad (2.4)$$

where $E_{LI}^{i}$ is a binding energy of one of the three L-subshells of Iodine indicated by the superscript *i*. This photoelectron produces an amount of light given by $L_{phe}^{L}$. The interaction also creates a hole in the L-shell which initiates a cascade of secondary processes involving the emission of Auger electrons and possibly low energy X-rays. In any case the total energy of the hole will be dissipated in the scintillator and converted to an amount of light given by $L_{cascade}^{L}$.

In the case of $K_\alpha$ X-ray escape we have photoelectric interaction at the Iodine K-shell. The energy of the photoelectron $E_{phe}^{K}$ in this case will be:

$$E_{phe}^{K} = E_X - E_{KI}. \qquad (2.5)$$

Next, a transition occurs of an electron from the L-shell to the K-shell with emission of the $K_{\alpha 1}$ or $K_{\alpha 2}$ X-ray which escapes the scintillator. Again a hole is created in the L-shell which produces as above the same amount $L_{cascade}^{L}$, of scintillation photons. Therefore, in both cases, i.e., photoelectric absorption at the Iodine L-shell or at the K-shell with subsequent X-ray escape, we have an L-shell photoelectron or a K-shell photoelectron of the same energy producing in first approximation the same amount of photons $L_{phe}$ and we have in both cases an L-shell hole producing $L_{cascade}^{L}$ amount of light. Therefore, as a first approximation both the photopeak-nPR should be about the same as the $K_\alpha$ escape-nPR in the energy range below $E_{KI}$. In second approximation, we can not treat the $K_\alpha$ escape-nPR as completely the same as a photopeak-nPR. $K_\alpha$ X-ray fluorescence is caused by a transition of an electron from the $L_3$ ($2p_{3/2}$ orbital) or the $L_2$ ($2p_{1/2}$ orbital) subshell to the K (1s orbital), see scheme of Fig. 2.4. The probabilities and the energies for the two transitions listed in Table 2.1 are not equal. The transition from the $L_1$ (2s orbital) to the K-shell is dipole forbidden and we can ignore that possibility. Because of the difference in the probability of a hole to be

created in the $L_1$, $L_2$ or $L_3$-subshell between photopeak-nPR and escape-nPR some deviation can arise.

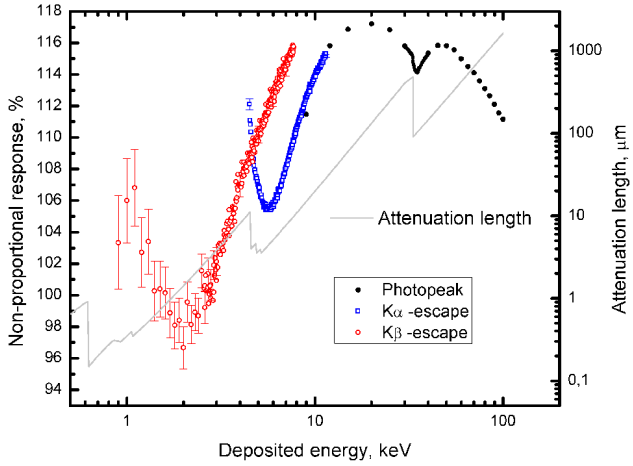


**Fig. 2.10** Photon nonproportional response of NaI:Tl as a function of deposited energy. Black solid circles, photopeak-nPR; blue open squares, $K_\alpha$ escape-nPR; red open circles, $K_\beta$ escape-nPR . The solid curve shows the X-ray attenuation length for NaI.

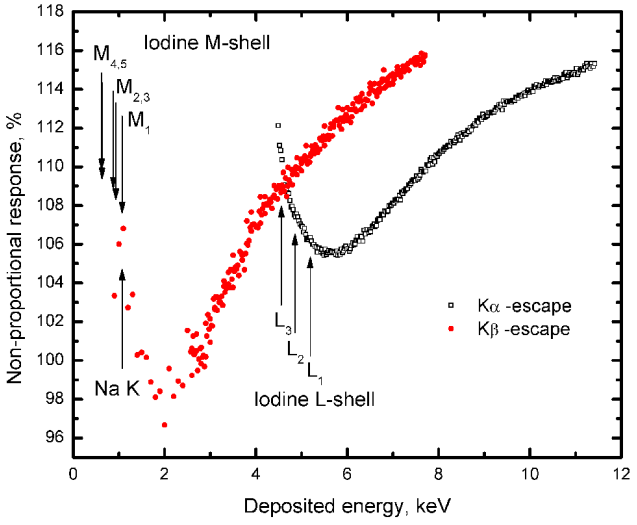


**Fig. 2.11** Escape nonproportional response of NaI:Tl as a function of deposited energy. Black open squares, $K_\alpha$ escape-nPR, red solid circles, $K_\beta$ escape-nPR.The arrows indicate the locations of K, L, and M-shell electron binding energies of Iodine and Sodium.

As can be seen in Figs. 2.10 and 2.11 there is a dip in the $K_\alpha$ escape-nPR with minima at energy about 5.5 keV. We call this the L-dip which is analogue to the K-dip that can be seen at energy around $E_{KI}$. The energy for both the K-dip and L-dip correspond with the discontinuities in the attenuation length curve presented in Fig. 2.10 and with the iodine electron binding energies indicated by arrows in Fig. 2.11. As compared to the K-dip, the L-dip is not as sharply defined because of the presence of three L-subshells with slightly different binding energies.

Next to the $K_\alpha$ escape-nPR we can define another photon-nPR that is based on $K_\beta$ escape peak analysis. We call this the $K_\beta$ escape-nPR, and the results are shown in Figs. 2.10 and 2.11. The $K_\beta$ escape-nPR data do not overlap the $K_\alpha$ escape-nPR but the two data sets cross each other around the Iodine $L_3$-subshell energy of 4.557 keV, shown as arrow $L_3$ in Fig. 2.11. Above we have argued that the $K_\alpha$ escape-nPR at energies below $E_{KI}$ in first approximation is similar to the photopeak-nPR. For the same reasoning the $K_\beta$ escape-nPR at energies below the energy of the $L_3$ subshell is as a first approximation the same as the photopeak-nPR. It is therefore not a coincidence that the $K_\beta$ escape-nPR crosses the $K_\alpha$ escape-nPR near the $L_3$ subshell energy. We anticipate similar behavior for other scintillation crystals. That reasoning is now as follows. For the photopeak event at energies $E_X$ below the $L_3$ subshell a hole is created in the Iodine M or N shells and the light yield observed is from the cascade of the hole in those shells plus the light produced by the photoelectron from those shells. For the $K_\beta$ escape peak event the light yield is from a K-shell photoelectron plus also from the cascade following the creation of a hole in the M, N subshells. Again in first approximation similar total light yield is expected for the beta escape event and the photopeak event. Similarly to the K and L-dips we can determine an M-dip with minimum at energy about 2 keV. M-dip seems to have a small shift to the higher energies in respect to the X-ray attenuation length in NaI Fig. 2.10 and M-shell binding energies shown in Fig. 2.11. One of the reasons for that can be the fact, that in second approximation the shape of the photopeak-nPR can differ from the shape of the $K_\beta$ escape-nPR because of the Sodium K-shell at energy 1.071 keV [22].

Values for the $K_\beta$ escape-nPR in the energy range above the Iodine $L_3$-subshell energy are higher then the values for the $K_\alpha$ escape-nPR in Figs. 2.10 and 2.11. We explain this as follows. For the same value of deposited energy $E_d$ in the case of $K_\beta$ escape the created photoelectron has higher energy as in the case of $K_\alpha$ escape. The difference between the photoelectron energy is equal to the difference between the electron binding energies of L and M or N-subshell electrons. The strong increase of photon-nPR in the range 9-20 keV implies that the scintillation efficiency increases with $E_X$ which suggests an increase with primary electron energy. In other words higher energy

electrons are more efficient in producing scintillation light. We believe that this is the reason that the $K_\beta$ escape-nPR curve is running above the $K_\alpha$ escape-nPR curve.
We have now demonstrated that by piecing together the $K_\beta$ escape-nPR below $E_{LI}$, the $K_\alpha$ escape-nPR between $E_{LI}$ and $E_{KI}$ and the photopeak-nPR between 9 keV and 100 keV we obtain the overall photon-nPR from 1 keV to 100 keV which could be further extended by utilizing radioactive sources up to say 10 MeV energy. This overall photon-nPR and the three other types of photon-nPR curves in Figure 2.10 reveal quite detailed and complex features especially near the binding energies of the iodine subshells. To further understand those features one needs to know the scintillation photon yield of NaI as function of electron energy. Below we will demonstrate that our data above $E_{KI}$ in Fig. 2.7 enables us to derive the the scintillator response to electrons and then also the electron-nPR curve down to energies as low as 30 eV.

### *2.3.4 K-electron nonproportional response*

Measuring the scintillator pulse height at energies below 9 keV is difficult because of the short attenuation length of X-ray absorption, and X-rays either do not transmit the Be-window or at best are absorbed close to the scintillator surface. However, then the surface may affect the scintillation yield. Usage of energies above 9 keV assures us that we are studying the properties of the bulk, not influenced by surface effects [23]. We therefore need other techniques to determine the nPR at energies below 9 keV.
To utilize K-dip spectroscopy, we need precise measurement of the photopeak-nPR in the energy range just above $E_{KI}$, i.e., like the results of the 25 eV step size measurement shown in Fig. 2.7. The drop of the photopeak-nPR in the range 33.0 – 34.5 keV is more then 1%. Showing error bars would blur all data and are therefore not shown in Fig. 2.7. In the presented range the average error is less then 0.1%. The main advantage of our method to obtain data compared to that from other methods is the high precision of the results.
The method can be described as follows. An X-ray, photoelectrically absorbed by Iodine, leads to the creation of a number of electrons; a photoelectron plus several Auger electrons. We assume that these electrons then act independently from each other. With this we mean that the number of photons $L_{phe}$ created by the photoelectron is not affected by the presence of the Auger electrons emitted from the same atom and vice versa. The total photon yield is the sum of the photons produced by the complete set of electrons. The response of a scintillator is then equivalent to the sum of two main interaction products: 1) a K-shell photo electron plus 2) the electrons emitted due to the sequence of processes following relaxation of the hole in the K-shell, the so-called K-cascade response. Our strategy is to employ X-ray energies just above $E_{KI}$. The K-

cascade response is assumed independent from the original X-ray energy. This response is found by tuning the X-ray energy very close above $E_{KI}$, see inset Fig. 2.5. By subtracting the K-cascade response from the total X-ray response we are left with the response in photoelectrons from the K-shell photo-electron alone with energy $E_X - E_{KI}$. The electron-nPR curve is then obtained by the $N_{phe}^{PMT}$/MeV at the energy of the K-photoelectron divided by the $N_{phe}^{PMT}$/MeV measured at 662 keV.

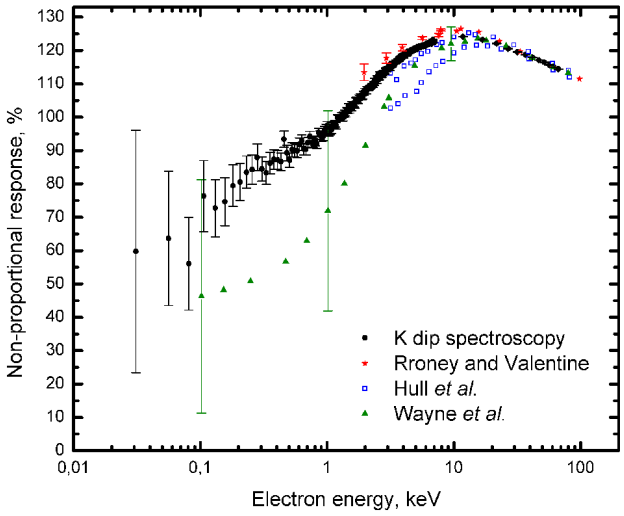


**Fig. 2.12.** Comparison of electron non-proportional response as a function of photoelectron energy inferred using K-dip spectroscopy with other data.

Figure 2.12 shows the K-electron-nPR for NaI:Tl using our K-dip spectroscopy method. An alternative method to obtain an electron-nPR curve is by means of CCT. Rooney and Valentine pioneered this method and used it to determine the Compton electron-nPR curve of NaI:Tl [13, 24]. Their results are also shown in Fig. 2.12. Choong *et al.* [15] further developed the CCT and the improved setup named SLYNCI was used by Hull *et al.* [25] to determine the Compton electron-nPR of different NaI:Tl crystals. Because for different NaI:Tl crystals the nPRs vary, in Fig. 2.12 we have shown the highest and the lowest values presented in [25]. The data measured by two different groups using the same method but different setups are in a good agreement with our data at energy above 20 keV. Below 20 keV, the Compton electron-nPR curve measured by Rooney and Valentine is at higher value. CCT and SLYNCI do not

provide reliable electron-nPR data below 3 keV, and here we think that our data is most reliable.

All presented curves in Fig. 2.12 have the same appearance. Starting with 100 keV the electron-nPR increase until a maximum is reached at 15 keV and then at even lower energies it decreases again. The increase of the electron-nPR is about 15% for the data reported by Rooney and Valentine in the range 10 – 100 keV; from 10% to 13% for Hull *et al.* in the range 15 – 100 keV; 12% for Wayne *et al.* in the range 15 -100 keV and 13% for K-electron-nPR in the range 10 – 100 keV. With further decreasing of the electron energy, the nPR starts to drop rather fast. In the low energy range, below 10 keV, electron response taken from Wayne et al. is showing lower values as compared with K-dip spectroscopy results. But, considering large error margins for both methods in the electron energy range below 1 keV, we can conclude that out K-dip spectroscopy data are in a good agreement with results from the modified Collinson and Hill method. However, our method provides much more data points with higher accuracy and extending to lower energy.

### *2.3.5 Comparison of the experimental data with simulations*

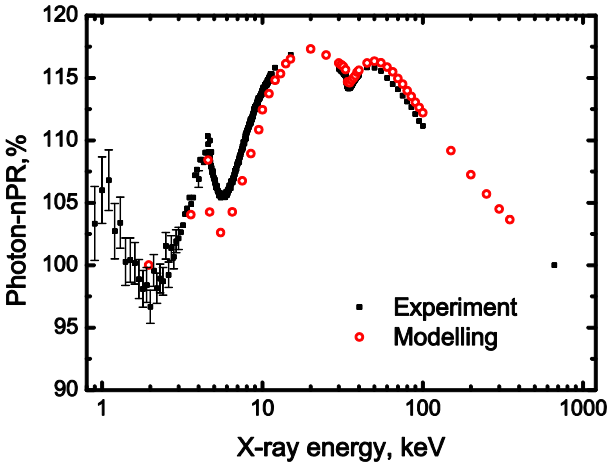


**Fig. 2.13** Comparison of the photon-nPR experimental data with GEANT4 simulated one. Simulation done by A. Lyssenko *et al*.

Using a specially developed Monte Carlo (MC) simulation code [26] the photon-nPR of NaI:Tl was simulated by our colleagues A. Lyssenko *et al.* from Ioffe Physical-Technical Institute of the Russian Academy of Sciences. Our data of the electron-nPR shown in Fig 2.12 was used as input. The simulation was done taking into account the

dimensions of the scintillator shown in Fig. 2.1 and the geometry of the experiment shown in Fig. 2.2. The γ- or X-ray photon interaction was simulated providing a list of primary and secondary electron energies. Using this list and the electron-nPR data pulse-height spectra were simulated for all corresponding X-ray energy values from 2 keV to 350 keV. For every pulse-height spectrum the number of scintillation photons corresponding to the maxima of the photopeak was determined.
Figure 2.13 compares the experimental data shown in Fig. 2.10 and data simulated with the MC code using as an input data in Fig. 2.12. Good to excellent agreement of the modeled data with experiment in the entire energy range exists and confirms that our electron-nPR derived using K-dip spectroscopy method must be reliable. That also evidences that the K-dip spectroscopy method can be used to determine the electron-nPR down to energies as low as tens of eV.

## 2.4 Conclusion

We have measured the nonproportional response of NaI:Tl to highly monochromatic X-ray photons in the energy range 9 – 100 keV. By utilizing the photopeak, the $K_\alpha$ escape peak, and the $K_\beta$ escape peaks in pulse height spectra we introduced three different types of strongly related non-proportionality curves. It enables us to obtain a good estimate for the non-proportionality curve of NaI:Tl to X-ray photons down to energies as low as 1 keV. Information that could not be obtained utilizing a 1 keV X-ray source because of unavoidable affects of the scintillator surface. We paid special emphasis to the scintillator response near the K-electron binding energy of the Iodine. From this data, we have inferred the non-proportional response curve (K-electron-nPR) of NaI:Tl to the iodine K-shell photoelectron in the energy range 0.03 – 65 keV. We have named this method K-dip spectroscopy, and it provides us with information on the electron response down to 30 eV. From 65 keV to 10 keV, K-electron-nPR increases from 114.5% to 124.6%; from 10 keV to 30 eV, K-electron-nPR appears to drop by more then 64% from 124.6% to 60%.
Our methods utilizing escape peaks and K-dip spectroscopy have the advantage that the non-proportionality curve can be extended to lower energies than possible with other methods. CCT becomes too inaccurate below 3 keV. With K-dip spectroscopy the curves are extended down to 30 eV. Detailed study of the non-proportionality in the photopeak-nPR just above the K-edge using energy steps as small as 25 eV enables this.
The CCT method has an advantage over K-dip spectroscopy. In K-dip spectroscopy we suppose that in the K-cascade a set of low energy electrons are emitted from the atom

and each produces an ionization track. We assumed that these tracks do not interact with the track created by the K-shell photoelectron. In that case the K-dip spectroscopy method provides us like the CCT method the genuine electron response. However, when tracks do influence each other, i.e., when the number of photons produced by the photoelectron is affected by the tracks from the cascade products, an error is introduced In this regard CCT may have an intrinsic advantage over the K-dip spectroscopy, by exciting the crystal with essentially just one electron at a time.

**Acknowledgments**

The research leading to these results has received funding from the Netherlands Technology Foundation (STW), Saint-Gobain, crystals and detectors division, Nemours, France, and by the European Community's Seventh Framework Programme (FP7/2007-2013) under grant agreement n° 226716. We thank the scientists and technicians of the X-1 beamline at the Hamburger Synhrotronstrahlungslabor (HASY-LAB) synchrotron radiation facilities for their assistance.

**References**

[1] R. Hofstadter, "Alkali Halide Scintillation Counters," *Physical Review*, vol. 74, pp. 100-101, 1948.

[2] E. V. D. van Loef, P. Dorenbos, C. W. E. van Eijk, K. Kramer, and H. U. Gudel, "High-energy-resolution scintillator: $Ce^{3+}$ activated $LaBr_3$," *Appl. Phys. Letters*, vol. 79, pp. 1573-1575, 2001.

[3] N. J. Cherepy, S. A. Payne, S. J. Asztalos, G. Hull, J. D. Kuntz, T. Niedermayr, S. Pimputkar, J. J. Roberts, R. D. Sanner, T. M. Tillotson, E. van Loef, C. M. Wilson, K. S. Shah, U. N. Roy, R. Hawrami, A. Burger, L. A. Boatner, C. Woon-Seng, and W. W. Moses, "Scintillators With Potential to Supersede Lanthanum Bromide," *Nuclear Science, IEEE Transactions on*, vol. 56, pp. 873-880, 2009.

[4] D. Engelkemeir, "Nonlinear Response of NaI(Tl) to Photons," *Review of Scientific Instruments*, vol. 27, pp. 589-591, 1956.

[5] C. D. Zerby, A. Meyer, and R. B. Murray, "Intrinsic line broadening in NaI(Tl) gamma-ray spectrometers," *Nuclear Instruments and Methods*, vol. 12, pp. 115-123, 1961/7// 1961.

[6] R. B. Murray and A. Meyer, "Scintillation Response of Activated Inorganic Crystals to Various Charged Particles," *Physical Review*, vol. 122, pp. 815-826, 1961.

[7] P. A. Rodnyi, P. Dorenbos, and C. W. E. van Eijk, "Energy Loss in Inorganic ScintiNators," *Phys. Statatus Solidi B*, vol. 187, pp. 15-29, 1995.

[8] P. Dorenbos, J. T. M. de Haas, and C. W. E. van Eijk, "Non-Proportionality in the Scintillation Response and the Energy Resolution Obtainable with Scintillation Crystals," *IEEE Trans. Nucl. Sci.*, vol. 42, pp. 2190-2202, 1995.

[9] G. Bizarri, W. W. Moses, J. Singh, A. N. Vasil'ev, and R. T. Williams, "An analytical model of nonproportional scintillator light yield in terms of recombination rates," *J. Appl. Phys.*, vol. 105, p. 044507, 2009.
[10] W. W. Moses, S. A. Payne, W. S. Choong, G. Hull, and B. W. Reutter, "Scintillator non-proportionality: Present understanding and future challenges," *IEEE Trans. Nucl. Sci.*, vol. 55, pp. 1049-1053, Jun 2008.
[11] A. N. Vasil'ev, "From luminescence non-linearity to scintillation non-proportionality," *IEEE Trans. Nucl. Sci.*, vol. 55, pp. 1054-1061, Jun 2008.
[12] R. T. Williams, J. Q. Grim, Q. Li, K. B. Ucer, and W. W. Moses, "Excitation density, diffusion-drift, and proportionality in scintillators," *Phys. Status Solidi B*, vol. 248, pp. 426-438, 2011.
[13] B. D. Rooney and J. D. Valentine, "Benchmarking the Compton Coincidence Technique for Measuring Electron Response Non-Proportionality in Inorganic Scintillators," *IEEE Trans. Nucl. Sci.*, vol. 43, pp. 1271-1276, 1996.
[14] W.-S. Choong, G. Hull, W. W. Moses, K. M. Vetter, S. A. Payne, N. J. Cherepy, and J. D. Valentine, "Performance of a Facility for Measuring Scintillator Non-Proportionality," *IEEE Trans. Nucl. Sci.*, vol. 55, pp. 1073-1078, 2008.
[15] W.-S. Choong, K. M. Vetter, W. W. Moses, G. Hull, S. A. Payne, N. J. Cherepy, and J. D. Valentine, "Design of a Facility for Measuring Scintillator Non-Proportionality," *IEEE Trans. Nucl. Sci.*, vol. 55, pp. 1753-1758, 2008.
[16] A. J. L. Collinson and R. Hill, "The Fluorescence Response of NaI(Tl) and CsI(Tl) to X Rays and g Rays," *Proc. Phys. Soc.*, vol. 81, pp. 883-892, 1963.
[17] L. R. Wayne, W. A. Heindl, P. L. Hink, and R. E. Rothschild, "Response of NaI(Tl) to X-rays and electrons," *Nuclear Instruments and Methods in Physics Research Section A: Accelerators, Spectrometers, Detectors and Associated Equipment*, vol. 411, pp. 351-364, 1998.
[18] http://www.crystals.saint-gobain.com/.
[19] J. T. M. de Haas, P. Dorenbos, and C. W. E. van Eijk, "Measuring the absolute light yield of scintillators," *Nucl. Instr. and Meth. A*, vol. 537, pp. 97-100, Jan 2005.
[20] http://hasylab.desy.de/facilities/doris_iii/beamlines/x1_roemo_ii/index_eng.html.
[21] J. T. M. de Haas and P. Dorenbos, "Advances in Yield Calibration of Scintillators," *IEEE Trans. Nucl. Sci.*, vol. 55, pp. 1086-1092, 2008.
[22] A. C. Thompson, *X-ray data booklet*. Berkeley: Lawrence Berkeley National Laboratory, 2009.
[23] G. C. Meggitt, "The effect of the crystal surface on the derived electron scintillation response of NaI(Tl)," *Nucl.Instr.and Meth.*, vol. 83, pp. 313-316, 1970.
[24] B. D. Rooney and J. D. Valentine, "Scintillator light yield nonproportionality: calculating photon response using measured electron response," *IEEE Trans. Nucl. Sci.*, vol. 44, pp. 509-516, 1997.

[25] G. Hull, C. Woon-Seng, W. W. Moses, G. Bizarri, J. D. Valentine, S. A. Payne, N. J. Cherepy, and B. W. Reutter, "Measurements of NaI(Tl) Electron Response: Comparison of Different Samples," *Nuclear Science, IEEE Transactions on*, vol. 56, pp. 331-336, 2009.

[26] M. M. Terekhov, R. L. Aptekar, D. D. Frederiks, S. V. Golenetskii, V. N. Il'inskii, and E. P. Mazets, "The Konus-Wind and Konus-A instrument response functions and the spectral deconvolution procedure," in *Gamma-Ray Bursts, Pts 1 and 2* Melville: Amer Inst Physics, 1998, pp. 894-898.

# Chapter 3 Nonproportionality of LSO:Ce, LuAG:Pr, LPS:Ce, and GSO:Ce

*Slightly modified version of this chapter has been published as: I.V. Khodyuk, J.T.M. de Haas, and P. Dorenbos, "Nonproportional response between 0.1-100keV energy by means of highly monochromatic synchrotron X-rays," IEEE Transactions on Nuclear Science, vol. 57, pp. 1175-1181, June 2010.*

Using highly monochromatic X-ray synchrotron irradiation ranging from 9 keV to 100 keV, accurate $Lu_2SiO_5:Ce^{3+}$ (LSO:Ce), $Lu_3Al_5O_{12}:Pr^{3+}$ (LuAG:Ce), $Lu_2Si_2O_7:Ce^{3+}$ (LPS:Ce) and $Gd_2SiO_5:Ce^{3+}$ (GSO:Ce) nonproportional response curves were determined. By utilizing information from escape peaks in pulse height spectra the response curve can be extended down to several keV. A detailed study of the non-proportionality just above the K-edge is presented and from that a method, which we named *K-dip spectroscopy*, is obtained to reconstruct the electron response curve down to energies as low as 100 eV.

## 3.1 Introduction

It was found 50 years ago [1] that the amount of light emitted in the scintillation spark caused by absorption of an X-ray or a γ-quantum in a crystal is not precisely proportional to its energy. This finding appears important because it causes the energy resolution achievable with scintillation material to deteriorate [2]. Although the phenomenon of non-proportional response and its relation with energy resolution has been studied quite intensively [3-8] there are still many major gaps in our understanding of the underlying physics. New theoretical models and accurate data by dedicated experimental techniques are needed to reveal the true origin of energy relaxation and dissipation inside the solid state. Better knowledge of the fundamental mechanisms of energy loss is necessary in the search for new highly effective and low energy resolution scintillators.

Nonproportional response as function of gamma energy is a direct consequence of the more fundamental non-proportional response to electrons. A powerful method to study the electron response of a scintillator is the Compton Coincidence Technique (CCT) introduced by Valentine and Rooney [9] and further developed by Choong *et al.* [10]. The main advantages of this method are the wide energy range covered, and the results are not affected by surface effects. Nevertheless, using CCT, it is not possible to obtain

accurate data on the electron response at energies below 3 keV. We will demonstrate in this work that measuring the photon response using highly monochromatic synchrotron X-rays, it is possible to get information of electron response starting from energy as low as 100 eV avoiding influence of surface effects. We are not aware of any other experimental method that provides information on electron response down to that low energy. Accurate experimental data is especially important in this low energy range because there the most dramatic drop in scintillator efficiency is expected.

In this chapter we will start from the nonproportionality response curves determined using direct observation of photo peaks from total absorption of highly monochromatic X-ray synchrotron irradiation; 9 – 100 keV X-rays were used. Typically 5 keV step size was used, much finer step size of 25 eV was used around the K absorption edge of the high Z atom in the scintillators. For each X-ray energy, energy resolution is determined as well. Next, a method to obtain the photon response curve in the low energy range down to 5 keV using $K_\alpha$ and $K_\beta$ escape peaks is presented. The nonproportionality curves as function of deposited energy are obtained for LSO:Ce, LuAG:Pr, LPS:Ce and GSO:Ce. Analysis of detailed data of the nonproportionality just above the K-edge, a method that we call *K-dip spectroscopy*, makes it possible to reconstruct the electron response curve that starts already at energies as low as 100 eV. Finally, a comparison of all three methods is presented for LSO:Ce and LuAG:Pr. The limitations of the methods and differences are discussed.

## 3.2 Materials and experiment

Table 3.1 compiles the studied samples. We decided to use these scintillators because LSO:Ce and GSO:Ce have similar chemical composition and crystal structure, and differ mainly by the atomic number of the lanthanide. LSO:Ce is a scintillator with high density 7.4 g/cm$^3$ and light yield of 38800 photons per MeV of absorbed gamma ray energy (ph/MeV) [11].

In spite of high photon yield, the energy resolution at 662 keV of the best LSO:Ce sample is not better than 7%. This is attributed to a high degree of intrinsic nonproportionality of the material. GSO:Ce with four times lower photon yield of 10500 ph/MeV [12] has a comparable energy resolution of 8%. LPS:Ce was chosen because it like LSO:Ce contains Lu and has relatively high photon yield of 26000 ph/MeV, and at the same time poor energy resolution of 10% [13]. LuAG:Pr has been chosen because it is also a Lu-based compound and it is a promising new scintillator material with good proportionality and low energy resolution of 4.6% at 662 keV [14].

***Table 3.1*** *Scintillation crystals used in the experiment.*

| Crystal | Size, $mm^3$ | Resolution at 662 keV, % | Photon yield, photons/MeV | Reference |
|---|---|---|---|---|
| LuAG:Pr | 6 × 6 × 1 | 4.6 | 19000 | [14] |
| GSO:Ce | 14 × 10 × 1.5 | 8.1 | 10500 | [12] |
| LSO:Ce,Ca | 10 × 10 × 2 | 7.7 | 38800 | [15] |
| LPS:Ce | 6 × 7 × 2 | 10 | 26000 | [16] |

Relatively thin samples 1–2 mm thick were used, to increase the probability of $K_\alpha$ and $K_\beta$ X-ray escape events, which we are interested in. To measure the pulse height spectra at many finely spaced energy values between 9 keV and 100 keV, experiments at the X-1 beamline at the Hamburger Synhrotronstrahlungslabor (HASYLAB) synchrotron radiation facility in Hamburg, Germany were carried out. The scheme of the experimental set-up and its in detail explanation can be found in the Chapter 2. Figure 3.1 shows the 70 keV synchrotron X-ray pulse height spectrum of LSO:Ce.

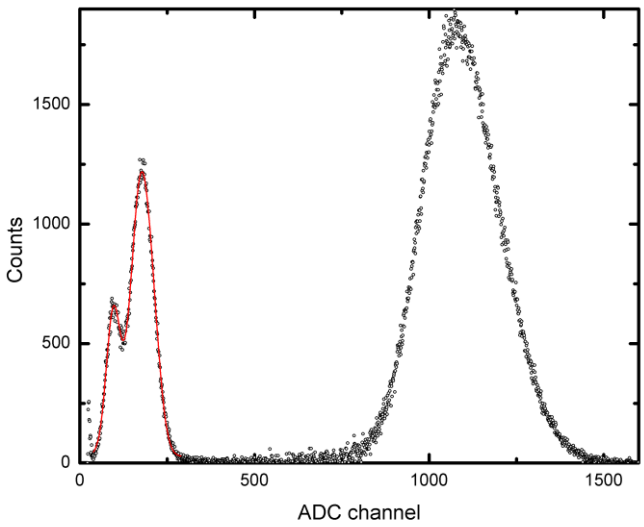


**Fig. 3.1.** Pulse height spectrum of LSO:Ce recorded using 70 keV monochromatic X-rays. The solid red line is the result of a fit of the escape peaks with five Gaussian peaks.

## 3.3 Results and discussion

### *3.3.1 Nonproportionality*

The photon response of the scintillators was determined using monoenergetic X-rays with energies between 9 and 100 keV with a 5 keV step size. In the low energy range 9 to 15 keV, a 1 keV step size was used. A much finer step size of 25 eV was used near the K-shell electron binding energy of 63.314 keV for Lu or 50.239 keV for Gd-based compounds. Figure 3.2 shows the relative scintillation photon yield as a function of X-ray energy for LuAG:Pr, GSO:Ce, LSO:Ce and LPS:Ce. The nonproportional response is defined as the photoelectron yield/MeV at energy E divided by the photoelectron yield/MeV at 662 keV and presented in percents. Error bars are not shown in Fig. 3.2, because the size of the error bars is comparable with the symbols size. Precision of the experimental data can be seen in the inset of Fig. 3.2 and in case of LSO relative error is less then 0.05% in the entire energy range.

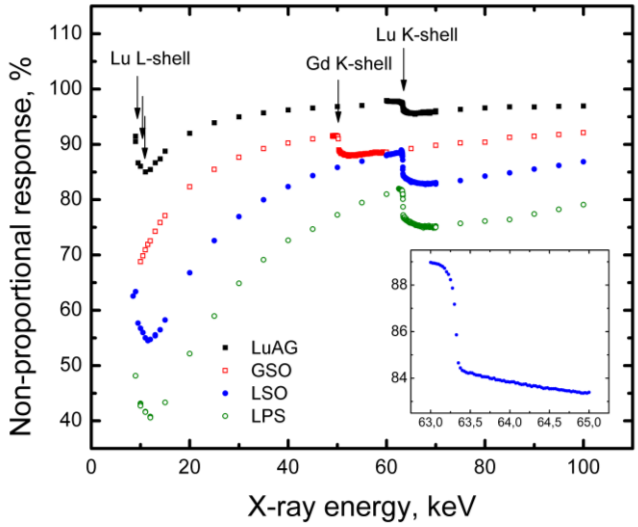


**Fig. 3.2** Scintillation photon yield at RT as a function of X-ray energy for LuAG, GSO, LSO and LPS, relative to the photon yield at 662 keV excitation. The inset shows a 25 eV step size energy scan between 63 and 65 keV for LSO. Error bars are not shown, because the size of the error bar is comparable with the symbol size.

All four materials reveal similar features. When moving from high energy towards low energy, we observe a relatively slow decrease of proportionality down to the K-edge energy. Table 3.2 compiles the K - and L -shell electron binding energies for Lu and

Gd. Figure 3.2 shows that at the Lu or Gd K-edge energy the non-proportionality curve increases with a clear discontinuity at the edge. For LuAG:Pr the response at the edge increases by about 2.1%, while for GSO:Ce it is 3.6%. LSO:Ce has a change in response of 5.9% and this increases to 6.8% for LPS. Moving further towards lower energy we observe a drop of proportionality below the K-edge. At 9 keV the efficiency has decreased by 15%, 31%, 45%, and 60% for LuAG:Pr, GSO:Ce, LSO:Ce, and LPS:Ce, respectively. For the Lu-based compounds there are also discontinuities in the non-proportionality curve at the Lu L-shell energy.

***Table 3.2*** *Electron binding energies.*

| Element | Electron binding energies, keV | | | |
|---|---|---|---|---|
| | K, 1s | $L_I$, 2s | $L_{II}$, $2p_{1/2}$ | $L_{III}$, $2p_{3/2}$ |
| Lutetium | 63.314 | 10.870 | 10.349 | 9.244 |
| Gadolinium | 50.238 | 8.376 | 7.930 | 7.243 |

We observe a proportional dependence between the magnitude of the drop $KL_{drop}$ of scintillator efficiency from below the K-shell to above the L-shell energy with the magnitude $K_{dip}$ of the drop at the K-edge. Empirically we can write

$$KL_{drop} = \xi \times K_{dip}, \qquad (3.1)$$

where for the Lu-based compounds $\xi = 6.01 \pm 0.04$.

### *3.3.2 Energy resolution*

The energy resolution, defined as Full Width at Half Maximum intensity (FWHM) over the peak position, determined from photopeaks like in Fig. 3.1, are plotted in Fig. 3.3 versus the X-ray energy and in Fig. 3.4 versus the number of photoelectrons. The solid curve in Fig. 3.4 represents the theoretical limiting resolution due to Poisson statistics in the number of detected photons [17]:

$$R_{stat} = 2.355\sqrt{\frac{1+\nu(M)}{N_{phe}}}, \qquad (3.2)$$

where $\nu(M) = 0.15$ is the variance in the PMT gain.

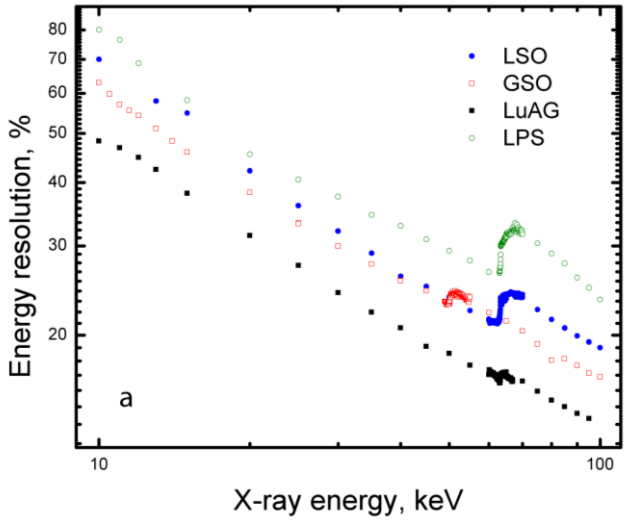


**Fig. 3.3** Energy resolution versus X-ray energy. Error bars are not shown, because the size of the error bar is comparable with the symbol size.

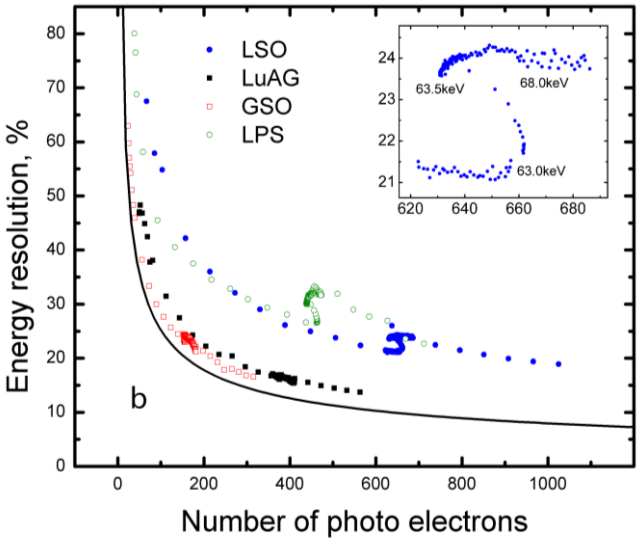


**Fig. 3.4** Energy resolution versus number of photo electrons. The inset shows the *S* type structure around the Lu K-shell in the case of LSO.

Fig. 3.4 shows that the energy resolution for GSO and LuAG are quite close to the theoretical limit. For GSO the most important factor limiting energy resolution is the

relatively low photon yield of 10500 photons/MeV. For LuAG the contribution from non-proportional response is very small. For LSO and LPS the values of their energy resolution are much further from the theoretical limit which is attributed to a large contribution from the nonproportional response.

An *S* type structure can be observed in the data at the Lu or Gd K-edges, see inset Fig. 3.4. For the LSO sample light yield starts to decrease approximately 300 eV below the Lu K-edge. With further increase of the X-ray excitation energy, the number of photoelectrons falls rapidly from 662 at 63.0 keV to 631 at 63.5 keV. A discontinuous increase of the energy resolution appeared in the same energy range 63.0 – 63.5 keV. Analogous features were observed for the other samples. LuAG shows the smallest resolution jump of only 0.9% at the K shell binding energy. For GSO the resolution jump is 1.4%, for LSO 3.2%, and for LPS 5.6%. There is not a linear relation between the magnitude of the resolution jump at the K-edge and $K_{dip}$, but a correlation clearly exists; the larger the resolution jump the larger the value for $K_{dip}$.

### *3.3.3 Information derived from escape peaks*

X-ray photons of energy between 9 keV and 100 keV interact with a sample almost exclusively by means of the photoelectric effect with a K-shell or L-shell electron. The electron is ejected from its shell, leaving a hole. As the atom returns to its stable lowest energy state, electrons from the outer shells relax to the inner shells, and in the process giving off a characteristic X-ray or Auger electrons. In the case that a characteristic X-ray photon escapes the bulk of the crystal we observe a so-called escape peak, shown in Fig. 3.1. The energy $E_{deposited}$ deposited in the bulk of the material is then:

$$E_{deposited} = E_X - E_{escape}, \qquad (3.3)$$

where $E_X$ is the energy of the incident X-ray photon and $E_{escape}$ - the energy of the fluorescent X-ray that escaped from the bulk of the material [18]. The ranges of Auger electrons are too short to escape the bulk of the material and we do not consider Auger electron escape here.

Using Eq. (3.3), we reconstructed the response curves for LuAG, GSO, LSO and LPS scintillators as shown in Fig. 3.5. The parts of the curves at energies above the L-edge are obtained by analyzing $K_{\alpha 1}$ and $K_{\alpha 2}$ – escape peaks. $K_\alpha$ X-ray fluorescence is caused by a transition of an electron from one of the subshells of the L-shell to the hole in the K-shell. In the case of transition from the M or N-shell to the hole in the K-shell, a $K_{\beta 1}$, $K_{\beta 2}$ or $K_{\beta 3}$ X-ray can be emitted and by utilizing the $K_\beta$ escape peaks the photon response below the L-edge can be reconstructed for LuAG and LSO. The probabilities

of other transitions leading to X-ray escape are very small and not considered here. It was not possible to resolve $K_\alpha$ and $K_\beta$ escape peaks for GSO and LPS, and hence no data below the L-edges could be retrieved. In the case of LPS the absence of the $K_\beta$ escape peak is due to a very poor energy resolution, and for GSO because of the lower energy of the Gd L-edge compared to that of Lu. The statistical contribution to the energy resolution becomes large in the low X-ray energy range and a high photon yield of the material is then important to be able to resolve the $K_\alpha$ and $K_\beta$ escape peaks.

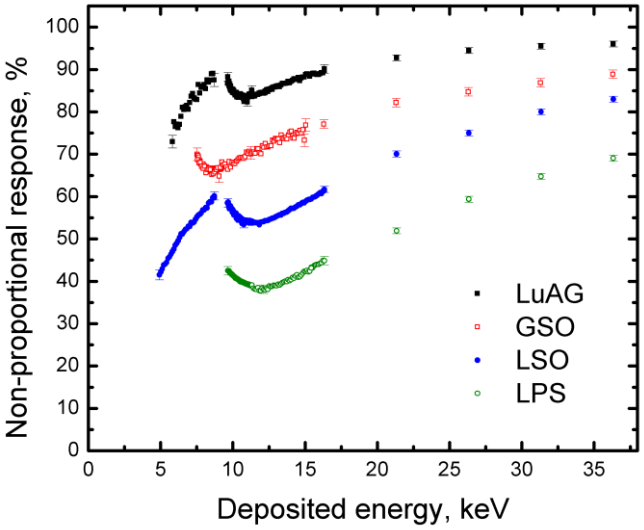


**Fig. 3.5** Scintillation photon yield relative to the photon yield at 662 keV. reconstructed using escape peaks as a function of deposited energy for LuAG, GSO, LSO and LPS.

Reconstructed data match data obtained from photopeak analysis well like in [19]. Rapid changes of the scintillator efficiency are observed near energies of Lu and Gd L-shell. A sharp discontinuity like in the case of the K-edge is not seen because there are three different L-subshell electron binding energies instead of only one for the K-shell.

### *3.3.4 K-dip spectroscopy*

Analysis of data on the nonproportionality response just above the K-edge Fig. 3.6, makes it possible to reconstruct the electron response curve that starts already at energies as low as 100 eV. We call this method *K-dip spectroscopy*. Briefly, the method can be described as follows. The response of a scintillator to an X-ray that has interacted with a K-shell electron is equivalent to the response of a scintillator to a sum

of two main interaction products: 1) a K-shell photo electron response plus 2) the sequence of processes following relaxation of the hole in the K-shell, the so-called K-cascade response. Our strategy is to employ X-ray energies just above the K-edge. The scintillator response due to the K-cascade is assumed independent from the original X-ray energy. This response is found by tuning the X-ray energy very close above the K-shell binding energy. By subtracting the K-cascade response from the total X-ray response we are left with the response in photoelectrons/MeV from the K-shell photo-electron alone with energy $E_X - E_{K_{binding}}$. To estimate the scintillator response due to the K-cascade, we fitted experimental data just above the K electron binding energy with polynomial fit Fig. 3.6. The mean value of the fit function at 63.314 keV was taken as light yield produced by K-cascade. The non-proportionality curve is then obtained by dividing with the photoelectron yield/MeV at energy of 662 keV. This procedure is analogous to the one developed by Collinson and Hill [20].

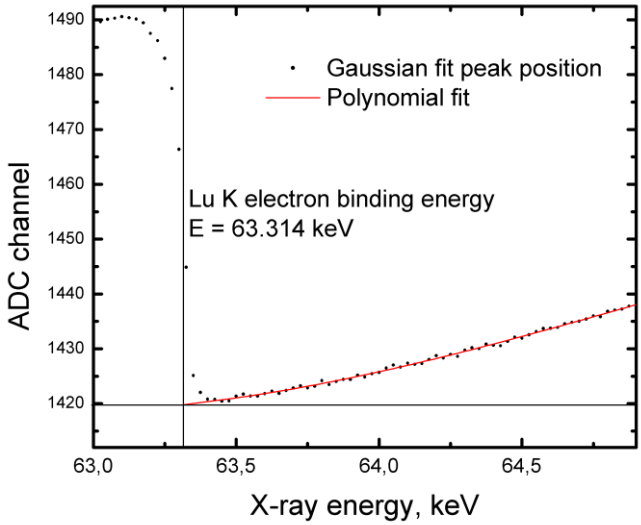


**Fig. 3.6** Position of the Gaussian fitted photopeak for LSO as a function of X-ray energy. Solid red line represents polynomial fit of the data above the Lu K electron binding energy.

Figure 3.7 shows the results obtained from this K-dip spectroscopy method. Our method is good enough to show shape and principal behavior of the electron response curve. The error bars, shown in Fig. 3.7 for LSO are substantial because of subtracting of two close quantities. We are not presenting error bars for the other samples in order to keep data readability.

A drop of 70% to 90% in the scintillator efficiency can be seen for the samples. Like in Fig. 3.2 we have the same ordering of the curves in Fig. 3.7; the most proportional one is for LuAG, then for GSO, LSO, and finally for LPS. Fig. 3.7 reveals a new finding. For all Lu based samples the slope of the electron nonproportional response curve tends to become less steep below 1 keV.

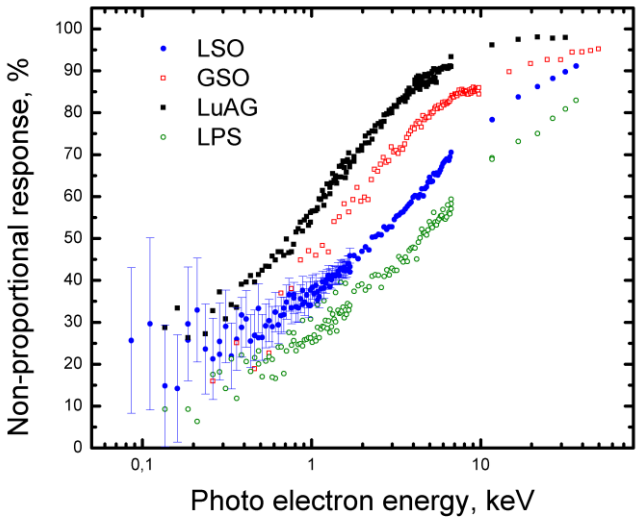


**Fig. 3.7** Relative photon yield as a function of photo electron energy inferred using K-dip spectroscopy.

According to theory [21] on electron inelastic mean free paths and stopping powers, the deposited energy density $dE/dx$ along the track as a function of electron energy increases rapidly with decrease of electron energy. In the low energy range peaking of the deposited energy density is observed in condensed matter. Position of the density maximum is material dependent, but is in order of few hundreds of electron volts. Since a high deposited energy density $dE/dx$ is thought to be the main reason for scintillator efficiency losses, we expect a relationship between the non-proportionality curve and the deposited energy density curve.

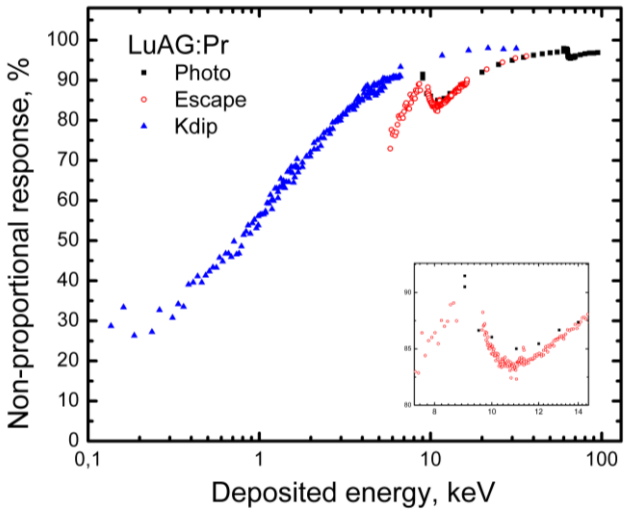


**Fig. 3.8** Comparison of direct photon response, response reconstructed using escape peaks and electron response inferred using K-dip spectroscopy for LuAG. The inset shows zoomed in part of the curves near L binding energies.

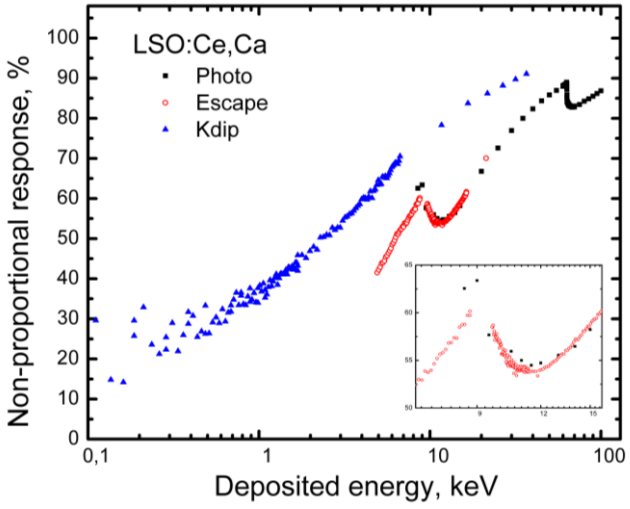


**Fig. 3.9** Comparison of direct photon response, response reconstructed using escape peaks and electron response inferred using K-dip spectroscopy for LSO. The inset shows zoomed in part of the curves near L binding energies.

### *3.3.5 Comparison of the three methods*

Figures 3.8 and 3.9 compare the three sets of response curve data of LSO and LuAG, obtained from X-ray photopeak position analysis, escape peak analysis, and K-dip spectroscopy. As shown in the insets, the shapes of the curves obtained from the photopeak and escape peaks agree well but do have small differences. Those differences we attribute to the fact that the atomic state after photoelectric interaction with the L-shell is different from the atomic state after X-ray fluorescence. In the former situation a hole is created with equal probability in the $L_I$, $L_{II}$, and $L_{III}$ subshells. In the latter situation the hole is preferably created in the $L_{III}$ and $L_{II}$ subshells [18]. The cascade products and the resulting photon yields are then not necessarily equal for both situation leading to the small differences in the data from both methods in Fig. 3.6 and 3.7. In the entire energy range, the K-shell photo-electron response curves are located above the X-ray photon response curves. It means that a single electron produces higher number of scintillating photons then an X-ray or gamma photon of the same energy. It can be understood by comparing the secondary reaction products from single electron and photon interaction in the sample. An X-ray photon, depending on its energy, can be photoelectrically absorbed by one of the atom's shells, creating a relatively energetic photoelectron and a set of electrons of low energies as a result of the cascade process following hole relaxation. Because of a high nonproportionality of the scintillator in the low energy range, the number of photons created by the set of low energy electrons will always be smaller then the yield from the single electron of the same total energy.

## 3.4 Conclusion

We have measured the scintillation response of LuAG, GSO, LSO, and LPS to X-rays in the energy range 9 – 100 keV, with special emphasis near the K-edge of the high Z atoms in the scintillator. From this data, we have inferred the electron response curves of the materials in the energy range 0.1 – 30 keV by a new method that we named K-dip spectroscopy. From 30 keV to 1 keV, scintillation yield for all samples appears to drop by 50 to 75%. Below 500 eV the response becomes proportional again. A means to construct the low energy photon response using analysis of escape peaks has been presented. Our methods utilizing escape peaks and K-dip spectroscopy have the advantage that the non-proportionality curve can be extended to lower energies than possible with other methods. CCT becomes too inaccurate below 3 keV. With K-dip spectroscopy the curves are extended down to 100 eV. Detailed study of the nonproportionality in the photon response just above the K-edge makes this possible.

The CCT method has an advantage over K-dip spectroscopy. In K-dip spectroscopy we suppose that in the K-cascade a set of low energy electrons are emitted from the atom and each produces an ionization track. We assumed that these tracks do not interfere with the track created by the K-shell photoelectron. In that case the K-dip spectroscopy method provides us like the CCT method the genuine electron response. However, when tracks do influence each other, i.e. when the number of photons produced by the photoelectron is affected by the tracks from the cascade products, an error is introduced In this regard CCT may have an intrinsic advantage over the K-dip spectroscopy, by exciting the crystal with essentially just one electron at a time.

**Acknowledgment**

Authors would like to thank Alan Owens and Francesco Quarati for providing beamtime and assisting with experiment at the X-1 beamline at the Hamburger Synhrotronstrahlungslabor (HASY – LAB) synchrotron radiation facility. These investigations have been supported by The Netherlands Technology Foundation (STW).

**References**

[1] D. Engelkemeir, "Nonlinear Response of NaI(Tl) to Photons," *Review of Scientific Instruments*, vol. 27, pp. 589-591, 1956.

[2] C. D. Zerby, A. Meyer, and R. B. Murray, "Intrinsic line broadening in NaI(Tl) gamma-ray spectrometers," *Nuclear Instruments and Methods*, vol. 12, pp. 115-123, 1961/7// 1961.

[3] R. B. Murray and A. Meyer, "Scintillation Response of Activated Inorganic Crystals to Various Charged Particles," *Physical Review*, vol. 122, pp. 815-826, 1961.

[4] P. A. Rodnyi, P. Dorenbos, and C. W. E. van Eijk, "Energy Loss in Inorganic ScintiNators," *Phys. Statatus Solidi B*, vol. 187, pp. 15-29, 1995.

[5] P. Dorenbos, J. T. M. de Haas, and C. W. E. van Eijk, "Non-Proportionality in the Scintillation Response and the Energy Resolution Obtainable with Scintillation Crystals," *IEEE Trans. Nucl. Sci.*, vol. 42, pp. 2190-2202, 1995.

[6] J. D. Valentine, B. D. Rooney, and J. Li, "The light yield nonproportionality component of scintillator energy resolution," *IEEE Trans. Nucl. Sci.*, vol. 45, pp. 512-517, 1998.

[7] W. W. Moses, S. A. Payne, W. S. Choong, G. Hull, and B. W. Reutter, "Scintillator non-proportionality: Present understanding and future challenges," *IEEE Trans. Nucl. Sci.*, vol. 55, pp. 1049-1053, Jun 2008.

[8] G. Bizarri, W. W. Moses, J. Singh, A. N. Vasil'ev, and R. T. Williams, "An analytical model of nonproportional scintillator light yield in terms of recombination rates," *J. Appl. Phys.*, vol. 105, p. 044507, 2009.

[9] B. D. Rooney and J. D. Valentine, "Benchmarking the Compton Coincidence Technique for Measuring Electron Response Non-Proportionality in Inorganic Scintillators," *IEEE Trans. Nucl. Sci.*, vol. 43, pp. 1271-1276, 1996.

[10] W.-S. Choong, K. M. Vetter, W. W. Moses, G. Hull, S. A. Payne, N. J. Cherepy, and J. D. Valentine, "Design of a Facility for Measuring Scintillator Non-Proportionality," *IEEE Trans. Nucl. Sci.*, vol. 55, pp. 1753-1758, 2008.

[11] M. A. Spurrier, P. Szupryczynski, Y. Kan, A. A. Carey, and C. L. Melcher, "Effects of $Ca^{2+}$ Co-Doping on the Scintillation Properties of LSO:Ce," *Nuclear Science, IEEE Transactions on*, vol. 55, pp. 1178-1182, 2008.

[12] M. Balcerzyk, M. Moszynski, M. Kapusta, D. Wolski, J. Pawelke, and C. L. Melcher, "YSO, LSO, GSO and LGSO. A Study of Energy Resolution and Nonproportionality," *IEEE Trans. Nucl. Sci.*, vol. 47, pp. 1319-1323, 2000.

[13] L. Pidol, B. Viana, A. e. Kahn-Harari, B. Ferrand, P. Dorenbos, and C. W. E. van Eijk, "Scintillation and thermoluminescence properties of Lu2Si2O7: Ce3+ crystals," *Nuclear Instruments and Methods in Physics Research Section A: Accelerators, Spectrometers, Detectors and Associated Equipment*, vol. 537, pp. 256-260, 2005.

[14] W. Drozdowski, P. Dorenbos, J. T. M. de Haas, R. Drozdowska, A. Owens, K. Kamada, K. Tsutsumi, Y. Usuki, T. Yanagida, and A. Yoshikawa, "Scintillation Properties of Praseodymium Activated $Lu_3Al_5O_{12}$ Single Crystals," *Nuclear Science, IEEE Transactions on*, vol. 55, pp. 2420-2424, 2008.

[15] C. L. Melcher, J. S. Schweitzer, C. A. Peterson, R. A. Manente, and H. Suzuki, "Crystal growth and scintillation properties of the rare earth orthosilicates," *Inorganic Scintillators and Their Applications, Delft Unviersity Press (SCINT95)*, vol. ISBN 90-407-1215-8, pp. 309-315, 1996.

[16] D. Pauwels, N. Le Masson, B. Vianna, A. Kahn-Harari, E. V. D. van Loef, P. Dorenbos, and C. W. E. van Eijk, "A novel inorganic scintillator: $Lu_2Si_2O_7:Ce^{3+}$ (LPS)," in *Nuclear Science Symposium, 1999. Conference Record. 1999 IEEE*, 1999, pp. 102-105.

[17] P. Dorenbos, "Fundamental Limitations in the Performance of $Ce^{3+}$–, $Pr^{3+}$–, and $Eu^{2+}$– Activated Scintillators," *IEEE Trans. Nucl. Sci.*, vol. 57, pp. 1162-1167, 2010.

[18] A. C. Thompson, *X-ray data booklet*. Berkeley: Lawrence Berkeley National Laboratory, 2009.

[19] M. Moszynski, M. Balcerzyk, W. Czarnacki, M. Kapusta, W. Klamra, A. Syntfeld, and M. Szawlowski, "Intrinsic energy resolution and light yield nonproportionality of BGO," *IEEE Trans. Nucl. Sci.*, vol. 51, pp. 1074-1079, 2004.

[20] A. J. L. Collinson and R. Hill, "The Fluorescence Response of NaI(Tl) and CsI(Tl) to X Rays and γ Rays," *Proc. Phys. Soc.*, vol. 81, pp. 883-892, 1963.

[21] G. F. Knoll, *Radiation Detection and Measurement*. the United States of America John Wiley & Sons, Inc., 1979.

# Chapter 4 Nonproportionality of $LaBr_3$:Ce and $LaCl_3$:Ce

*Sligtly modified version of this chapter has been published as: I.V. Khodyuk and P. Dorenbos, "Nonproportional response of $LaBr_3$:Ce and $LaCl_3$:Ce scintillators to synchrotron x-ray irradiation," Journal of Physics: Condensed Matter, vol. 22(48), art. 485402, December 2010.*

The nonproportional scintillation response of $LaBr_3$ doped with 5% $Ce^{3+}$ and of $LaCl_3$ doped with 10% $Ce^{3+}$ was measured using highly monochromatic synchrotron irradiation. To estimate the photon response, pulse height spectra at many finely spaced energy values between 9 keV and 100 keV were measured. The experiment was carried out at the X-1 beamline at the Hamburger Synhrotronstrahlungslabor (HASYLAB) synchrotron radiation facility in Hamburg, Germany. Special attention was paid to the X-ray fluorescence escape peaks as they provide us with additional information about photon response in the range 1.2 - 14.5 keV for $LaBr_3$:Ce and 2.0 - 11.6 keV for $LaCl_3$:Ce. A rapid variation of the photon response curve is observed near the Lanthanum K- electron binding energy for both scintillators. A dense sampling of data is performed around this energy and that data are used to apply a method, which we call K-dip spectroscopy. This method allows us to derive the electron response curves of $LaBr_3$:Ce and $LaCl_3$:Ce down to energies as low as 0.1 keV.

## 4.1 Introduction

Nonproportional response (nPR) of inorganic scintillators to ionizing radiation is one of the key problems that limits the development of new high energy resolution scintillation detectors [1-6]. The energy resolution $R$, defined as the full width ($\Delta E$) of the full absorption peak in the pulse height spectrum, see Fig. 4.1, at half the maximum intensity (FWHM) divided by its energy $E$, of a scintillator detector can be written as

$$\left(\frac{\Delta E}{E}\right)^2 = R^2 = R_{nPR}^2 + R_{inh}^2 + R_p^2 + R_M^2 , \qquad (4.1)$$

where $R_{nPR}$ is the contribution of the nonproportional response of the scintillator to the energy resolution, $R_{inh}$ is connected with inhomogeneities in the crystal, which can cause local fluctuations in the scintillation light output, $R_p$ the transfer resolution and

$R_M$ the contribution of the photomultiplier tube (PMT) and Poisson statistics in the number of detected photons to the resolution [2]

$$R_M = 2.35\sqrt{\left(1+\mathrm{var}\left(M\right)\right)/N_{phe}^{PMT}}\ , \qquad (4.2)$$

where var*(M)*=0.25 is the contribution from the variance in the gain of the Hamamatsu R6231-100 PMT.

For an absolutely homogeneous scintillation crystal with perfect transfer efficiency, $R_{inh}$ and $R_p$ can be set as zero. Then resolution is given by $R_M$, determined by the variance in the PMT gain and in the number of photoelectrons $N_{phe}^{PMT}$ produced in the PTM, plus $R_{nPR}$. It is important to have $R_{nPR}$ as low as possible to get the best energy resolution at a given $N_{phe}^{PMT}$. To reduce $R_{nPR}$ we need to understand the internal physical cause for the nPR of inorganic scintillators.

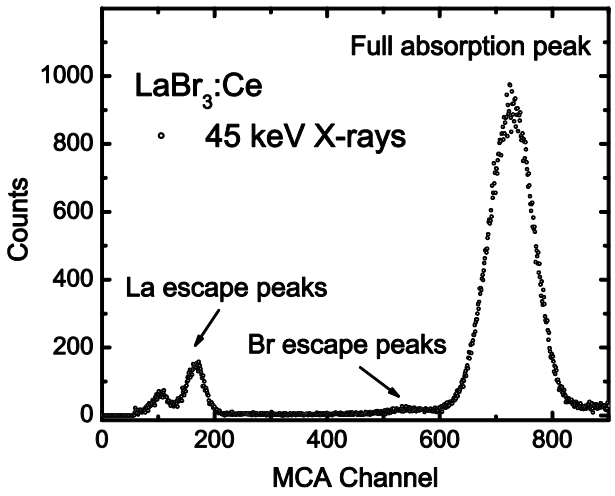


**Fig. 4.1** Pulse height spectrum measured with $LaBr_3$:Ce at 45 keV monochromatic x-ray irradiation.

In principle, scintillation light yield nonproportionality can be characterized as a function of either photon or electron energy. The scintillation response as a function of X-ray and gamma photon energy, hereafter referred to as the photon nonproportional response (photon-nPR), is in general easy to measure and is an indication of scintillator quality [7]. However, the scintillation nonproportional response as function of electron energy, hereafter referred to as electron nonproportional response (electron-nPR), is more fundamental [8, 9]. For a better understanding of the true cause of nPR,

measurements of both the photon and the electron response of the scintillator in question are needed. The most dramatic changes in the nPR occur in the 0.1 keV-10 keV energy range, where the ionization density along the track is higher than at energies of say 100 keV to 1 MeV [1, 10]. To study the nonproportional response in the 0.1 keV – 10 keV range we will apply escape peak analysis and K-dip spectroscopy. To measure photon-nPR, a set of radioactive sources or an energy tunable monochromatic X-ray facility can be used. Figure 4.1 shows a pulse height spectrum measured by $LaBr_3$:Ce at 45 keV monochromatic x-ray irradiation. From this spectrum we can determine the photon-nPR of $LaBr_3$:Ce at 45 keV. Measuring pulse height spectra at many finely spaced energy values between 9 keV and 100 keV we can determine the entire curve. Due to a short attenuation length of X-rays with energy below 9 keV the scintillator surfaces may affect the scintillation output. It is then difficult to measure the genuine photon-nPR below that energy. Extracting additional data of photon-nPR by analyzing X-ray fluorescence escape peaks, gives us information about nonproportionality in the low energy range down to 1 keV. We call this type of nonproportionality curve, escape-nPR.

For determining the electron-nPR, the Compton Coincidence Technique (CCT) [11] is a powerful measurement technique. Unfortunately, CCT is not very accurate for the measurement of electron-nPR below 3 keV. An alternative technique that we call K-dip spectroscopy allows us to estimate K-electron-nPR down to energies as low as 70 eV.

Discovered in 2001 and 2002, $LaCl_3$:Ce and $LaBr_3$:Ce [12, 13] are among the best scintillators available for X-ray and gamma ray detection [14]. With a high light output of 70000 photons/MeV [15] and low energy resolution of 2.9% observed for the 662 keV full absorption peak, $LaBr_3$:Ce is the benchmark for new potentially high performance scintillation materials. $LaCl_3$:Ce with light output of 49000 photons/MeV [15] and energy resolution of 3.3% at 662 keV is a very good scintillator as well. The nonproportional scintillation response of $LaBr_3$:Ce and $LaCl_3$:Ce was measured by several groups [8, 16, 17] using various methods down to photon energies of 5 keV and electron energy of 3 keV. In this chapter we extended those measurements to 1 keV for X-rays and 0.1 keV for electrons. Such data is needed to better understand the true origin of nPR. The main aim of this chapter is to present new data on photon-nPR and electron-nPR of the scintillators $LaBr_3$:Ce and $LaCl_3$:Ce and to present the new methods used to obtain it.

## 4.2 Experimental methods

$LaBr_3$:Ce and $LaCl_3$:Ce are hygroscopic and to study their photon-nPR down to X-ray energies of 9 keV, the same X-ray assemblies as described in Chapter 2 were manufactured by the company Saint-Gobain. Since we intended to exploit X-ray escape peaks for our studies, small 10 mm diameter and 2 mm thick crystals were used to increase the probability of X-ray fluorescence escape. 220 μm thick beryllium was used as an entrance window for the X-rays in order to avoid too much absorption at low energies. The crystals are sealed in aluminum housing with 1 mm thick quartz windows, and the 2 mm edge of the crystal is covered with a white reflector to maximize the photon collection at the PMT photocathode.

The number of photoelectrons $N_{phe}^{PMT}$ per MeV of absorbed energy produced in a Hamamatsu R6231-100 PMT by $LaBr_3$:Ce or $LaCl_3$:Ce was determined by comparing the position of the $^{137}$Cs 662 keV photopeak or of the $^{241}$Am 59.5 keV photopeak in recorded pulse height spectra with the mean value of the so-called single photoelectron pulse height spectrum. The procedure has been described in detail by de Haas *et al.* [18, 19].

## 4.3 Results

Figure 4.1 shows a typical pulse height spectrum recorded with $LaBr_3$:Ce at 45 keV monochromatic x-ray irradiation. The full absorption peak used to determine the photopeak-nPR and the energy resolution is located around channel 710. This peak is a result of the complete deposit of the 45 keV energy of the x-ray photons in the crystal. At channels 167 and 105 lanthanum $K_\alpha$ and $K_\beta$ escape peaks are located. These peaks are the result of x-ray fluorescence escape. X-ray photons of energy between the lanthanum K-electron binding energy $E_{KLa}$=38.925 keV [20] and 100 keV interact with the scintillators almost exclusively by means of the photoelectric effect. After interaction, the electron is ejected from the atom's K-shell, leaving a hole. As the atom returns to its stable lowest energy state, an electron from one of its outer shells jumps into the hole in the K-shell, and in the process giving off a characteristic X-ray photon or Auger electrons. In the case that characteristic X-ray photons escape the bulk of the crystal we observe an escape peak. Since we know precisely the energy of the characteristic X-ray photon the energy deposited in the material is known as well. The procedure has been described by us in detail in Chapter 2. Around channel 530 in Fig. 4.1 weak bromine escape peaks can be seen. The amplitude of those peaks is too low so we did not incorporate them in any further analysis.

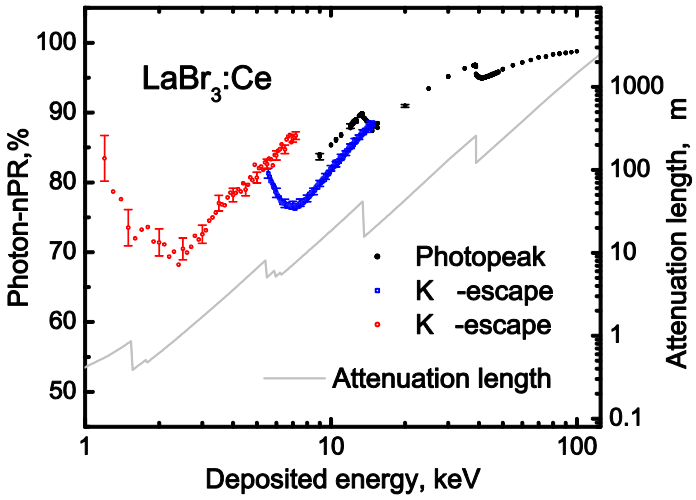


**Fig. 4.2** Photon nonproportional response of $LaBr_3$:Ce as a function of deposited energy. Black solid circles, photopeak-nPR; blue open squares, $K_\alpha$ escape-nPR; red open circles, $K_\beta$ escape-nPR .The solid curve shows the calculated X-ray attenuation length for $LaBr_3$.

Figure 4.2 shows the photon-nPR as function of the energy deposited in the bulk of the $LaBr_3$:Ce scintillator while that of the $LaCl_3$:Ce scintillator is shown in Fig. 4.3. There are three different types of strongly related photon-nPR curves. The first type is the photopeak-nPR which is derived from a single Gaussian fit of the full absorption peaks in the pulse height spectra recorded with X-ray energies ($E_X$) in the range 9 - 100 keV. We define the nPR of a scintillator at $E_X$ as the number $N_{phe}^{PMT}/MeV$ observed at energy $E_X$ divided by the number $N_{phe}^{PMT}/MeV$ observed at $E_X$ = 662 keV energy. The nPR is expressed as a percentage value. The second and the third types of photon-nPR curves are the $K_\alpha$-escape-nPR and $K_\beta$-escape-nPR, they are derived from a multi-Gaussian fit of the lanthanum X-ray escape peaks. In order not to blur the data, error bars are only shown for few data points in Figs. 4.2 and 4.3. The typical error in the data for both $LaBr_3$:Ce and $LaCl_3$:Ce is less then 0.05% at 100 keV, rising to 3% at 1.2 keV.

Precision tuning of the x-ray excitation energy at the X-1 beamline at HASYLAB allows us to observe relatively small variations in the photon response near the K, L, and M-shell electron binding energies of the atoms in the compounds. For example for $LaBr_3$:Ce in Fig. 4.2 we observe a discontinuity in the photon response curve not only

at the lanthanum K-electron binding energy $E_{KLa}$=38.925 keV, but at the bromine K-electron binding energy $E_{KBr}$=13.474 keV [20] as well. The sizes of the jumps in photopeak-nPR are 1.7% and 1.5% the $E_{KLa}$ and $E_{KBr}$ respectively. The total decrease of the photopeak-nPR in the studied range 9 – 100 keV is 15.0%.

The $K_\alpha$-escape-nPR curve of $LaBr_3$:Ce has a dip value of 76.7% at 7.0 keV which is in the energy range above the three lanthanum L-electron shell binding energies of $E_{LLa}$: 5.483 keV, 5.891 keV, and 6.266 keV [20]. The $K_\beta$- escape-nPR curve reaches its minimal value of 68.2% at 2.4 keV which is more then 1 keV above the highest energy lanthanum M-electron shell binding energy of 1.362 keV [20].

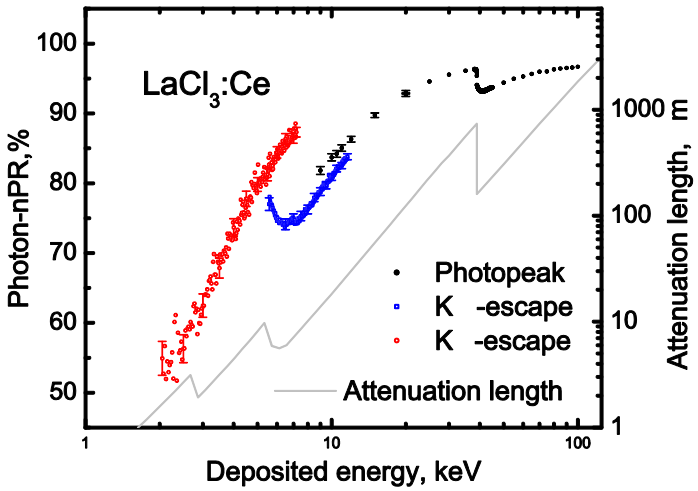


**Fig. 4.3** Photon nonproportional response of $LaCl_3$:Ce as a function of deposited energy. Black solid circles, photopeak-nPR; blue open squares, $K_\alpha$ escape-nPR; red open circles, $K_\beta$ escape-nPR .The solid curve shows the calculated X-ray attenuation length for $LaCl_3$.

The photopeak-nPR curve of $LaCl_3$:Ce as shown in Fig. 4.3 has a similar shape as seen for $LaBr_3$:Ce. The curve increases in the energy range from 9 keV to 100 keV by 14.9%. The magnitude of the jump downwards at $E_{KLa}$ is 3.1%. The $K_\alpha$-escape-nPR reaches the lowest value at 6.5 keV and the $K_\beta$-escape-nPR decreases to 54.9% at 2 keV. The photopeak-nPR curves for the two La-halides show similar features as that of the photopeak-nPR curves of LSO:Ce, LuAG:Pr, LPS:Ce and GSO:Ce presented in Chapter 3.

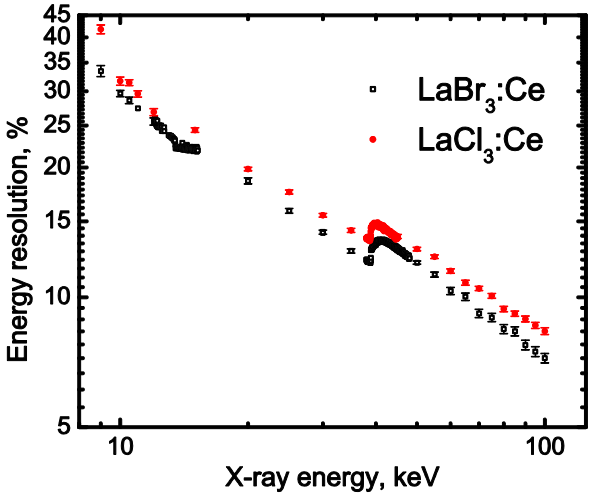


**Fig. 4.4** Energy resolution of the X-ray photopeak as a function of X-ray energy. $LaBr_3$:Ce – black open squares, $LaCl_3$:Ce – red solid circles.

The attenuation length for X-ray and gamma ray photons in $LaBr_3$ and $LaCl_3$ are also shown in Figs. 4.2 and 4.3. The short attenuation length of low energy X-rays complicates the determination of the photon-nPR of scintillators. These X-rays can be absorbed by air, the beryllium entrance window, the reflector, etc. severely reducing the count rate. More importantly, when X-rays are absorbed within say the first 1 μm, the scintillator light output may be affected by surface effects [21, 22]. By using escape peaks analysis we can avoid these complications.

The energy resolution $R$ of the X-ray photopeaks for $LaBr_3$:Ce and $LaCl_3$:Ce is plotted on a double-log scale in Fig. 4.4 as function of $E_X$. Ideally when only $R_M$ contributes to the energy resolution a straight line with slope -0.5 is expected [23]. For $LaBr_3$:Ce $R$ decreases from 33.4% to 7.2%. A clear step-like increase of almost 1.3% can be seen at energy $E_{KLa}$. A small deviation from a straight line can also be seen at energy around $E_{KBr}$. For $LaCl_3$:Ce in Fig. 4.4, $R$ decreases from 41.8% to 8.3%. A step-like increase of 1.1%, analogous to $LaBr_3$:Ce, can be seen around $E_{KLa}$. In the entire range 9 – 100 keV the energy resolution of $LaBr_3$:Ce is better then that of $LaCl_3$:Ce.

Figure 4.5 shows the energy resolution $R$ versus the number of photoelectrons $N_{phe}^{PMT}$ produced in the Hamamatsu R6231-100 PMT for both scintillators. The solid line

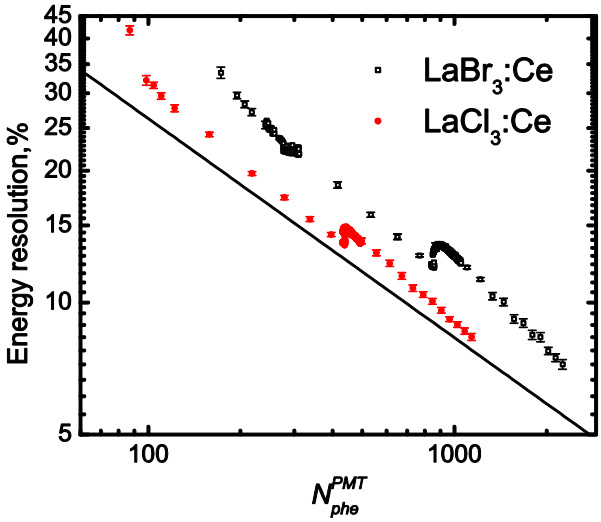


**Fig. 4.5** Energy resolution as function of the number of photoelectrons $N_{phe}^{PMT}$. $LaBr_3$:Ce – black open squares, $LaCl_3$:Ce – red solid circles. Solid line – contribution predicted from Poisson statistics.

represents the theoretical limiting resolution due to the always present Poisson statistics in the number of detected photons, equation (4.2). The step like increases of resolution at $E_{KLa}$ has actually an "*S*-shape" which can be better seen in the enlarged views on a lin-lin scale of Figures 4.6 and 4.7. The data point at $E_{KLa}$ is encircled in both of those Figures. For both $LaBr_3$:Ce and $LaCl_3$:Ce we observe with increasing $E_X$ that energy resolution starts to increase significantly at 38.8 keV which is approximately 0.1 keV before $E_{KLa}$ is reached. Along with an increase in the resolution, the number of photoelectrons $N_{phe}^{PMT}$ decreases rapidly with the increase in X-ray energy. After further increase of energy by 0.5 keV for $LaBr_3$:Ce and by 1.0 keV for $LaCl_3$:Ce, $N_{phe}^{PMT}$ returns to the value observed at 38.8 keV. In Chapter 3 a similar type of "S-shape" behavior for LSO:Ce and other scintillators was observed.

Using the K-dip spectroscopy method we derived the K-electron-nPR curves for $LaBr_3$:Ce and $LaCl_3$:Ce which are shown in Figs. 4.8 and 4.9. The method is briefly described as follows. An X-ray that photoelectrically interacts with the lanthanum K-shell leads to the creation of a K-shell photoelectron plus several Auger electrons. The response of a scintillator is then equivalent to the sum of two main interaction products: 1) the K-shell photo electron response plus 2) the response from the electrons emitted

due to the sequence of processes following relaxation of the hole in the K-shell, the so-called K-cascade response. Our strategy is to employ X-ray energies just above $E_{KLa}$.

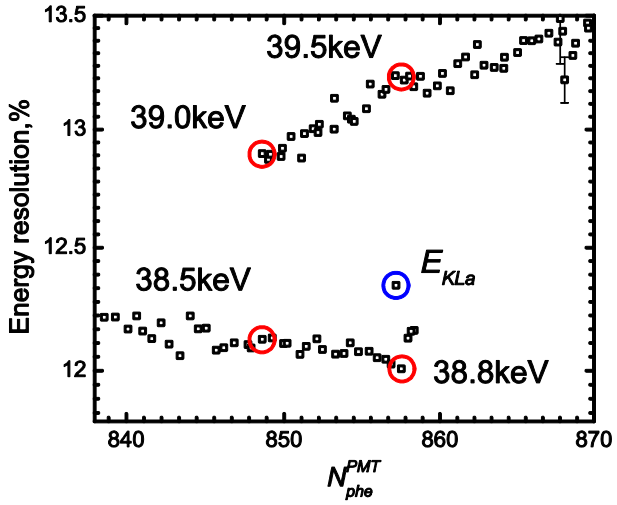


**Fig. 4.6** *S*-type structure near the Lanthanum K-electron binding energy $E_{KLa}$=38.925 keV for $LaBr_3$:Ce.

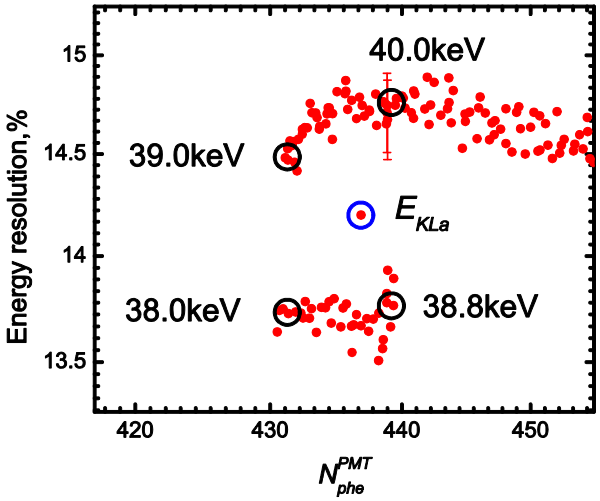


**Fig. 4.7** *S*-type structure near the Lanthanum K-electron binding energy $E_{KLa}$=38.925 keV for $LaCl_3$:Ce.

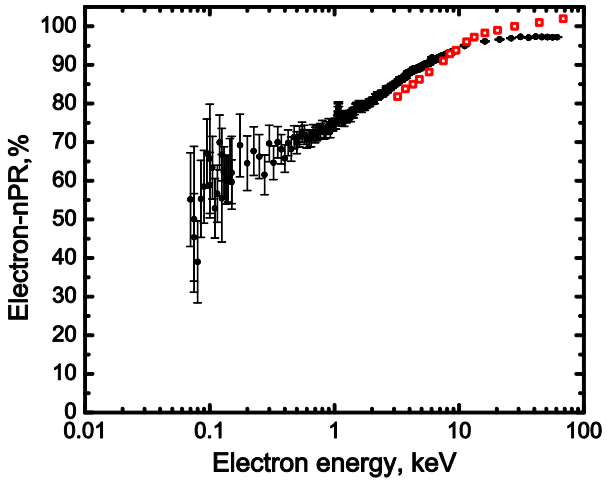


**Fig. 4.8** Black solid circles, electron nonproportional response of $LaBr_3$:Ce as a function of K-photoelectron energy obtained from K-dip spectroscopy. Red open squares, electron-nPR obtained with SLYNCI from [7].

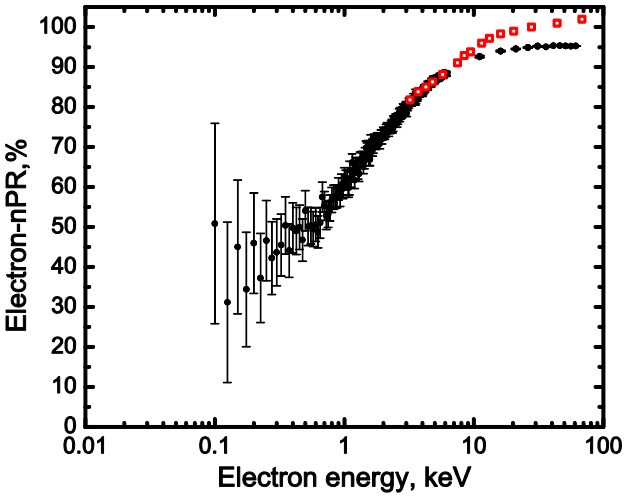


**Fig. 4.9** Black solid circles, electron nonproportional response of $LaCl_3$:Ce as a function of K-photoelectron energy obtained from K-dip spectroscopy. Red open squares, electron-nPR obtained with SLYNCI from [7].

The K-cascade response is assumed independent from the original X-ray energy. This response is found by tuning the X-ray energy to just above $E_{KLa}$ [10, 24]. By subtracting the K-cascade response from the total X-ray response we are left with the response in photoelectrons from the K-shell photoelectron alone with energy $E_X - E_{KLa}$.

The K-electron-nPR curve is then obtained from the number $N_{phe}^{PMT}$ /MeV at the energy of the K-photoelectron divided by the number $N_{phe}^{PMT}$ /MeV measured at 662 keV. A more detailed description of the K-dip spectroscopy method can be found in Chapter 2. Figure 4.8 shows the K-electron-nPR of $LaBr_3$:Ce as function of K-photoelectron energy. Across the range 0.07 keV to 61 keV, K-electron-nPR continuously increases from 60% to 96%. The estimated error decreases from ±19% to ±0.05% with increasing energy over the same energy range. Figure 4.9 shows the K-electron-nPR of $LaCl_3$:Ce as function of K-photoelectron energy. The increase of the K-electron-nPR with increasing K-photoelectron energy for $LaCl_3$:Ce is significantly stronger than for $LaBr_3$:Ce. It rises from 40% at 0.1 keV to 95.3% at 61 keV and the error decreases from ±25% to ±0.05%.

## 4.4 Discussion

The photon-nPR of $LaBr_3$:Ce and $LaCl_3$:Ce shown in Figs. 4.2 and 4.3 are displayed against the deposited amount of energy in the scintillator. This allows us to present the photopeak-nPR, the $K_\alpha$-escape-nPR, and $K_\beta$-escape-nPR curves in one figure. Photopeak-nPR is the standard type of nonproportionality curve that can also be obtained with a set of radioactive sources. In the X-ray energy range from 9 – 100 keV the results match well with the data of other research groups [4, 16] for both scintillators. To extend the nonproportionality curve towards lower energy than 9 keV we performed an analysis of the lanthanum escape peaks to derive the $K_\alpha$-escape-nPR and $K_\beta$-escape-nPR curves. This provides us with the photon-nPR down to energies as low as 1.2 keV for $LaBr_3$:Ce. Figure 4.2 shows that the $K_\alpha$-escape-nPR curve of $LaBr_3$:Ce does not overlap with the photopeak-nPR curve. The two curves join together only in the small energy range 14.0 -14.6 keV. Below 14.0 keV until 9 keV the photopeak-nPR is almost 4% higher than the $K_\alpha$- escape-nPR. Similarly Fig. 4.3 shows that the difference between the photopeak-nPR and the $K_\alpha$-escape-nPR of $LaCl_3$:Ce in the range 9 – 11.6 keV is about 3%. The error of the nPR data in this range is about 0.7% and therefore it can not explain this difference. With $K_\alpha$ or $K_\beta$ X-ray escape, a different set of electrons is generated than without X-ray escape, and although the deposited

energy is the same the total light yield will then be different. This is what is seen in Fig. 4.2 and 4.3. When the scintillator response to electrons is available, we expect that all three nPR curves can be reproduced by means of a Monte Carlo simulation of the cascade processes following X-ray interaction in the crystal as it was done for NaI:Tl in Chapter 2. It is noted that no significant differences between photopeak-nPR and $K_\alpha$-escape-nPRs were observed for the previously studied inorganic scintillators NaI:Tl, LSO:Ce, LuAG:Pr, GSO:Ce and LPS:Ce.

Comparison of the results of the photon-nPRs for $LaBr_3$:Ce and $LaCl_3$:Ce show a difference in the magnitude of the drop at $E_{KLa}$. For $LaBr_3$:Ce it is 1.7%, and for $LaCl_3$:Ce it is 3.1%. According to our results for Lu-based materials and calculations by van Loef et al. [9] the magnitude of the drop at the Lutetium K-edge is strongly related to the magnitude of the photon-nPR drop over the entire range. For LSO:Ce, LuAG:Pr and LPS:Ce we observed a proportional dependence between the magnitude of the drop $KL_{drop}$ of scintillator efficiency from below the K-shell to above the L-shell energy of Lu and the magnitude $K_{dip}$ of the drop at the Lu K-edge. It was written as $KL_{drop} = \xi \times K_{dip}$, and empirically we found $\xi \approx 6$. If we use this equation for $LaBr_3$:Ce and $LaCl_3$:Ce we can expect $KL_{drop}$ of 10.2% and 18.6%. The observed $KL_{drop}$ of the photon-nPR is 20.0% for $LaBr_3$:Ce and 22.2% for $LaCl_3$:Ce. Apparently, the relationship is not a rigorous scintillator law.

Figure 4.4 shows that the energy resolution $R$ of $LaBr_3$:Ce in the entire measurement range 9-100 keV is lower than that of $LaCl_3$:Ce. The 1.3% step-like increase in the energy resolution near $E_{KLa}$ for $LaBr_3$:Ce is higher than the 1.1% increase observed for $LaCl_3$:Ce. This is different from what we observed earlier for LSO:Ce, LuAG:Pr, LPS:Ce and GSO:Ce, where the size of the resolution step increases with $K_{dip}$.

In Fig. 4.5 energy resolution is presented as function of the number of created photoelectrons $N_{phe}^{PMT}$. The solid line represents the theoretical contribution due to Poisson statistics. Fig. 4.5 shows that the energy resolution achieved with $LaCl_3$:Ce as function of the number of detected photons is closer to the statistical limit then that achieved with $LaBr_3$:Ce. However, Fig. 4.4 shows that the energy resolution as function of X-ray energy is definitely better for $LaBr_3$:Ce. For $LaBr_3$:Ce the light output is higher and Figs. 4.8 and 4.9 show that it is more proportional. In Fig. 4.5 statistical contribution $R_M$ goes with $\sqrt{1/N_{phe}^{PMT}}$ whereas the nonproportionality contribution $R_{nPR}$ is not directly related with the $N_{phe}^{PMT}$. Therefore for poor light output scintillators always the statistical contribution dominates. From Fig. 4.5 we can

conclude that for the high light output crystals the nonproportionality becomes the resolution determining property and this increases the need to estimate the true origin of nonproportionality. $LaCl_3$:Ce is still a crystal where statistics dominates, but for the high output $LaBr_3$:Ce nonproportionality becomes highly important.

The presence of the so-called *S-shape* structures, shown in Figs. 4.6 and 4.7, for $LaBr_3$:Ce and $LaCl_3$:Ce makes these materials not suitable for X-ray spectroscopy in the energy ranges 38.5-39.5 keV and 38.0-40.0 keV respectively. In these ranges there is no unique relationship between $N_{phe}^{PMT}$ and $E_X$. The *S-shape* structures reveal that as the energy of the x-ray photon increases, $N_{phe}^{PMT}$ decreases and the energy resolution deteriorates. The deterioration of the energy resolution starts already at energies approximately 0.1 keV lower then the $E_{KLa}$. This means that some of the processes that cause this deterioration start even before $E_{KLa}$ due to the arising photoabsorption at the lanthanum K-shell electron.

Electron-nPRs of $LaBr_3$:Ce and $LaCl_3$:Ce obtained with the K-dip spectroscopy method are shown in Figs. 4.8 and 4.9. Using K-dip spectroscopy we extended the electron response curve down to 70 eV for $LaBr_3$:Ce and down to 100 eV for $LaCl_3$:Ce. We can divide the energy range covered by the K-dip spectroscopy method into three ranges: a) from 61 to 10 keV is a relatively proportional range with slow decrease of scintillator efficiency with decrease of electron energy; b) from 10 to 1 keV there is a fast decrease of scintillator efficiency with decrease of electron energy; and c) below 1 keV there is again like for a) a relatively slow decrease of scintillator efficiency with decrease of electron energy. For $LaCl_3$:Ce shown in Fig. 4.9 this division is somewhat clearer visible than for $LaBr_3$:Ce shown in Fig. 4.8. We already observed similar type of electron nonproportional response curve structure before for LSO:Ce, LuAG:Pr and LPS:Ce. Our experimental findings were recently supported by the theoretical model developed by Kozorezov *et al.* [25].

In Fig. 4.8 and 4.9 we have added data for the electron response measured with SLYNCI, the instrument based on the Compton Coincidence Technique (CCT) by Choong et al. [26]. The data agree reasonably well with each other. Like for our data, the SLYNCI data shows that below 10 keV the nPR starts to decrease. However, for both $LaBr_3$:Ce and $LaCl_3$:Ce in the range 10 – 60 keV the SLYNCI- electron-nPR is higher than the K- electron-nPR. It could be caused by different methods of normalization. The SLYNCI- electron-nPR is normalized at 466 keV, while our K-electron-nPR is normalized at 662 keV. Furthermore it was assumed by us that the amount of $N_{phe}^{PMT}$ produced by the crystal after absorption of a 662 keV gamma-

quantum is equal to the amount produced after absorption of a 662 keV electron. After proper normalization and combining data from SLYNCI with K-dip spectroscopy we aim to obtain a reliable electron-nPR curve in the range 0.07 – 466 keV. By means of Monte Carlo ionization track simulation software we then aim to reproduce the escape-nPR and photopeak-nPR curves of Fig. 4.2 and 4.3.

## 4.5 Conclusion

The nonproportional scintillation response of $LaBr_3:Ce^{3+}$ and of $LaCl_3$:10% $Ce^{3+}$ was measured using highly monochromatic synchrotron irradiation in the energy range 9 – 100 keV. Special attention was paid to the X-ray fluorescence escape peaks as they provide us with additional information about photon response in the range 1.2 - 14.5 keV for $LaBr_3$:Ce and 2.0 - 11.6 keV for $LaCl_3$:Ce. In the X-ray energy range from 9 – 100 keV the results are in a good agreement with the data of other research groups for both scintillators. A rapid variation of the photon response curve is observed near the Lanthanum K- electron binding energy for both scintillators. No relation can be seen between the magnitude of the drop at the Lanthanum K-edge and the magnitude of the photon-nPR drop over the entire range for $LaBr_3$:Ce and $LaCl_3$:Ce.

The presence of the *S-shape* structures in the energy resolution versus $N_{phe}^{PMT}$ curves makes $LaBr_3$:Ce and $LaCl_3$:Ce not suitable for X-ray spectroscopy in the energy ranges 38.5-39.5 keV and 38.0-40.0 keV respectively. In these ranges there is no unique relationship between $N_{phe}^{PMT}$ and $E_X$.

Using K-dip spectroscopy we extended the electron response curve down to 70 eV for $LaBr_3$:Ce and down to 100 eV for $LaCl_3$:Ce. We are not aware of any other experimental method that provides information on electron response to that low energy. Combined data from SLYNCI and K-dip spectroscopy can give us electron-nPR in the entire energy range.

**Acknowledgments**

The research leading to these results has received funding from the Netherlands Technology Foundation (STW), Saint Gobain, crystals and detectors division, Nemours, France, and by the European Community's Seventh Framework Programme (FP7/2007-2013) under grant agreement n° 226716. We thank the scientists and technicians of the X-1 beamline at the Hamburger Synhrotronstrahlungslabor (HASY-LAB) synchrotron radiation facilities for their assistance.

## References


[1] G. Bizarri, W. W. Moses, J. Singh, A. N. Vasil'ev, and R. T. Williams, "An analytical model of nonproportional scintillator light yield in terms of recombination rates," *J. Appl. Phys.*, vol. 105, p. 044507, 2009.

[2] P. Dorenbos, J. T. M. de Haas, and C. W. E. van Eijk, "Non-Proportionality in the Scintillation Response and the Energy Resolution Obtainable with Scintillation Crystals," *IEEE Trans. Nucl. Sci.*, vol. 42, pp. 2190-2202, 1995.

[3] W. W. Moses, G. Bizarri, R. T. Williams, and S. A. Payne, "The Origins of Scintillator Non-Proportionality," *IEEE Trans. Nucl. Sci.*, vol. 59, 2012.

[4] S. A. Payne, W. W. Moses, S. Sheets, L. Ahle, N. J. Cherepy, B. Sturm, S. Dazeley, G. Bizarri, and C. Woon-Seng, "Nonproportionality of Scintillator Detectors: Theory and Experiment. II," *IEEE Trans. Nucl. Sci.*, vol. 58, pp. 3392-3402, 2011.

[5] P. A. Rodnyi, *Physical Processes in Inorganic Scintillators*. NY: CRC Press, 1997.

[6] P. A. Rodnyi, P. Dorenbos, and C. W. E. van Eijk, "Energy Loss in Inorganic ScintiNators," *Phys. Statatus Solidi B,* vol. 187, pp. 15-29, 1995.

[7] P. Dorenbos, "Light output and energy resolution of $Ce^{3+}$-doped scintillators," *Nucl. Instr. and Meth. A,* vol. 486, pp. 208-213, 2002.

[8] W. W. Moses, S. A. Payne, W. S. Choong, G. Hull, and B. W. Reutter, "Scintillator non-proportionality: Present understanding and future challenges," *IEEE Trans. Nucl. Sci.*, vol. 55, pp. 1049-1053, Jun 2008.

[9] E. V. D. van Loef, W. Mengesha, J. D. Valentine, P. Dorenbos, and C. W. E. van Eijk, "Nonproportionality and energy resolution of a $LaCl_3$:10% $Ce^{3+}$ scintillation crystal," *IEEE Trans. Nucl. Sci.*, vol. 50, pp. 155-158, 2003.

[10] A. J. L. Collinson and R. Hill, "The Fluorescence Response of NaI(Tl) and CsI(Tl) to X Rays and γ Rays," *Proc. Phys. Soc.*, vol. 81, pp. 883-892, 1963.

[11] B. D. Rooney and J. D. Valentine, "Benchmarking the Compton Coincidence Technique for Measuring Electron Response Non-Proportionality in Inorganic Scintillators," *IEEE Trans. Nucl. Sci.*, vol. 43, pp. 1271-1276, 1996.

[12] J. Andriessen, O. T. Antonyak, P. Dorenbos, P. A. Rodnyi, G. B. Stryganyuk, C. W. E. van Eijk, and A. C. Voloshinovskii, "Experimental and theoretical study of the spectroscopic properties of $Ce^{3+}$ doped LaCl single crystals," *Optics Communications,* vol. 178, pp. 355–363, 2000.

[13] E. V. D. van Loef, P. Dorenbos, C. W. E. van Eijk, K. Kramer, and H. U. Gudel, "High-energy-resolution scintillator: $Ce^{3+}$ activated $LaBr_3$," *Appl. Phys. Letters,* vol. 79, pp. 1573-1575, 2001.

[14] http://www.crystals.saint-gobain.com/.

[15] N. J. Cherepy, S. A. Payne, S. J. Asztalos, G. Hull, J. D. Kuntz, T. Niedermayr, S. Pimputkar, J. J. Roberts, R. D. Sanner, T. M. Tillotson, E. van Loef, C. M. Wilson, K. S. Shah, U. N. Roy, R. Hawrami, A. Burger, L. A. Boatner, C. Woon-Seng, and W. W. Moses, "Scintillators With Potential to Supersede Lanthanum Bromide," *Nuclear Science, IEEE Transactions on*, vol. 56, pp. 873-880, 2009.

[16] A. Owens, A. J. J. Bos, S. Brandenburg, P. Dorenbos, W. Drozdowski, R. W. Ostendorf, F. Quarati, A. Webb, and E. Welter, "The hard X-ray response of Ce-doped lanthanum halide scintillators," *Nucl. Instr. and Meth. A*, vol. 574, pp. 158-162, 2007.

[17] S. A. Payne, N. J. Cherepy, G. Hull, J. D. Valentine, W. W. Moses, and C. Woon-Seng, "Nonproportionality of Scintillator Detectors: Theory and Experiment," *IEEE Trans. Nucl. Sci.*, vol. 56, pp. 2506-2512, 2009.

[18] J. T. M. de Haas and P. Dorenbos, "Advances in Yield Calibration of Scintillators," *IEEE Trans. Nucl. Sci.*, vol. 55, pp. 1086-1092, 2008.

[19] J. T. M. de Haas, P. Dorenbos, and C. W. E. van Eijk, "Measuring the absolute light yield of scintillators," *Nucl. Instr. and Meth. A*, vol. 537, pp. 97-100, Jan 2005.

[20] A. C. Thompson, *X-ray data booklet*. Berkeley: Lawrence Berkeley National Laboratory, 2009.

[21] A. M. Kudin, B. V. Grinyov, V. Y. Gres', and A. I. Mitichkin, "A possible reason for non-proportionality of response in NaI:Tl and CsI:Tl scintillation crystals," *Functional Materials*, vol. 13, pp. 54-58, 2006.

[22] G. C. Meggitt, "The effect of the crystal surface on the derived electron scintillation response of NaI(Tl)," *Nucl.Instr.and Meth.*, vol. 83, pp. 313-316, 1970.

[23] P. Dorenbos, "Fundamental Limitations in the Performance of $Ce^{3+}$–, $Pr^{3+}$–, and $Eu^{2+}$– Activated Scintillators," *IEEE Trans. Nucl. Sci.*, vol. 57, pp. 1162-1167, 2010.

[24] L. R. Wayne, W. A. Heindl, P. L. Hink, and R. E. Rothschild, "Response of NaI(Tl) to X-rays and electrons," *Nuclear Instruments and Methods in Physics Research Section A: Accelerators, Spectrometers, Detectors and Associated Equipment*, vol. 411, pp. 351-364, 1998.

[25] A. Kozorezov, J. K. Wigmore, and A. Owens, "Picosecond dynamics of hot carriers and phonons and scintillator non-proportionality," *arXiv:1206.1780v1 [cond-mat.mtrl-sci]*, 2012.

[26] W.-S. Choong, G. Hull, W. W. Moses, K. M. Vetter, S. A. Payne, N. J. Cherepy, and J. D. Valentine, "Performance of a Facility for Measuring Scintillator Non-Proportionality," *IEEE Trans. Nucl. Sci.*, vol. 55, pp. 1073-1078, 2008.

# Chapter 5 Trends and patterns of scintillator nonproportionality

*Slightly modified version of this chapter has been accepted for publication as: I.V. Khodyuk and P. Dorenbos, "Trends and patterns of scintillator nonproportionality," IEEE Transactions on Nuclear Science, December 2012.*

Data on the photon nonproportional response of 35 inorganic scintillation materials are systemized and analyzed. Main trends of nonproportionality typical for different groups of inorganic scintillators, especially for complex oxides and halides, are highlighted. The dependence of the shape and degree of photon nonproportional response versus chemical composition, dopant type, refractive index and some other fundamental properties of the materials is studied. Better proportionality appears to be correlated with higher refractive index of the compound. Another related factor is the width of the valence band in halide compounds. With larger valence band width from fluorides, to chlorides, to bromides, and to iodides, a better proportionality is observed.

## 5.1 Introduction

One of the most important requirements imposed on new scintillators is a high energy resolution for gamma ray detection. There are two fundamental factors that determine energy resolution: Poisson statistics in the number of detected photons and the nonproportionality of the light yield of scintillators with gamma-ray energy. Nonproportionality means that the total light output of a scintillator is not precisely proportional to the energy of the absorbed gamma-ray photon. This has a deteriorating effect on energy resolution. As the light yield and the PMT performance is already close to optimal we need to reduce nonproportionality in order to improve energy resolution, and for that we wish to understand the causes of nonproportionality.

The aim of this chapter is to overview, systematize, analyze and interpret the data on the photon nonproportional response (photon-nPR) of inorganic scintillation materials. The main trends and patterns of the photon-nPR typical for the different groups of scintillators, especially for complex oxides and halides, are highlighted. The dependence of the shape of the photon-nPR curve and the degree of the photon-nPR is studied as a function of chemical composition, dopant type, refractive index and other fundamental properties of the materials. To analyze trends and patterns of

nonproportionality the photon-nPRs of 23 inorganic scintillators were measured using synchrotron irradiation in the energy range from 9 to 100 keV. The data on the photon-nPR of 12 other inorganic scintillators were obtained from the publications.

The scintillation response as a function of X-ray or gamma photon energy will hereafter be referred to as the photon-nPR. We define the photon-nPR of a scintillator at energy $E$ as the number of photoelectrons $N_{phe}^{PMT}$ per MeV of absorbed energy observed at energy $E$ divided by the number $N_{phe}^{PMT}/MeV$ observed at $E$ = 662 keV energy. The photon-nPR is expressed as a percentage value. The energy resolution is defined as the full width at half maximum of the photoabsorption peak divided by the energy of the centroid of the peak.

## 5.2 Experimental methods

To determine the photon-nPR of scintillators, scintillation pulse height spectra at many finely spaced X-ray energy values between 9 keV and 100 keV at the X-1 beamline at the Hamburger Synchrotronstrahlungslabor (HASYLAB) synchrotron radiation facility in Hamburg, Germany were carried out. The scheme of the experimental set-up can be found in Chapter 2 and [1, 2]. A monochromatic pencil X-ray beam was used as an excitation source. A tunable double Bragg reflection monochromator using a Si[511] set of silicon crystals providing an X-ray resolution of 2 eV at 9 keV rising to 20 eV at 100 keV was used to select the X-ray energies. The beam spot size was set by a pair of precision stepper-driven slits, positioned immediately in front of the sample coupled to the PMT. The intensity of the synchrotron beam was reduced in order to avoid pulse pileup.

To record synchrotron X-ray pulse height spectra of a scintillator, a Hamamatsu R6231-100 PMT connected to a homemade preamplifier, an Ortec 672 spectroscopic amplifier and an Amptek 8000A multichannel analyzer were used. The crystal was optically coupled to the window of the PMT with Viscasil 60000 cSt from General Electric. The crystal was covered with several layers of ultraviolet reflecting Teflon tape (PFTE tape) forming an “umbrella” configuration [3]. Scintillation photons reflected from the photocathode are then reflected back by the umbrella thus enhancing detection efficiency. All measurements were carried out at room temperature and were repeated several times.

The number of photoelectrons $N_{phe}^{PMT}$ per MeV of absorbed energy produced by the scintillator in the PMT at 662 keV was determined by comparing the positions of the

***Table 5.1*** *Properties of the scintillation materials studied in this work.*

| Scintillator | R,% at 662 keV | Light yield, photons/keV at 662 keV | Index of refraction, n | Photon-nPR,% at 10keV | Degree of photon-nPR, $\sigma_{photon\text{-}nPR}$,% | Reference |
|---|---|---|---|---|---|---|
| YAP:Ce | 4.4 | 16 | 1.95 | 95.2 | 0.13 | [4-7] |
| $Cs_2LiYCl_6$:Ce | 3.9-5.1 | 21 | | 102.2 | 0.38 | [8-10] |
| $K_2LaCl_5$:Ce | 5.1 | 28 | | ~95 | 0.52 | [4, 11] |
| GYGAG:Ce (ceramics) | 5.4 | 60 | | 85 | 0.61 | [12] |
| YSO:Pr | 8 | 6 | 1.8 | 85.3 | 0.72 | [5] |
| LuAP:Ce | 7.1-9.5 | 12 | 1.95 | ~87 | 0.94 | [13-15] |
| $LaBr_3$:Ce | 2.7-3.1 | 75 | 2.05 | 87.2 | 1.10 | [16-19] |
| ZnO (ceramics) | 11.8 | 25 | 2.03 | 82.7 | 1.33 | [20-23] |
| $SrI_2$:Eu | 2.8-3.7 | 115 | 2.05 | 96.1 | 1.35 | [12, 24, 25] |
| LuAG:Sc | 6.5 | 23 | 1.84 | ~90 | 1.36 | [4] |
| ZnSe:Te | 5.4 | 28 | 2.67 | ~85 | 1.43 | [26] |
| $SrI_2$ | 6.7 | 38 | 2.05 | 87 | 1.61 | [24] |
| LuAG:Pr | 4.6 | 16 | 1.84 | 86 | 1.98 | [18, 27] |
| $LuI_3$:Ce | 3.3 | 98 | | 85 | 2.12 | [28] |
| $LaCl_3$:Ce | 3.1 | 49 | 1.9 | 83.7 | 2.16 | [16, 17, 29] |
| $CeBr_3$ | 4-4.4 | 68 | | ~80 | 2.42 | [30] |
| LuYAP:Ce | 8-10 | 15 | 1.94 | ~75 | 2.77 | [14, 31, 32] |
| $BaF_2$ | 7-8 | 11 | 1.51 | 80 | 3.54 | [4, 33, 34] |
| YAG:Ce | 3.5-15 | 17 | 1.82 | ~82 | 3.64 | [35, 36] |
| LuAG:Ce | 11 | 12.5 | 1.84 | ~70 | 4.04 | [18, 35] |
| $CaF_2$:Eu | 5.7 | 24 | 1.44 | ~72 | 4.45 | [37] |
| GSO:Ce | 9.2-9.5 | 12 | 1.85 | 68.8 | 5.03 | [27, 38] |
| YAP | 13.3 | 1.5 | 1.95 | ~70 | 5.70 | [39] |
| YSO:Ce | 9.4-11.1 | 24 | 1.792 | ~65 | 6.71 | [38, 40] |
| CsI:Tl | 5.8-6.2 | 57 | 1.78 | 112 | 6.78 | [37, 41] |
| NaI:Tl | 5.6-7.8 | 45 | 1.85 | 114 | 6.83 | [1, 37, 42] |
| $YPO_4$:Ce | | | 1.65 | 58.3 | 7.06 | [5] |
| CWO | 6.6 | 15 | 2.25 | 47.3 | 7.11 | [4, 43, 44] |
| BGO | 7.8-10 | 8 | 2.15 | ~70 | 7.15 | [4, 45, 46] |
| LSO:Ce | 7.9-11.9 | 29 | 1.82 | 56.7 | 8.40 | [4, 18, 27, 38, 47] |
| CsI:Na | 6.5 | 49 | 1.84 | ~130 | 8.46 | [37] |
| LPS:Ce | 10 | 26 | 1.74 | ~42 | 8.94 | [27, 48] |
| LYSO:Ce,Ca | 8.7 | 38 | 1.81 | ~45 | 11.24 | [49] |
| LGSO:Ce | 12.4 | 20 | | 45 | 12.56 | [38] |
| NaI | 16.2-18.1 | 1-3 | 1.80 | ~170 | 18.14 | [50] |

$^{137}$Cs photopeak in recorded pulse height spectra with the mean value of the single photoelectron pulse height spectrum. To collect as much of the emitted light as possible, the shaping time of an Ortec 672 spectroscopic amplifier was set at 10 μs. In some cases for slower scintillators such as tungstates 10 μs shaping time can be insufficient and further research might be necessary to correct the experimental data.

## 5.3 Results

In this section data on the photon-nPR of 35 inorganic scintillation materials are presented. The photon-nPRs of 23 inorganic scintillators were measured using synchrotron irradiation in the energy range from 9 to 100 keV at HASYLAB. Data on the photon-nPR of 12 other inorganic scintillators were obtained from published works. All investigated scintillators and their properties are listed in Table 5.1. In addition to properties, such as energy resolution, light yield and refractive index, Table I compiles the photon-nPR at 10 keV and the degree of photon-nPR ($\sigma_{photon\text{-}nPR}$). If the exact value of the photon-nPR at 10 keV has not been determined in the measurement, we used an approximate value obtained by extrapolating the response from a fit at higher excitation energies. The degree of photon-nPR was determined following the ideas in [51, 52]. Its numerical value was calculated using

$$\sigma_{photon-nPR} = \frac{1}{\left(E_{\max} - E_{\min}\right)} \int_{E_{\min}}^{E_{\max}} \left| f_{photon-nPR}\left(E_{\max}\right) - f_{photon-nPR}\left(E\right) \right| dE \qquad (5.1)$$

where $E_{max}$ = 662 keV, $E_{min}$ = 10 keV, $f_{photon\text{-}nPR}(E_{max})$ = 100%, and $f_{photon\text{-}nPR}(E)$ is the value of the photon-nPR at the excitation energy E. For a perfectly proportional scintillator the value of the degree of photon-nPR is zero. As a result, scintillators with a lower value of the $\sigma_{photon\text{-}nPR}$ are considered to be more proportional.

## 5.4 Oxide scintillators

A large number of currently known and applied scintillators are oxides. Oxides are generally nonhygroscopic dense scintillators with high gamma stopping power. According to the type of rare earth (RE) cation and chemical composition, oxides will be divided into the groups shown in Table 5.2.

### *5.4.1 Influence of chemical composition*

An effect of the chemical composition on the shape and degree of the photon-nPR was noted by many authors. For the majority of cerium doped RE-oxides regardless of the RE-cation in the composition, a trend in the photon-nPR can be observed. In Figs. 5.2

and 5.3 the photon-nPR as a function of energy of the incident X-ray or gamma photon is shown. All data presented are normalized at 662 keV. The yttrium and lutetium based compounds show similar shape of photon-nPR curves.

***Table 5.2*** *Classification of oxide scintillators.*

| Chemical composition | | RE-cation | | | |
|---|---|---|---|---|---|
| | | $Y^{3+}$ | $Gd^{3+}$ | $Lu^{3+}$ | Mixed Y-Gd-Lu |
| Aluminum perovskites | $REAlO_3$ | YAP:Ce<br>YAP:Pr<br>YAP | | LuAP:Ce | LuYAP:Ce |
| Aluminum garnets | $RE_3Al_5O_{12}$ | YAG:Ce | | LuAG:Ce<br>LuAG:Pr<br>LuAG:Sc | GYGAG:Ce (ceramics) |
| Oxyorthosilicates | $RE_2SiO_5$ | YSO:Ce<br>YSO:Pr | GSO:Ce | LSO:Ce | LYSO:Ce,Ca<br>LGSO:Ce |
| Pyrosilicates | $RE_2Si_2O_7$ | YPO:Ce | | | |
| Phosphates | $REPO_4$ | | | LPS:Ce | |

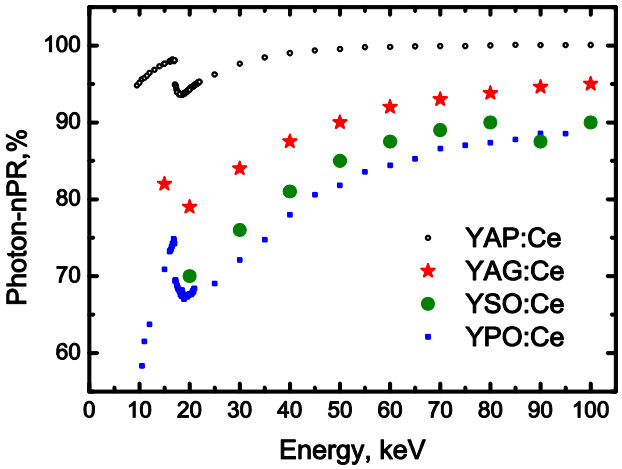


**Fig. 5.2** Photon nonproportional response of Ce-doped Y-based scintillators as a function of X-ray or gamma photon energy. Black open dots – YAP:Ce; red stars – YAG:Ce [35]; olive circles – YSO:Ce [40]; and blue squares – $YPO_4$:Ce.

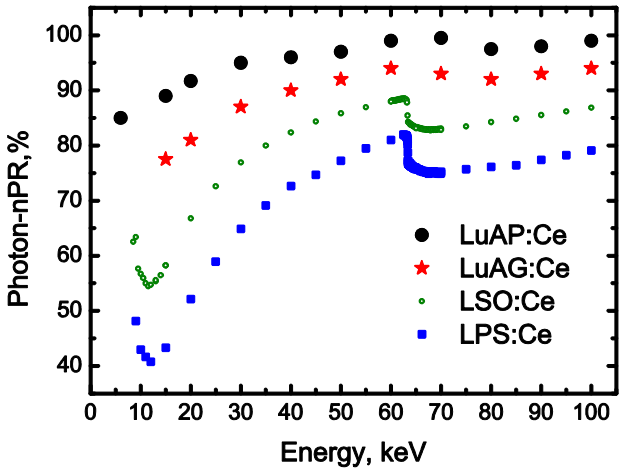


**Fig. 5.3** Photon nonproportional response of Ce-doped Lu-based scintillators as a function of X-ray or gamma photon energy. Black circles – LuAP:Ce [13]; red stars – LuAG:Ce [18]; olive open dots – LSO:Ce; and blue squares – LPS:Ce.

The most proportional response is shown by aluminum perovskites with composition $REAlO_3$:Ce, next are aluminum garnets $RE_3Al_5O_{12}$:Ce, oxyorthosilicates $RE_2SiO_5$:Ce, phosphates $REPO_4$:Ce and pyrosilicates $RE_2Si_2O_7$:Ce, where RE = Lu or Y. In contradiction to the statement in [40] that LuAP:Ce has a high degree of photon-nPR, Fig. 5.3 shows that it has the same relatively low degree of photon-nPR as YAP:Ce. The degree of photon-nPR increases from 0.13% for YAP:Ce up to 7.06% for $YPO_4$:Ce and from 0.94% for LuAP:Ce up to 8.94% for LPS:Ce.

Despite the strong dependence of the degree of photon-nPR on the chemical composition, the shape of the photon-nPR curves appears similar for all scintillators in Figs. 5.2 and 5.3. It is always characterized by a lowest value of the photon-nPR at the lowest energies, a dip in the photon-nPR curve near K-shell and L-shell absorption edges of yttrium or lutetium, and a smooth monotonic increase of the photon-nPR curve with increasing photon energy up to 662 keV.

### *5.4.2 Influence of dopant*

The influence of dopant on nonproportionality and energy resolution was discussed in [12, 18, 53]. A clear correlation between the degree of photon-nPR and the concentration or type of the dopant was not established yet. Figures 5.4, 5.5 and 5.6 show the photon-nPR as a function of energy for YAP, LuAG and YSO pure materials

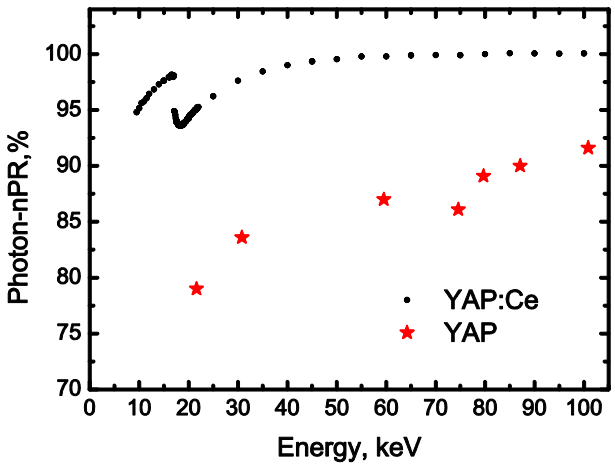


**Fig. 5.4** Photon nonproportional response of YAP scintillators as a function of X-ray or gamma photon energy. YAP:Ce – black dots; pure YAP – red stars [39].

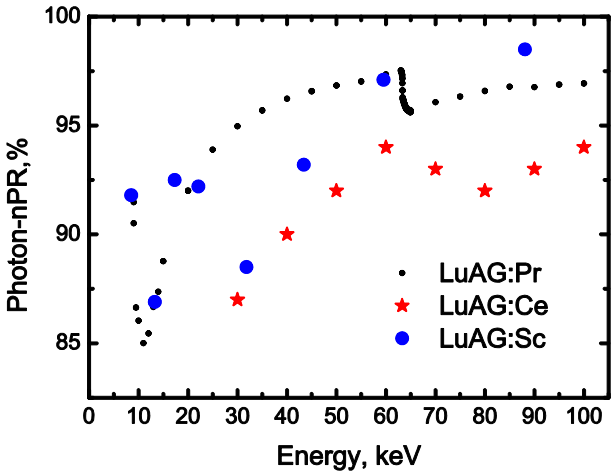


**Fig. 5.5** Photon nonproportional response of LuAG scintillators as a function of X-ray or gamma photon energy. LuAG:Pr – black dots [27]; LuAG:Sc – blue circles [4]; LuAG:Ce – red stars [18].

or activated with different dopants. The most pronounced observation is the improvement of nonproportionality with $Pr^{3+}$ doping in comparison with $Ce^{3+}$ doping for LuAG and YSO. LuAG doped with praseodymium shows lower $\sigma_{photon\text{-}nPR}$ = 1.98% in comparison with the cerium doped material $\sigma_{photon\text{-}nPR}$ = 4.04%. The same was

observed for YSO scintillators: 0.72% and 6.71% for praseodymium and cerium doped, respectively. A relatively good proportionality of YSO:Pr scintillator leads to the fact that even with low light yield 6000 photons/MeV this material shows energy resolution of about 8% at 662 keV.

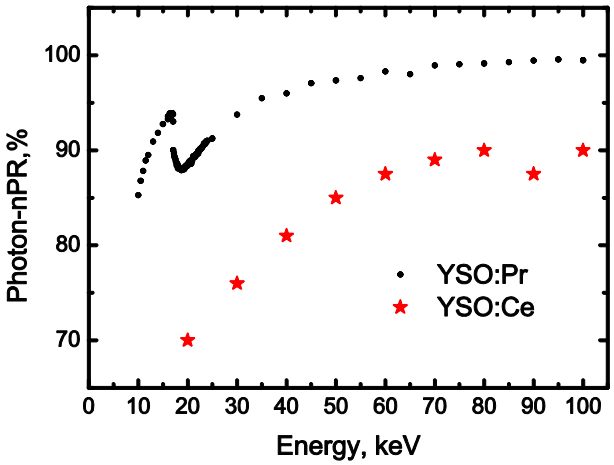


**Fig. 5.6** Photon nonproportional response of YSO scintillators as a function of X-ray or gamma photon energy. YSO:Pr – black dots; YSO:Ce – red stars [40].

Together with the doped scintillator YAP:Ce, Fig. 5.4 shows the photon-nPR curve for undoped YAP [39]. Undoped YAP shows much larger $\sigma_{photon\text{-}nPR}$ = 5.70% then that of Ce-doped material $\sigma_{photon\text{-}nPR}$ = 0.13%. The light yield of the pure material is less than 10% of the light output of YAP:Ce, which leads to a substantial contribution made to the overall energy resolution 13.3% at 662 keV by photo-detector statistics [4].

Figure 5.5 shows the photon-nPR as a function of X-ray or gamma energy for LuAG crystals doped not only with $Ce^{3+}$ and $Pr^{3+}$, but also with $Sc^{3+}$. In the case of Pr-doped scintillator the photon-nPR is more proportional in comparison with LuAG:Ce. The values of the LuAG:Sc photon-nPR with the exception of two values at energies of 30 and 45 keV almost coincide with the numbers of the LuAG:Pr photon-nPR. The most proportional LuAG:Sc with $\sigma_{photon\text{-}nPR}$ = 1.36% and LuAG:Pr with $\sigma_{photon\text{-}nPR}$ = 1.98% have energy resolutions of 6.5% and 4.6% at 662 keV, respectevily, whereas less proportional LuAG:Ce with $\sigma_{photon\text{-}nPR}$ = 4.04% shows energy resolution of 11% at 662 keV.

### *5.4.3 Cation substitution effect*

To improve scintillation properties like afterglow, decay time and light yield, and to improve stability of the crystal during the growth process, fraction of the RE-cations in a material composition can be replaced by RE-cations of lower atomic number. The most widely known and used material of this kind is LYSO:Ce in which about 10% of the lutetium in LSO:Ce is replaced by yttrium. Sometimes in order to improve the scintillation properties of LYSO:Ce co-doping with calcium or magnesium can be used [49]. Another well-known example of a scintillator with mixed RE-cation is LGSO:Ce [38].

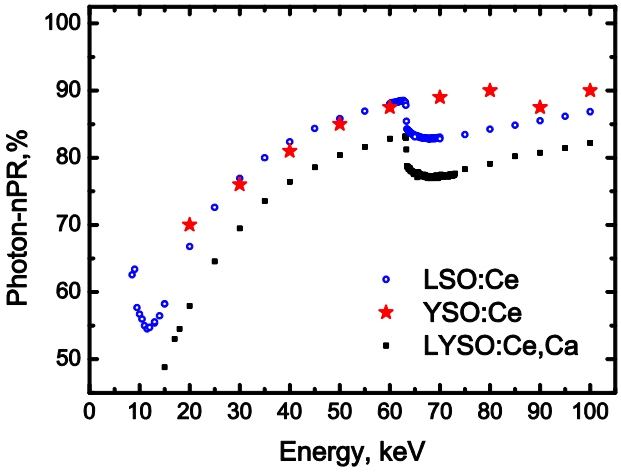


**Fig. 5.7** Photon nonproportional response of Ce-doped oxyorthosilicates as a function of X-ray or gamma photon energy. LSO:Ce – blue open dots; YSO:Ce – red stars [40]; LYSO:Ce,Ca – black squares.

Figure 5.7 compares the LYSO:Ce,Ca photon-nPR with that of LSO:Ce and YSO:Ce. A similar comparison of the LGSO:Ce photon-nPR with that of LSO:Ce and GSO:Ce is shown in Fig. 5.8. The mixed RE-cation compounds, show a high degree of photon-nPR: 11.24% and 12.56% for LYSO:Ce,Ca and LGSO:Ce, respectively. An effect similar to the photon-nPR deterioration for the mixed-cation compounds can be observed for aluminum perovskites, as shown in Fig. 5.9. In this figure, the photon-nPR of LuYAP:Ce is compared with the photon-nPRs of YAP:Ce and LuAP:Ce scintillators. YAP:Ce and LuAP:Ce have low $\sigma_{photon\text{-}nPR}$ = 0.13% and 0.94%, compared with other oxides. Whereas the degree of LuYAP:Ce photon-nPR is 2.77%. Similar to the case of oxyorthosilicates, shown in Figs. 5.7 and 5.8, and similar to the case of

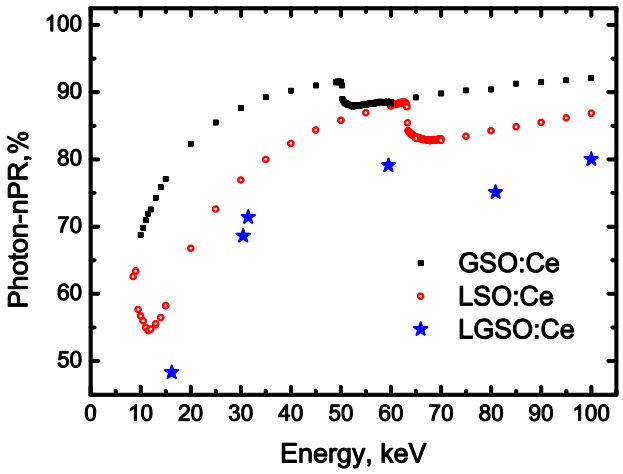


**Fig. 5.8** Photon nonproportional response of Ce-doped oxyorthosilicates as a function of X-ray or gamma photon energy. GSO:Ce – black squares; LSO:Ce – red open dots; LGSO:Ce – blue stars [38].

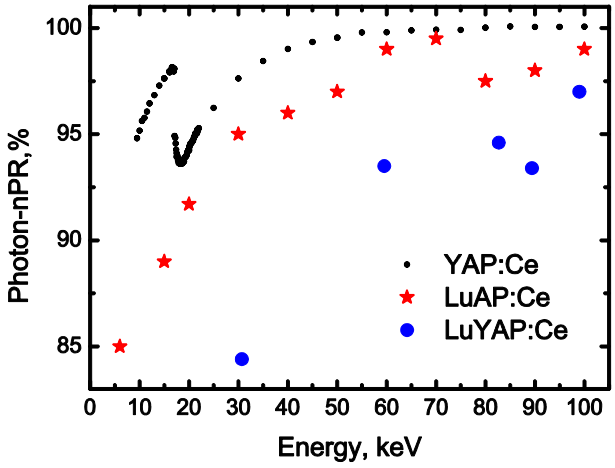


**Fig. 5.9** Photon nonproportional response of Ce-doped aluminum perovskites scintillators as a function of X-ray or gamma photon energy. YAP:Ce – black dots; LuAP:Ce – red stars [13]; LuYAP:Ce – blue circles [31].

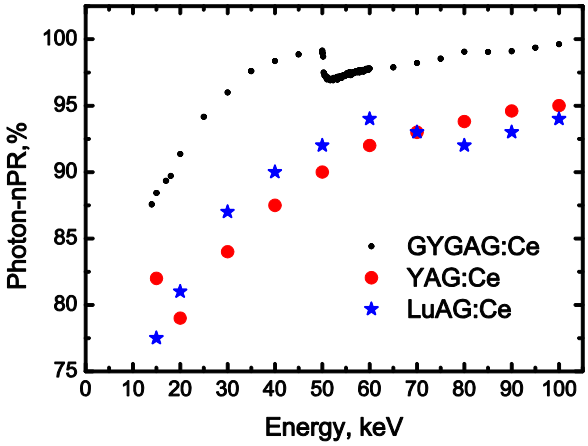


**Fig. 5.10** Photon nonproportional response of Ce-doped aluminum garnets as a function of X-ray or gamma photon energy. GYGAG:Ce – black dots; YAG:Ce – red circles [35]; LuAG:Ce – blue stars [18].

aluminum perovskites, shown in Fig. 5.9, the complete replacement of yttrium or gadolinium for lutetium did not significantly change the degree of photon-nPR. Only a slight improvement of $\sigma_{photon\text{-}nPR}$ can be noticed for GSO:Ce and YAP:Ce.

The opposite to the trend identified for LGSO:Ce, LYSO:Ce,Ca and LuYAP:Ce is observed for the ceramic garnet GYGAG:Ce; a scintillator with mixed gadolinium and yttrium, and mixed gallium and aluminum cations [54]. Figure 5.10 shows the photon-nPR of GYGAG:Ce in comparison with those of YAG:Ce and LuAG:Ce. Ceramic GYGAG:Ce shows low degree of photon-nPR $\sigma_{photon\text{-}nPR}$ = 0.61%, which in combination with a high light output 60000 photons/MeV leads to the energy resolution of about 5% at 662 keV, see Table 5.1. The degree of photon-nPR of YAG:Ce is 3.64% and of LuAG:Ce is 4.04%, both are much higher than that of the ceramic. Direct comparison of the photon-nPR of GYGAG:Ce to the photon-nPR of YAG:Ce or LuAG:Ce is not entirely legitimate, because GYGAG:Ce is a ceramics. Moreover in the paper by Payne et. al [12] materials containing gadolinium are identified as a separate class of materials. The authors motivate this identification, saying that carriers and excitons rapidly transfer their energy through Gd sub-lattice to a cerium ion in materials with gadolinium, and this migration mechanism is more efficient compared to usual migration of carriers and excitons.

### *5.4.4 Other oxides*

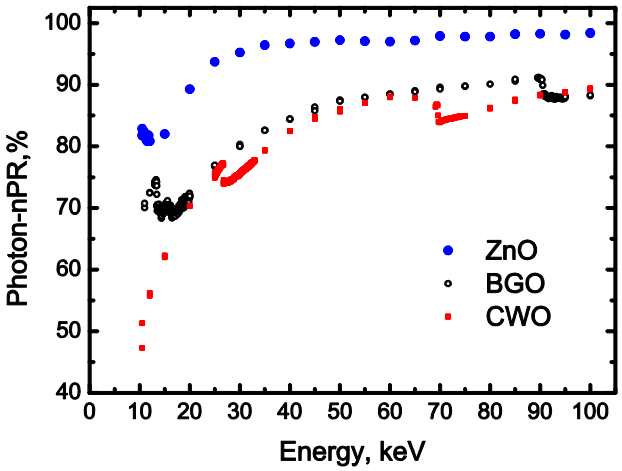


**Fig. 5.11** Photon nonproportional response of oxide scintillators as a function of X-ray or gamma photon energy. ZnO – blue circles [21]; BGO – black open dots; CWO – red squares.

Fig. 5.11 shows the photon-nPR curves for ceramic ZnO, BGO and CWO. ZnO shows the smallest degree of photon-nPR $\sigma_{photon\text{-}nPR}$ = 1.33. The ceramic sample was 1.5 mm thick with a transmittance of about 50% at the maximum of the luminescence wavelength [22]. Synchrotron X-ray excitation was on one side of the sample and the registration of the luminescence on the other [1]. Part of the light, especially at low X-ray energy, can be self-absorbed, which may lead to an increased downturn in the photon-nPR at low excitation energies than in fully transparent ZnO. As shown in Fig. 10 the photon-nPRs of BGO and CWO show similar shape and degree of photon-nPR above 7%. With a light output equal to 8000 photons/MeV for BGO and 15000 photons/MeV for CWO and the observed photon-nPRs, the energy resolution of these materials is about 8% and 7%, respectively.

### *5.4.5 Semiconductor scintillators*

In addition to being an oxide, ZnO is a well-known semiconductor with a band gap of 3.4 eV [23]. Zinc oxide is non-hygroscopic, stable over a wide range of temperatures, mechanically robust, and medium dense 5.61 g/cm$^3$ material. Due to its unique optical, acoustic, and electric properties, zinc oxide finds use in gas sensors varistors, and generators of surface acoustic waves. ZnO single crystals are also used as substrates for obtaining gallium nitride thin films. Recently, powders, films and ceramics of zinc

oxide have been finding use in the scintillation technique [20, 22]. Figure 5.12 shows the photon-nPR of ZnO ceramics compared to the photon-nPR of another semiconductor scintillator ZnSe:Te with an even lower value of the band gap of 2.7 eV. Taking into account the measurement errors, the photon-nPRs of both semiconductor scintillators are approximately equal. The degree of photon-nPR is 1.33% for ZnO and 1.43% for ZnSe:Te The photon-nPRs of studied semiconductor scintillators are not something exceptional compared to other scintillators, mostly insulators.

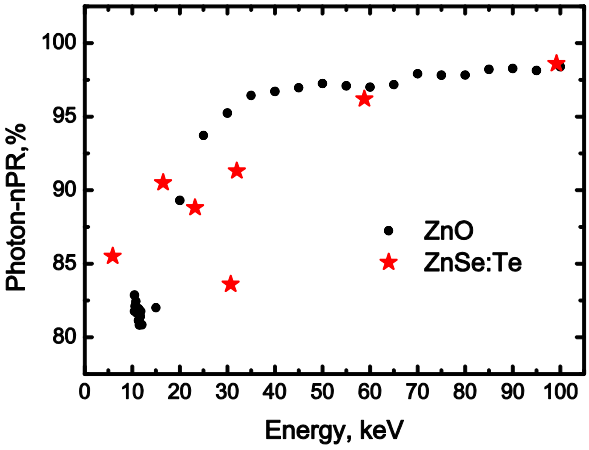


**Fig. 5.12** Photon nonproportional response of semiconductor scintillators as a function of X-ray or gamma photon energy. ZnO – black circles [21]; ZnSe:Te – red stars [26].

## 5.5 Halide scintillators

Halide scintillators play an important role among the presently known scintillation materials. Doped with rare-earth ions $Ce^{3+}$ and $Eu^{2+}$ they are especially important. In this section the effect of anion and cation on the shape and degree of photon-nPR of fluorides, chlorides, bromides and iodides is considered. Also the photon-nPR of pure iodides, iodides doped with $Tl^{+}$, $Na^{2+}$ or $Eu^{2+}$ is compared.

### *5.5.1 Anion effect (F – Cl – Br – I)*

Figure 5.13 shows the photon-nPRs of $SrI_2:Eu^{2+}$, $LaBr_3:Ce^{3+}$, $LaCl_3:Ce^{3+}$, and $CaF_2:Eu^{2+}$. The concentration of $Eu^{2+}$ in $SrI_2$:Eu was 5% [24], while for $LaBr_3$:Ce and $LaCl_3$:Ce the standard commercially available scintillators BrilLanCe 380 and

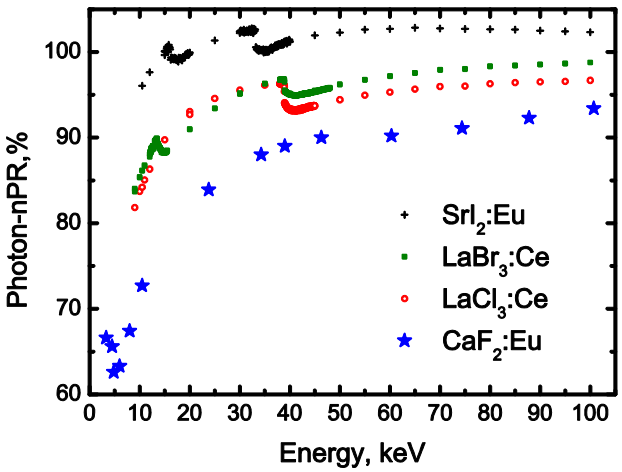


**Fig. 5.13** Photon nonproportional response of halide scintillators as a function of X-ray or gamma photon energy. $SrI_2$:Eu – black crosses [24]; $LaBr_3$:Ce – olive squares [17]; $LaCl_3$:Ce – red open dots [17]; $CaF_2$:Eu – blue stars [37].

BrilLanCe 350 containing 5% and 10% of $Ce^{3+}$ were used. The $CaF_2$:Eu data were taken from the paper by Aitken et. al [37], where the concentration of $Eu^{2+}$ was not specified.

Table 5.1 shows that $LaBr_3$:Ce has the lowest degree of photon-nPR 1.10%. The value of the photon-nPR at 10 keV increases from fluoride to chloride to bromide to iodide. The photon-nPRs of all investigated scintillators were normalized to the corresponding value at 662 keV. If normalization is at a different energy, e.g. at 100keV, $SrI_2$:Eu will show the lowest degree of photon-nPR. In the energy range 10 – 100 keV, the $SrI_2$:Eu photon-nPR is always within 8% from 100%, that is twice smaller than for $LaBr_3$:Ce. Among the scintillators presented in Fig. 5.13, $SrI_2$:Eu is the only material with the photon-nPR values exceeding 100% in the energy range 10- 100 keV.

### *5.5.2 Fluorides*

Comparing the photon-nPR, that we measured for pure $BaF_2$ and the photon-nPR of $CaF_2$:Eu, taken from the reference [37], it can be seen that $BaF_2$ is a more proportional scintillator. $BaF_2$ shows two types of luminescence; the core to valence luminescence (CVL) showing peaks at 195 and 220 nm [55-57] and excitonic luminescence with a broad band peaking around 310 nm. The quantum efficiency of the Hamamatsu R6231-100 PMT that was used is low below 300 nm [58]. Thus Fig. 5.14 shows the photon-nPR mainly for the excitonic luminescence of $BaF_2$.

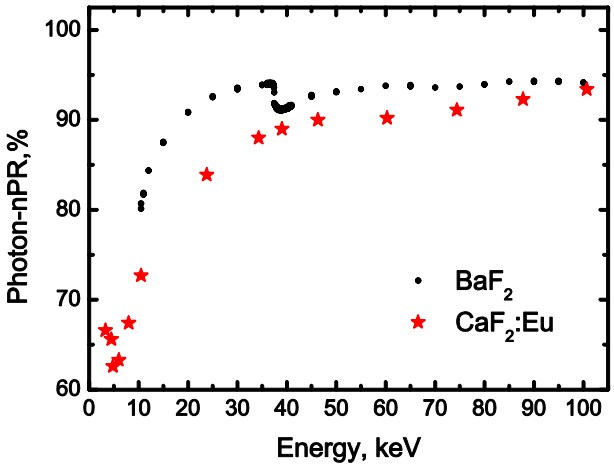


**Fig. 5.14** Photon nonproportional response of fluoride scintillators as a function of X-ray or gamma photon energy. $BaF_2$ – black dots; $CaF_2$:Eu – red stars [37].

### *5.5.3 Chlorides*

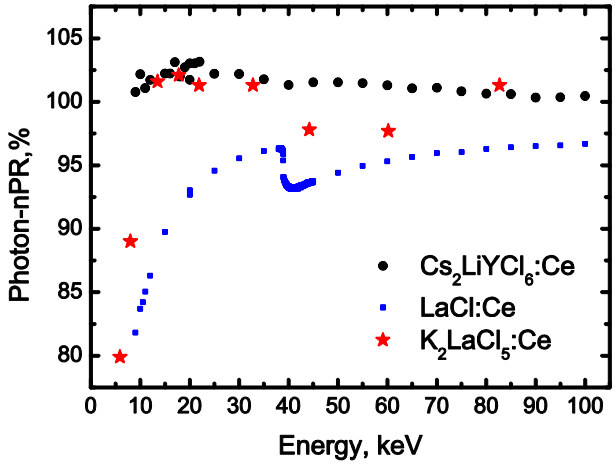


**Fig. 5.15.** Photon nonproportional response of chloride scintillators as a function of X-ray or gamma photon energy. $Cs_2LiYCl_6$:Ce – black dots; $K_2LaCl_5$:Ce – red stars [4]; $LaCl_3$:Ce – blue squares [17].

Fig. 5.15 shows shows photon-nPRs for chloride scintillators. The data on $K_2LaCl_5$:Ce were taken from [4]. CLYC:Ce was studied at the end of 90's [59, 60] and in the early 2000's [8, 61]. It is a very proportional scintillator with small degree of photon-nPR

0.38% making it one of the most proportional scintillators. Only YAP:Ce with $\sigma_{photon\text{-}nPR}$ = 0.13% appears better. $K_2LaCl_5$:Ce also demonstrates small photon-nPR except at low excitation energies of about 6 and 10 keV. However, these data points contain large errors. As for the photon-nPR of $LaCl_3$:Ce, it has the highest $\sigma_{photon\text{-}nPR}$ = 2.16% among the three investigated chlorides.

Nonproportionality is just one of the factors affecting the total energy resolution of a scintillator. So the even less proportional material $LaCl_3$:Ce with higher light yield, shows an energy resolution of 3.1% at 662 keV, while the more proportional materials CLYC:Ce and $K_2LaCl_5$:Ce both show only 5.1% at 662 keV. From the standpoint of the highest possible energy resolution it should always be the optimal combination of low nonproportionality and high light output.

### *5.5.4 Bromides*

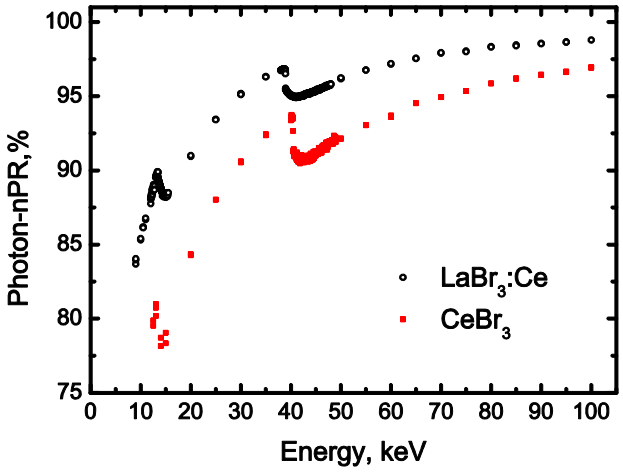


**Fig. 5.16** Photon nonproportional response of bromide scintillators as a function of X-ray or gamma photon energy. $LaBr_3$:Ce – black open dots [17]; $CeBr_3$ – red squares.

Figure 5.16 shows the photon-nPR of $LaBr_3$:Ce and $CeBr_3$ scintillators. $CeBr_3$ shows high light yield, but the 4% energy resolution at 662 keV is worse than that of $LaBr_3$:Ce. As can be seen in Fig. 5.16, poorer energy resolution of $CeBr_3$ can be related to the higher degree of photon-nPR $\sigma_{photon\text{-}nPR}$ = 2.42% as compared with $\sigma_{photon\text{-}nPR}$ = 1.10% of $LaBr_3$:Ce.

### *5.5.5 Iodides*

Figure 5.17 shows photon-nPRs of CsI:Tl, NaI:Tl, $SrI_2$:Eu and $LuI_3$:Ce. The data on the CsI:Na photon-nPR were taken from [37]. The photon-nPR curves in Fig. 5.17 vary a lot. $LuI_3$:Ce has a shape more similar to $LaBr_3$:Ce than to NaI:Tl. $SrI_2$:Eu shows a low degree of photon-nPR, the 1.35%. Its photon-nPR curve runs between that of $LuI_3$:Ce and NaI:Tl. CsI:Tl, NaI:Tl and CsI:Na, show the typical shape of the photon-nPR for iodides [37] with a maximum near 10 - 20 keV.

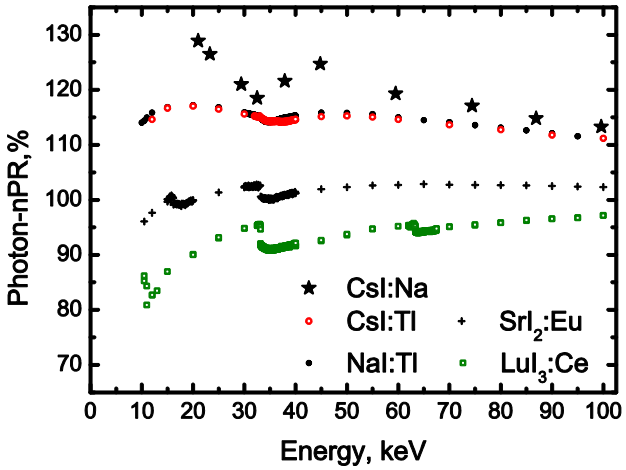


**Fig. 5.17** Photon nonproportional response of iodide scintillators as a function of X-ray or gamma photon energy. CsI:Na – black stars [37]; NaI:Tl – black dots [1]; CsI:Tl – red open dots; $SrI_2$:Eu – black crosses [24]; $LuI_3$:Ce – olive open squares [7, 17].

Figure 5.18 compares the photon-nPRs for pure $SrI_2$ and NaI, with that of $SrI_2$:Eu and NaI:Tl at room temperature. For $SrI_2$ the change of the photon-nPR with the introduction of $Eu^{2+}$ is relatively small. As seen in Table 5.1, doping by $Eu^{2+}$ substantially increases the light output of $SrI_2$, but the degree of photon-nPR is only slightly reduced from 1.61% to 1.34%. For NaI the photon-nPR improves considerably by doping with $Tl^+$. Figure 16 shows that the value of the photon-nPR of pure NaI reaches 170% at 17 keV X-ray energy. In fact, this means that the energy conversion efficiency of 17 keV X-ray or gamma radiation into the optical photons is 1.7 times higher than that of 662 keV. This leads to the largest degree of photon-nPR, 18.14%, among all the scintillators considered in this paper. The large degree of photon-nPR of pure NaI, combined with low light yield leads to an energy resolution of 16.2 – 18.1% at 662 keV [50].

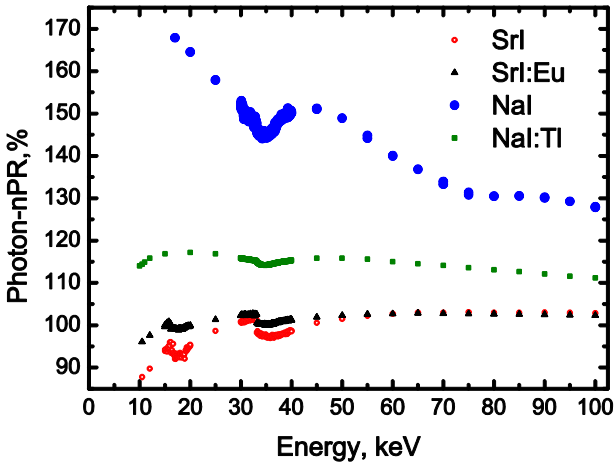


**Fig. 5.18** Photon nonproportional response of iodde scintillators as a function of X-ray or gamma photon energy. NaI – blue ciricles; NaI:Tl – olive squares [1]; $SrI_2$:Eu – black triangles [24]; $SrI_2$ – red open dots [24].

## 5.6 Discussion

Several models were proposed to explain the origin of nonproportionality and the shape of the photon- and electron-nPR curves [12, 62-65]. In all those models, the cause of nonproportionality is a high concentration of charge carriers resulting from the interaction of ionizing radiation with a scintillator material. According to the Bethe equation, with decrease in the energy of the primary electron, the ionization density (*dE/dx*) along the track grows [66]. This leads to larger radiationless electron hole recombination rate which forms the basis of increasing nonproportionality with smaller X-ray or gamma-ray energy. This increase can be clearly observed for the scintillators investigated in this study by the downward curvature of the photon-nPR curves when going to smaller energy. Exceptions are CLYC:Ce shown in Fig. 5.15, CsI:Na shown in Fig. 5.17, and NaI shown in Fig. 5.18. Probably their nonproportionality curve does not differ fundamentally from that of the others; the only difference is that the dropping of the photon-nPR starts at X-ray energy below 10 keV that is out of the scope of our experiments. The models presented use slightly different arguments to explain the degree of photon- or electron-nPR. A comprehensive overview of the currently available models and ideas was presented by Moses et. al [67]. The basis of all those models is the competition between two opposing processes: 1) quenching due to

radiationless electron hole recombination inside the volume of high ionization density along the track, and 2) diffusion of the charge carriers from the point of creation towards a volume of lower ionization density. The faster the charge carriers escape the volume of high ionization density in which quenching occurs, the higher the probability of converting the energy of the carriers into optical photons. An important factor determining the rate at which carriers leave this volume is the carrier diffusion coefficient [65, 68, 69]. A high diffusion coefficient contributes to a more rapid transport of electrons, holes and excitons to regions further from the track where the radiationless recombination rate does not depend on ionization density.

According to the diffusion equation [70]:

$$\frac{\partial n(r,t)}{\partial t} = \nabla\left[ D(n)\nabla n(r,t)\right], \qquad (5.2)$$

where $n$ is the concentration of charge carriers, $r$ is the radial coordinate perpendicular to the ionization track, $t$ is the time and $D$ is the diffusion coefficient. Assuming that in the high ionization density volume the diffusion coefficient is independent of concentration: $D(n) = const$ [71], and using the Einstein relation $D = \mu \cdot kT$, one obtains

$$\left.\frac{\partial n(r,t)}{\partial t}\right|_{diffusion} = \mu \cdot kT \cdot \nabla^2 n(r,t), \qquad (5.3)$$

where $\mu$ is the mobility of carriers, $k$ is the Boltzmann constant, $T$ is the effective temperature of the carriers and $e$ is the elementary charge.

Based on Eq. (5.3), the transport of the charge carriers is faster when mobility and temperature increases. Hence, the photon-nPR is expected to depend on carrier mobility and temperature. Such dependence on temperature was indeed observed for $LaBr_3$:Ce [72] and Chapter 6 and $SrI_2$:Eu [24].

According to theory [71, 73], the mobility for thermalized carriers in wide band gap semiconductors is determined by lattice scattering and impurity scattering. The mobility determined by the lattice scattering mechanism $\mu_L$ is given by:

$$\mu_L = \frac{e}{2\alpha\omega_0 m^*}\left( \exp\left( \frac{\hbar\omega_0}{kT} \right) - 1 \right), \qquad (5.4)$$

$$\alpha = \left( \frac{1}{\varepsilon_\infty} - \frac{1}{\varepsilon} \right)\sqrt{\frac{m^* E_H}{m_e \hbar\omega_0}}$$

where $\alpha$ is the polaron coupling constant, $\omega_0$ is the longitudinal optical phonon

frequency, $m^*$ is the effective mass of the carriers – holes or electrons, $\hbar$ is the reduced Planck constant, $m_e$ is the rest mass of the electron, $E_H$ is the first ionization energy of the hydrogen atom (13.595 eV), $\varepsilon_\infty$ and $\varepsilon$ are the high frequency and the static dielectric permittivity constants [71]. In turn, the mobility determined by the impurity scattering mechanism $\mu_I$ is given by:

$$\mu_I = \frac{2^{7/2}\left(\varepsilon\varepsilon_0\right)^2\left(kT\right)^{3/2}}{\pi^{3/2}z^2e^3\left(m^*\right)^{1/2}N_i}\cdot F\left(3kT\right), \qquad (5.5)$$

where $z$ is the effective charge of the impurity with concentration $N_i$ and $\varepsilon_0$ is the vacuum permittivity and *F(3kT)* is the averaged Coulomb screening factor [73].

Equations (5.4) and (5.5) are valid for thermalized carriers in wide band gap semiconductors. In the case of charge carrier transfer from the primary track to the luminescence centers in scintillators, the picture can be different. For example it is not clear if we can speak about thermalized carriers or if extra kinetic energy should be taken into account. Anyway, in both the lattice scattering mechanism Eq. (5.4) and the impurity scattering mechanism Eq. (5.5) the carrier mobility increases with increasing value of the high frequency or static dielectric permittivities of the material. Unfortunately, the dielectric permittivities are not known for all scintillators discussed in this paper. However the refractive index is well known for the scintillators. Refractive indexes are listed in Table I. The high frequency refractive index is related to the dielectric permittivity as

$$n = \sqrt{\varepsilon_r\mu_r}, \qquad (5.6)$$

where the relative permittivity is given by $\varepsilon_r = \frac{\varepsilon(\omega)}{\varepsilon_0}$ and $\mu_r$ is the relative permeability. For the majority of scintillators $\mu_r \approx 1$ ; and, consequently, $n^2 \sim \varepsilon(\omega)$ . For higher values of the refractive index there is a higher dielectric permittivity and, consequently, a higher carrier mobility, faster diffusion of carriers from the high ionization density volume of the track, lower radiationless electron hole recombination and as a result a better proportionality. Figure 5.19 shows the degree of photon-nPR versus the refractive index of the Ce-doped RE oxides from Table 5.2 and Figs. 5.1, 5.2. With increasing refractive index the degree of photon-nPR is decreasing. A similar dependence is observed for halide scintillators, shown in Fig. 5.20.

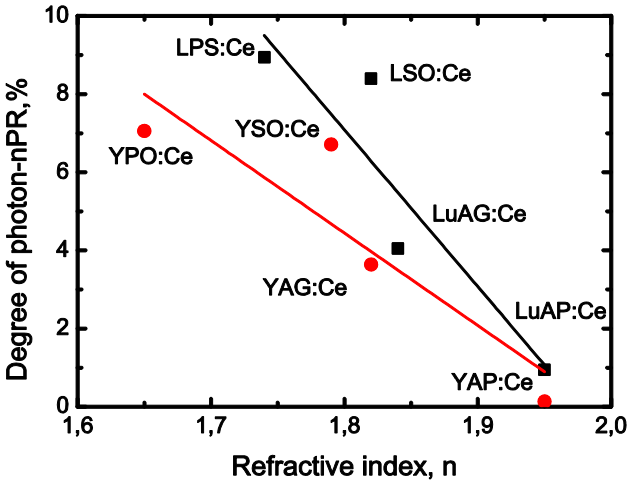


**Fig. 5.19** Degree of photon-nPR as a function of refractive index of the oxides. Solid lines – linear approximation.

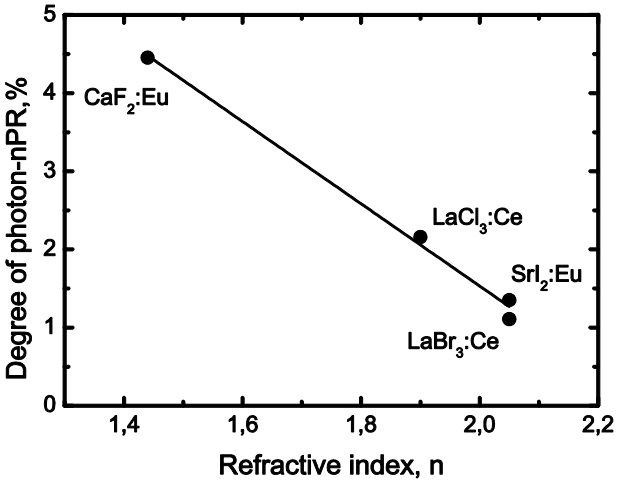


**Fig. 5.20** Degree of photon-nPR as a function of refractive index of the halides. Solid line – linear approximation.

Figure 5.19 shows that dependence of the photon-nPR degree on the refractive index is less steep for the Y-based complex oxide scintillators compared to the Lu-based scintillators. This can be interpreted as a lower ionization density due to longer ionization track in Y-based scintillators. The average length of the ionization tracks at equal energy of the incident X-ray or gamma photon is inverse proportional to the

density of the compound and its effective atomic number. The longer the ionization track the lower the high ionization density volume. This leads to a decrease in the radiationless electron hole recombination and reduced degree of photon-nPR.

The high frequency dielectric permittivity and hence the refractive index are determined by how strongly valence electrons are bonded to atoms in a scintillator material. The lower the bonding energy of the electrons, the higher the dielectric permittivity and the refractive index and thus the lower the degree of photon-nPR. This rule is not absolute, and as can be seen from Table 5.1 and Fig. 5.10, some oxide scintillators with high refractive index show a relatively high degree of photon-nPR, e.g. BGO $\sigma_{photon\text{-}nPR}$ = 7.15% and CWO $\sigma_{photon\text{-}nPR}$ = 7.15%. However, when considering the general patterns of nonproportionality attention should be paid to the refractive index, dielectric constant, carriers mobility and bonding energy of the valence electrons.

The high frequency dielectric constant and the refractive index depend on the electrons in the compound. The larger the concentration of electrons and the weaker they are bonded the larger the refractive index tends to be. The weaker bonded electrons are the valence band electrons and they contribute most to the refractive index. Within the halides the valence band electrons bonding decreases in the sequence fluorides-chlorides-bromides-iodides, and within the oxides bonding depends on the cations like P, S, Si, Al that bind the oxygen ligands. Since a relationship exists between valence band electron binding and bandgap one, the refractive index tends to increase with smaller bandgap.

According to [52] the nonproportionality is influenced not only by the mobility of electrons but also by the mobility of holes. Hole mobility is related to the width of the valence band that tends to increase from fluorides to chlorides to bromides and to iodides [74]. At the higher width of the valence band the probability for hole to be trapped is lower, thus the probability of radiative recombination is higher. In the sequence fluorides-chlorides-bromides-iodides the width of the band gap on average decreases, while the width of the valence band increases, thereby resulting in higher hole mobility and better proportionality. So in Fig. 5.20 decrease of $\sigma_{photon\text{-}nPR}$ is explained not only by increasing refractive index, but also by increasing width of the valence band.

## 5.7 Conclusion

Complex oxides show a decrease in the degree of photon-nPR in the sequence $RE_2Si_2O_7$:Ce – $REPO_4$:Ce – $RE_2SiO_5$:Ce – $RE_3Al_5O_{12}$:Ce – $REAlO_3$:Ce, where RE is

Y or Lu. The decrease of the photon-nPR degree is correlated with an increase in the refractive index of the compounds. Refractive index is related to dielectric constant, carrier mobility and bonding energy of electrons. A decrease in the degree of photon-nPR similar to the complex oxides was observed for the halide scintillators with the anion replacement: fluoride to chloride to bromide and to iodide. In some materials the dopant has influence on the shape and degree of the photon-nPR. So for LuAG and YSO hosts a decrease in the degree of photon-nPR was observed after doping with $Pr^{3+}$ compared to doping with $Ce^{3+}$. Full or partial replacement of the RE-cation in the complex oxides does not lead to a significant decrease in the degree of photon-nPR. In most cases oxides with a mixed type of RE-cation, e.g. LYSO:Ce, LGSO:Ce or LuYAP:Ce show a higher degree of photon-nPR. The semiconductor scintillators ZnO, ZnSe:Te did not show photon-nPRs significantly different from the photon-nPRs of other scintillators, mostly insulators. An important factor in the halides nonproportionality is the width of the valence band. As the width of the valence band increases from fluorides to chlorides, to bromides and to iodides, a higher value for the photon-nPR at 10 keV is observed.

**Acknowledgement**

We thank the scientists and technicians of the X-1 beamline at the Hamburger Synhrotronstrahlungslabor (HASY-LAB) synchrotron radiation facilities for their assistance. Also we want to express our gratitude to our colleagues Mikhail Alekhin, Francesco Quarati and Johan de Haas who have made a significant contribution to the experimental activities and data analysis. We would like to thank Alan Owens from the European Space Agency for sharing with us some of the beamtime at X-1, Vladimir Ouspenski from Saint-Gobain Crystals for the LYSO, $LaBr_3$, $LaCl_3$ and NaI crystals, Karl Kramer from University of Bern for $SrI_2$ crystals, Piotr Rodnyi from St. Petersburg State Politechnical University and Elena Gorokhova from the Scientific Research and Technological Institute of Optical Material Science for the ZnO ceramics, and Paul Schotanus from SCIONIX Holland B.V. for the $CeBr_3$ crystal.

**References**

[1] I. V. Khodyuk, P. A. Rodnyi, and P. Dorenbos, "Nonproportional scintillation response of NaI:Tl to low energy x-ray photons and electrons," *J. Appl. Phys.*, vol. 107, p. 113513, Jun 2010.

[2] A. Owens, "Synchrotron light sources and radiation detector metrology," *Nucl. Instr. and Meth. A*, 2012.

[3] J. T. M. de Haas and P. Dorenbos, "Advances in Yield Calibration of Scintillators," *IEEE Trans. Nucl. Sci.*, vol. 55, pp. 1086-1092, 2008.

[4] P. Dorenbos, J. T. M. de Haas, and C. W. E. van Eijk, "Non-Proportionality in the Scintillation Response and the Energy Resolution Obtainable with Scintillation Crystals," *IEEE Trans. Nucl. Sci.*, vol. 42, pp. 2190-2202, 1995.

[5] I. V. Khodyuk, P. A. Rodnyi, and P. Dorenbos, "Energy dependence of the relative light output of $YAlO_3$:Ce, $Y_2SiO_5$:Ce and $YPO_4$:Ce scintillators," *Instruments and Experimental Techniques*, vol. 55, pp. 187-197, 2012.

[6] M. Moszyn´ski, M. Kapusta, D. Wolski, W. Klamra, and B. Cederwall, "Properties of the YAP:Ce scintillator," *Nucl. Instr. and Meth. A*, vol. 404, pp. 157-165, 1998.

[7] M. Nikl, J. A. Mares, A. Vedda, M. Fasoli, V. Laguta, E. Mihokova, J. Pejchal, M. Zhuravleva, A. Yoshikawa, and K. Nejezchleb, "Can Pr-Doped YAP Scintillator Perform Better?," *IEEE Trans. Nucl. Sci.*, vol. 57, pp. 1168-1174, 2010.

[8] A. Bessiere, P. Dorenbos, C. W. E. van Eijk, K. W. Kramer, and H. U. Gudel, "New thermal neutron scintillators: $Cs_2LiYCl_6:Ce^{3+}$ and $Cs_2LiYBr_6:Ce^{3+}$," *IEEE Trans. Nucl. Sci.*, vol. 51, pp. 2970-2972, 2004.

[9] J. Glodo, E. van Loef, R. Hawrami, W. H. Higgins, A. Churilov, U. Shirwadkar, and K. S. Shah, "Selected Properties of Scintillators," *IEEE Trans. Nucl. Sci.*, vol. 58, pp. 333-338, 2011.

[10] J. Glodo, W. M. Higgins, E. V. D. van Loef, and K. S. Shah, "Scintillation Properties of 1 Inch  Crystals," *IEEE Trans. Nucl. Sci.*, vol. 55, pp. 1206-1209, 2008.

[11] E. V. D. van Loef, P. Dorenbos, C. W. E. van Eijk, K. W. Kramer, and H. U. Gudel, "Scintillation properties of $K_2LaX_5:Ce^{3+}$ (X=Cl, Br, I)," *Nucl. Instr. and Meth. A*, vol. 537, pp. 232-236, 2005.

[12] S. A. Payne, W. W. Moses, S. Sheets, L. Ahle, N. J. Cherepy, B. Sturm, S. Dazeley, G. Bizarri, and C. Woon-Seng, "Nonproportionality of Scintillator Detectors: Theory and Experiment. II," *IEEE Trans. Nucl. Sci.*, vol. 58, pp. 3392-3402, 2011.

[13] M. Balcerzyk, M. Moszynski, Z. Galazka, M. Kapusta, A. Syntfeld, and J. L. Lefaucheur, "Perspectives for high resolution and high light output LuAP:Ce crystals," in *Nuclear Science Symposium Conference Record, 2004 IEEE*, 2004, pp. 986-992.

[14] J. Trummer, E. Auffray, P. Lecoq, A. Petrosyan, and P. Sempere-Roldan, "Comparison of LuAP and LuYAP crystal properties from statistically significant batches produced with two different growth methods," *Nucl. Instr. and Meth. A*, vol. 551, pp. 339-351, 2005.

[15] A. G. Petrosyan, M. Derdzyan, K. Ovanesyan, G. Shirinyan, P. Lecoq, E. Auffray, M. Kronberger, B. Frisch, C. Pedrini, and C. Dujardin, "Comparison of Spectral and Scintillation Properties of LuAP:Ce and LuAP:Ce,Sc Single Crystals," *IEEE Trans. Nucl. Sci.*, vol. 56, pp. 2574-2579, 2009.

[16] A. Owens, A. J. J. Bos, S. Brandenburg, P. Dorenbos, W. Drozdowski, R. W. Ostendorf, F. Quarati, A. Webb, and E. Welter, "The hard X-ray response of

Ce-doped lanthanum halide scintillators," *Nucl. Instr. and Meth. A*, vol. 574, pp. 158-162, 2007.

[17] I. V. Khodyuk and P. Dorenbos, "Nonproportional response of $LaBr_3$:Ce and $LaCl_3$:Ce scintillators to synchrotron x-ray irradiation," *J. Phys. Condens. Matter*, vol. 22, p. 485402, Dec 2010.

[18] L. Swiderski, M. Moszynski, A. Nassalski, A. Syntfeld-Kazuch, T. Szczesniak, K. Kamada, K. Tsutsumi, Y. Usuki, T. Yanagida, A. Yoshikawa, W. Chewpraditkul, and M. Pomorski, "Scintillation Properties of Praseodymium Doped LuAG Scintillator Compared to Cerium Doped LuAG, LSO and $LaBr_3$," *IEEE Trans. Nucl. Sci.*, vol. 56, pp. 2499-2505, 2009.

[19] F. Quarati, A. J. J. Bos, S. Brandenburg, C. Dathy, P. Dorenbos, S. Kraft, R. W. Ostendorf, V. Ouspenski, and A. Owens, "X-ray and gamma-ray response of a $LaBr_3$:Ce scintillation detector," *Nucl. Instr. and Meth. A*, vol. 574, pp. 115-120, 2007.

[20] P. A. Rodnyi, I. V. Khodyuk, and E. I. Gorokhova, "Integral, Absolute, and Relative Light Yield of ZnO-Based Ceramics," *Tech. Phys. Lett.*, vol. 36, pp. 714-716, 2010.

[21] I. V. Khodyuk, P. A. Rodnyi, and E. I. Gorokhova, "Scintillation properties of Zinc oxide based optical ceramics," *NAUCH TEKHN VED SPBG*, vol. 109, pp. 28-38, 2010.

[22] V. A. Demidenko, E. I. Gorokhova, I. V. Khodyuk, O. A. Khristicha, S. B. Mikhrin, and P. A. Rodnyi, "Scintillation properties of ceramics based on zinc oxide," *Radiation Measurements*, vol. 42, pp. 549-552, Apr-May 2007.

[23] P. Rodnyi and I. Khodyuk, "Optical and luminescence properties of zinc oxide (Review)," *Optics and Spectroscopy*, vol. 111, pp. 776-785, 2011.

[24] M. S. Alekhin, I. V. Khodyuk, J. T. M. De Haas, and P. Dorenbos, "Non-proportional response and energy resolution of pure $SrI_2$ and $SrI_2$:5%Eu scintillators," *IEEE Trans. Nucl. Sci.*, vol. 59, 2012.

[25] M. S. Alekhin, J. T. M. de Haas, K. W. Kramer, I. V. Khodyuk, L. de Vries, and P. Dorenbos, "Scintillation properties and self absorption in $SrI_2:Eu^{2+}$," in *Nuclear Science Symposium Conference Record (NSS/MIC), 2010 IEEE*, 2011, pp. 1589-1599.

[26] M. Balcerzyk, W. Klamra, M. Moszynski, M. Kapusta, and M. Szawlowski, "Energy resolution and light yield non-proportionality of ZnSe:Te scintillator studied by large area avalanche photodiodes and photomultipliers," *Nucl. Instr. and Meth. A*, vol. 482, pp. 720-727, 2002.

[27] I. V. Khodyuk, J. T. M. de Haas, and P. Dorenbos, "Nonproportional Response Between 0.1-100 keV Energy by Means of Highly Monochromatic Synchrotron X-Rays," *IEEE Trans. Nucl. Sci.*, vol. 57, pp. 1175-1181, Jun 2010.

[28] M. D. Birowosuto, P. Dorenbos, C. W. E. van Eijk, K. W. Kramer, and H. U. Gudel, "High-light-output scintillator for photodiode readout: $LuI_3:Ce^{3+}$," *J. Appl. Phys.*, vol. 99, pp. 123520-123520-4, 2006.

[29] E. V. D. van Loef, W. Mengesha, J. D. Valentine, P. Dorenbos, and C. W. E. van Eijk, "Nonproportionality and energy resolution of a $LaCl_3$:10% $Ce^{3+}$ scintillation crystal," *IEEE Trans. Nucl. Sci.*, vol. 50, pp. 155-158, 2003.

[30] K. S. Shah, J. Glodo, W. Higgins, E. V. D. van Loef, W. W. Moses, S. E. Derenzo, and M. J. Weber, "$CeBr_3$ scintillators for gamma-ray spectroscopy," *IEEE Trans. Nucl. Sci.*, vol. 52, pp. 3157-3159, 2005.

[31] C. Kuntner, E. Auffray, P. Lecoq, C. Pizzolotto, and M. Schneegans, "Intrinsic energy resolution and light output of the $Lu_{0.7}Y_{0.3}$AP:Ce scintillator," *Nucl. Instr. and Meth. A*, vol. 493, pp. 131-136, 2002.

[32] A. Baberdin, A. Dutova, A. Fedorov, M. Korzhik, V. Ligoun, O. Missevitch, V. Kazak, A. Vinokurov, and S. Zagumenov, "(Lu-Y)$AlO_3$:Ce Scintillator for Well Logging," *IEEE Trans. Nucl. Sci.*, vol. 55, pp. 1170-1173, 2008.

[33] P. A. Rodnyi, "Core-valence luminescence in scintillators," *Radiation Measurements*, vol. 38, pp. 343-352, 2004.

[34] P. A. Rodnyi, S. D. Gain, I. A. Mironov, E. A. Garibin, A. A. Demidenko, D. M. Seliverstov, Y. I. Gusev, P. P. Fedorov, and S. V. Kuznetsov, "Spectral-kinetic characteristics of crystals and nanoceramics based on $BaF_2$ and $BaF_2$: Ce," *Phys. Solid State*, vol. 52, pp. 1910-1914, 2010.

[35] W. Chewpraditkul, L. Swiderski, M. Moszynski, T. Szczesniak, A. Syntfeld-Kazuch, C. Wanarak, and P. Limsuwan, "Scintillation Properties of LuAG:Ce, YAG:Ce and LYSO:Ce Crystals for Gamma-Ray Detection," *IEEE Trans. Nucl. Sci.*, vol. 56, pp. 3800-3805, 2009.

[36] F. A. Selim, D. Solodovnikov, M. H. Weber, and K. G. Lynn, "Identification of defects in $Y_3Al_5O_{12}$ crystals by positron annihilation spectroscopy," *Applied Physics Letters*, vol. 91, pp. 104105-3, 2007.

[37] D. W. Aitken, B. L. Beron, G. Yenicay, and H. R. Zulliger, "The Fluorescent Response of NaI(Tl), CsI(Tl), CsI(Na) and $CaF_2$(Eu) to X-Rays and Low Energy Gamma Rays," *IEEE Trans. Nucl. Sci.*, vol. 14, pp. 468-477, 1967.

[38] M. Balcerzyk, M. Moszynski, M. Kapusta, D. Wolski, J. Pawelke, and C. L. Melcher, "YSO, LSO, GSO and LGSO. A Study of Energy Resolution and Nonproportionality," *IEEE Trans. Nucl. Sci.*, vol. 47, pp. 1319-1323, 2000.

[39] W. Klamra, M. Balcerzyk, W. Czarnacki, V. Kozlov, and M. Moszynski, "Light yield non-proportionality of undoped YAP scintillator " *Journal of Instrumentation*, vol. 4, p. P05006, 2009.

[40] P. A. Cutler, C. L. Melcher, M. A. Spurrier, P. Szupryczynski, and L. A. A. Eriksson, "Scintillation Non-Proportionality of Lutetiumand Yttrium-Based Silicates and Aluminates," *IEEE Trans. Nucl. Sci.*, vol. 56, pp. 915-919, 2009.

[41] W. Mengesha, T. D. Taulbee, B. D. Rooney, and J. D. Valentine, "Light yield nonproportionality of CsI(Tl), CsI(Na), and YAP," *IEEE Trans. Nucl. Sci.*, vol. 45, pp. 456-461, 1998.

[42] M. Moszyn'ski, A. Nassalski, A. Syntfeld-Kaz'uch, T. Szczes'niak, W. Czarnacki, D. Wolski, G. Pausch, and J. Stein, "Temperature dependences of $LaBr_3$(Ce), $LaCl_3$(Ce) and NaI(Tl) scintillators," *Nucl. Instr. and Meth. A*, vol. 568, pp. 739–751, 2006.

[43] V. Nagirnyi, S. Dolgov, R. Grigonis, M. Kirm, L. L. Nagornaya, F. Savikhin, V. Sirutkaitis, S. Vielhauer, and A. Vasil'ev, "Exciton-Exciton Interaction in $CdWO_4$ Under Resonant Excitation by Intense Femtosecond Laser Pulses," *IEEE Trans. Nucl. Sci.*, vol. 57, pp. 1182-1186, Jun 2010.

[44] R. F. Lang, G. Angloher, M. M. Bauer, I. Bavykina, and A. Bento, "Scintillator Non-Proportionality and Gamma Quenching in $CaWO_4$," vol. arXiv:0910.4414v1, 2009.

[45] M. Moszynski, M. Balcerzyk, W. Czarnacki, M. Kapusta, W. Klamra, A. Syntfeld, and M. Szawlowski, "Intrinsic energy resolution and light yield nonproportionality of BGO," *IEEE Trans. Nucl. Sci.*, vol. 51, pp. 1074-1079, 2004.

[46] T. D. Taulbee, B. D. Rooney, W. Mengesha, and J. D. Valentine, "The measured electron response nonproportionalities of $CaF_2$, BGO, and LSO," *IEEE Trans. Nucl. Sci.*, vol. 44, pp. 489-493, 1997.

[47] M. Kapusta, P. Szupryczynski, C. L. Melcher, M. Moszynski, M. Balcerzyk, A. A. Carey, W. Czarnacki, M. A. Spurrier, and A. Syntfeld, "Non-Proportionality and Thermoluminescence of LSO:Ce," *IEEE Trans. Nucl. Sci.*, vol. 52, pp. 1098-1104, 2005.

[48] D. Pauwels, N. Le Masson, B. Vianna, A. Kahn-Harari, E. V. D. van Loef, P. Dorenbos, and C. W. E. van Eijk, "A novel inorganic scintillator: $Lu_2Si_2O_7:Ce^{3+}$ (LPS)," in *Nuclear Science Symposium, 1999. Conference Record. 1999 IEEE*, 1999, pp. 102-105.

[49] S. Blahuta, A. Bessiere, B. Viana, V. Ouspenski, E. Mattmann, J. Lejay, and D. Gourier, "Defects Identification and Effects of Annealing on $Lu_{2(1-x)}Y_{2x}SiO_5$ (LYSO) Single Crystals for Scintillation Application," *Materials*, vol. 4, pp. 1224-1237, Jul 2011.

[50] M. Moszynski, W. Czarnacki, A. Syntfeld-Kazuch, A. Nassalski, T. Szczesniak, L. Swiderski, F. Kniest, and A. Iltis, "A Comparative Study of Undoped NaI Scintillators With Different Purity," *IEEE Trans. Nucl. Sci.*, vol. 56, pp. 1655-1660, 2009.

[51] P. Dorenbos, "Light output and energy resolution of $Ce^{3+}$-doped scintillators," *Nucl. Instr. and Meth. A*, vol. 486, pp. 208-213, 2002.

[52] W. Setyawan, R. M. Gaume, R. S. Feigelson, and S. Curtarolo, "Comparative Study of Nonproportionality and Electronic Band Structures Features in Scintillator Materials," *IEEE Trans. Nucl. Sci.*, vol. 56, pp. 2989-2996, 2009.

[53] P. A. Rodnyi, P. Dorenbos, and C. W. E. van Eijk, "Energy Loss in Inorganic ScintiNators," *Phys. Statatus Solidi B*, vol. 187, pp. 15-29, 1995.

[54] N. J. Cherepy, S. A. Payne, B. W. Sturm, J. D. Kuntz, Z. M. Seeley, B. L. Rupert, R. D. Sanner, O. B. Drury, T. A. Hurst, S. E. Fisher, M. Groza, L. Matei, A. Burger, R. Hawrami, K. S. Shah, and L. A. Boatner, "Comparative gamma spectroscopy with $SrI_2$(Eu), GYGAG(Ce) and Bi-loaded plastic scintillators," in *Nuclear Science Symposium Conference Record (NSS/MIC), 2010 IEEE*, 2011, pp. 1288-1291.

[55] N. N. Ershov, N. G. Zakharov, and P. A. Rodnyi, "Spectral-Kinetic Study of Intrinsic Luminescence Characteristics for a Fluorite-Type Crystal," *Optika I Spektroskopiya*, vol. 53, pp. 89-93, 1982.

[56] P. A. Rodnyi, M. A. Terekhin, and E. N. Melchakov, "Radiative Core-Valence Transitions in Barium-Based Fluorides," *Journal of Luminescence*, vol. 47, pp. 281-284, Mar-Apr 1991.

[57] Y. M. Aleksandrov, V. N. Makhov, P. A. Rodnyi, T. I. Syreishchikova, and M. N. Yakimenko, "Intrinsic Luminescence of $Baf_2$ at Pulsed Synchrotron Radiation Excitation," *Fizika Tverdogo Tela*, vol. 26, pp. 2865-2867, 1984.

[58] J. T. M. de Haas and P. Dorenbos, "Methods for accurate measurement of the response of photomultiplier tubes and intensity of light pulses," *IEEE Trans. Nucl. Sci.*, vol. 58, pp. 1290-1296, 2011.

[59] J. C. van't Spijker, P. Dorenbos, C. W. E. van Eijk, M. S. Wickleder, H. U. Gudel, and P. A. Rodnyi, "Scintillation properties of some Ce doped chloride elpasolites," *Journal of Luminescence*, vol. 72-74, pp. 786-788, 1997.

[60] C. M. Combes, P. Dorenbos, C. W. E. van Eijk, K. W. Kramer, and H. U. Gudel, "Optical and scintillation properties of pure and $Ce^{3+}$-doped $Cs_2LiYCl_6$ and $Li_3YCl_6$ crystals," *Journal of Luminescence*, vol. 82, pp. 299-305, 1999.

[61] A. Bessiere, P. Dorenbos, C. W. E. van Eijk, K. W. Kramer, and H. U. Gudel, "Luminescence and scintillation properties of $Cs_2LiYCl_6$:$Ce^{3+}$ for gamma and neutron detection," *Nucl. Instr. and Meth. A*, vol. 537, pp. 242-246, 2005.

[62] G. Bizarri, W. W. Moses, J. Singh, A. N. Vasil'ev, and R. T. Williams, "An analytical model of nonproportional scintillator light yield in terms of recombination rates," *J. Appl. Phys.*, vol. 105, p. 044507, 2009.

[63] S. Kerisit, K. M. Rosso, B. D. Cannon, F. Gao, and Y. Xie, "Computer simulation of the light yield nonlinearity of inorganic scintillators," *J. Appl. Phys.*, vol. 105, p. 114915, 2009.

[64] J. Singh, "Study of nonproportionality in the light yield of inorganic scintillators," *J. Appl. Phys.*, vol. 110, pp. 024503-8, 2011.

[65] R. T. Williams, J. Q. Grim, Q. Li, K. B. Ucer, and W. W. Moses, "Excitation density, diffusion-drift, and proportionality in scintillators," *Phys. Status Solidi B*, vol. 248, pp. 426-438, 2011.

[66] G. F. Knoll, *Radiation Detection and Measurement*. the United States of America John Wiley & Sons, Inc., 1979.

[67] W. W. Moses, G. Bizarri, R. T. Williams, and S. A. Payne, "The Origins of Scintillator Non-Proportionality," *IEEE Trans. Nucl. Sci.*, vol. 59, 2012.

[68] Q. Li, J. Q. Grim, R. T. Williams, G. Bizarri, and W. W. Moses, "The role of hole mobility in scintillator proportionality," *Nucl. Instr. and Meth. A*, vol. 652, pp. 288-291, 2010.

[69] Q. Li, J. Q. Grim, R. T. Williams, G. Bizarri, and W. W. Moses, "A transport-based model of material trends in nonproportionality of scintillators," *J. Appl. Phys.*, vol. 109, p. 123716, 2011.

[70] J. Crank, *The Mathematics of Diffusion*. Oxford: Clarendon Press, 1956.

[71] K. Ellmer, A. Klein, and B. Rech, *Transparent Conductive Zinc Oxide*. Berlin: Springer, 2008.
[72] I. V. Khodyuk, M. S. Alekhin, J. T. M. de Haas, and P. Dorenbos, "Improved scintillation proportionality and energy resolution of $LaBr_3$:Ce at 80K," *Nucl. Instr. and Meth. A*, vol. 642, pp. 75-77, 2011.
[73] J. M. Ziman, *Electrons and phonons*. Oxford: The Clarendon Press, 1960.
[74] K. S. Song and R. T. Williams, *Self-Trapped Excitons*: Springer-Verlag, 1993.

# Chapter 6 Charge carrier mobility and nonproportionality of $LaBr_3$:Ce scintillators

*Slightly modified version of this chapter has been submitted for publication at Physical Review B: I.V. Khodyuk, F.G.A. Quarati, M.S. Alekhin, P. Dorenbos, "Charge carrier mobility and nonproportionality of $LaBr_3$:Ce scintillators."*

The nonproportional response and related energy resolution of $LaBr_3:Ce^{3+}$ scintillation crystals doped with different concentrations of cerium were studied between 80K and 450K. For $Ce^{3+}$ concentration of 5% and 30%, $LaBr_3$ showed best proportionality and energy resolution at 80K. For $LaBr_3$:0.2%Ce the best energy resolution and the lowest degree of nonproportional response were instead observed around room temperature. The experimental results were analyzed in terms of charge carrier mobility and using theory of carrier transport in wide band gap semiconductors. We found that scattering of carriers by both lattice and impurity are the key processes determining the particular temperature dependence of carrier mobility and ultimately the scintillation nonproportionality. The calculated maximum of the $LaBr_3$:0.2%Ce carrier mobility corresponds well with the experimentally observed minima of its degree of nonproportionality, when assuming about 100ppm ionized impurity concentration.

## 6.1 Introduction

The nonproportionality of scintillators is attributed to radiationless recombination of electron-hole pairs with a recombination rate that increases with the ionization density [1-7]. This process together with an ionization density that changes along an electron track and with primary electron energy causes the deterioration of the energy resolution. To avoid the recombination losses, charge carriers should be effectively transferred from the primary track to luminescence centers. The faster the charge carriers escape the volume of high ionization density shown in Fig. 1.2 (Capter 1), in which quenching occurs, the higher the probability of converting carriers into optical photons. An important factor determining the rate at which carriers leave this volume is the carrier diffusion coefficient [2, 3, 5]. A high diffusion coefficient contributes to a more rapid transport of electrons, holes and excitons to regions further from the track where the radiationless recombination rate does not depend on ionization density.

In this Chapter the dependence of $LaBr_3$ nonproportionality on temperature and $Ce^{3+}$ concentration has been studied. For $LaBr_3$ with 0.2%, 5% and 30% of $Ce^{3+}$ the nonproportional response is determined at 80K, 300K and 450K and as a function of photon energy (photon-nPR) and as a function of electron energy (electron-nPR). Scintillation yield and energy resolution was measured in the energy range from 10.5 keV to 100 keV and at 662 keV. A specific model will be presented able to predict the electron-nPR results, and the degree of electron-nPR will be introduced and determined. Its dependence on temperature and concentration will be compared with our model estimate of the mobility for thermalized carriers in wide band gap semiconductors.

## 6.2 Experimental methods

To record scintillation pulse height spectra as a function of temperature, a $LaBr_3$:Ce sample was fixed at the bottom of a parabolic-like stainless steel cup covered with a reflective Al-foil, mounted onto the cold finger of a liquid nitrogen bath cryostat. The cup directs the scintillation light through a quartz window towards a photomultiplier tube (PMT) situated outside the cryostat chamber [8]. The Hamamatsu R6231-100 PMT at -680V bias voltage remained at room temperature and observes about 20% of the emitted scintillation light. To collect as much of the PMT output charge pulse as possible, the shaping time of an Ortec 672 spectroscopic amplifier was set at 10 μs. The temperature of the sample was controlled by two thermocouples attached to different parts of the sample holder. The yield of the scintillator will be expressed by the number of photoelectrons created in the PMT per MeV ( $N_{phe}^{PMT}$/MeV) of absorbed gamma or X-ray photon energy. The energy resolution $R$ of a peak in the pulse height spectrum at energy $E$ is defined as the ratio of the full width at half maximum $\Delta E$ of that peak to the energy $E$, and it will be expressed as a percentage value.

To measure X-ray pulse height spectra at many finely spaced energy values between 10.5 keV and 100 keV, experiments were carried out at the X-1 beam line at the Hamburger Synchrotronstrahlungslabor (HASYLAB) synchrotron radiation facility in Hamburg, Germany. A highly monochromatic pencil X-ray beam in the energy range 10.5 – 100 keV was used as an excitation source. A tunable double Bragg reflection monochromator using a Si[511] set of silicon crystals providing an X-ray resolution of 1 eV at 10.5 keV rising to 20 eV at 100 keV was used to select the X-ray energies. A sketch of the experimental set-up can be found in Chapter 2. The beam spot size was set by a pair of precision stepper-driven slits, positioned immediately in front of the cryostat chamber. For all measurements, a slit size of $50 \times 50$ μm$^2$ was used.

A dense sampling of data performed around the lanthanum K-electron binding energy $E_{KLa}$=38.925 keV was done in order to apply the K-dip spectroscopy method [9]. This method allows to derive the response of $LaBr_3$:Ce to photoelectrons down to energies as low as 100 eV. The method is briefly described as follows. An X-ray with energy $E_X$ that photoelectrically interacts with the lanthanum K-shell leads to the creation of a photoelectron with energy $E_e$ and a hole in the lanthanum *K*-shell,

$$E_e = E_X - E_{KLa}\,. \qquad (6.1)$$

The hole relaxes to the ground state with the emission of a cascade of secondary X-ray fluorescence photons and/or Auger electrons. The response of a scintillator is then equivalent to the sum of two main interaction products: 1) the K-shell photo electron response and 2) the response from the electrons emitted due to the sequence of processes following relaxation of the hole in the K-shell, the so-called K-cascade response. Our strategy is to employ X-ray energies just above $E_{KLa}$. The K-cascade response is assumed to be independent from the original X-ray energy. This response is found by tuning the X-ray energy to just above $E_{KLa}$. By subtracting the K-cascade response from the total X-ray response we are left with the response in photoelectrons from the K-shell photoelectron alone with energy $E_e$. The K-electron-nPR curve is then obtained from the number $N_{phe}^{PMT}$ /MeV at the energy of the K-photoelectron divided by the number $N_{phe}^{PMT}$ /MeV measured at 662 keV.

## 6.3 Photon response

The photon nonproportional response (photon-nPR) written as $f_{ph}(E)$ is defined as the number of photoelectrons $N_{phe}^{PMT}$ /MeV of absorbed energy observed at energy $E$ divided by the number $N_{phe}^{PMT}$ /MeV observed at $E$ = 662 keV energy. $f_{ph}(E)$ is expressed as a percentage value. For an ideal proportional scintillator it is 100% at all energies. Figure 6.1 shows $f_{ph}(E)$ for $LaBr_3$ doped with 0.2%, 5% and 30% $Ce^{3+}$ studied at 80K, 300K, and 450K. The shape of the $f_{ph}(E)$ curve depends not only on the temperature as was reported in [4], but also on $Ce^{3+}$ concentration.

As a figure of merit the degree of photon-nPR $\sigma_{ph}$ will be used. It has been defined following ideas in [10-12]

$$\sigma_{ph} = \frac{1}{\left(E_{\max} - E_{\min}\right)} \int_{E_{\min}}^{E_{\max}} \left| f_{ph}\left(E_{\max}\right) - f_{ph}\left(E\right) \right| dE\,, \qquad (6.2)$$

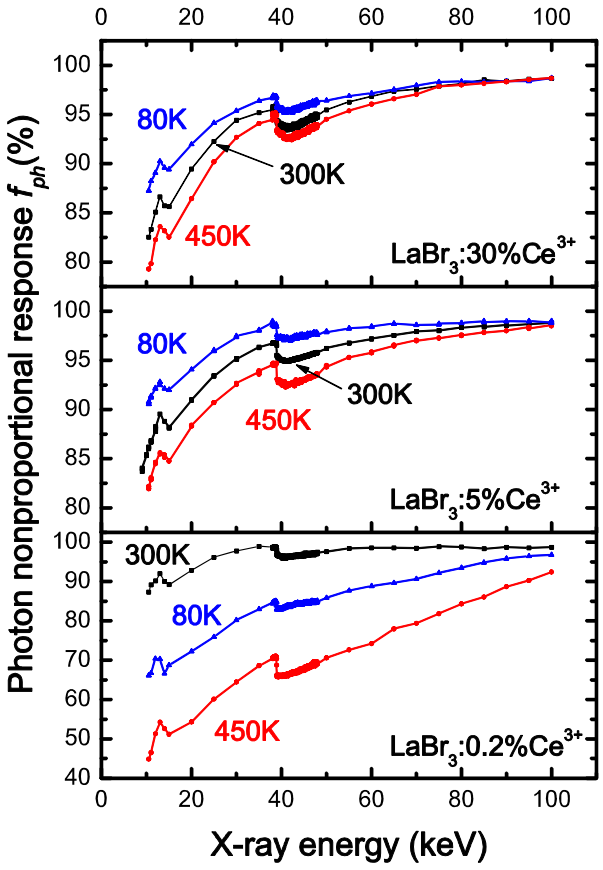


**Fig. 6.1** Photon nonproportional response of $LaBr_3$ doped with 0.2%, 5% and 30% $Ce^{3+}$ as a function of X-ray or gamma photon energy at 80K, 300K and 450K.

***Table 6.1*** *Degree (in %) of $LaBr_3$:Ce photon-nPR $\sigma_{ph}$ in the energy range from $E_{min}$ = 10.5 keV to $E_{max}$ = 662 keV.*

| $Ce^{3+}$ concentration (%) | Temperature, K | | |
|---|---|---|---|
| | 80 | 300 | 450 |
| 0.2 | 3.31 | 0.95 | 6.98 |
| 5 | 0.78 | 1.07 | 1.43 |
| 30 | 1.09 | 1.22 | 1.37 |

where $E_{max}$ = 662 keV, $E_{min}$ = 10.5 keV, and $f_{ph}(E_{max})$ is set equal to 100%. $\sigma_{ph}$ for $LaBr_3$ at different temperatures and $Ce^{3+}$ concentrations obtained from the results in Fig. 6.1 are listed in Table 6.1. For $LaBr_3$:5%Ce and $LaBr_3$:30%Ce $\sigma_{ph}$ increases with temperature. The behavior is different for $LaBr_3$:0.2%Ce where the lowest value for $\sigma_{ph}$ is observed at 300K. The smallest $\sigma_{ph}$ is measured for $LaBr_3$:5%Ce at 80K.

## 6.4 Energy resolution

### *6.4.1 Energy resolution as a function of energy at different temperatures*

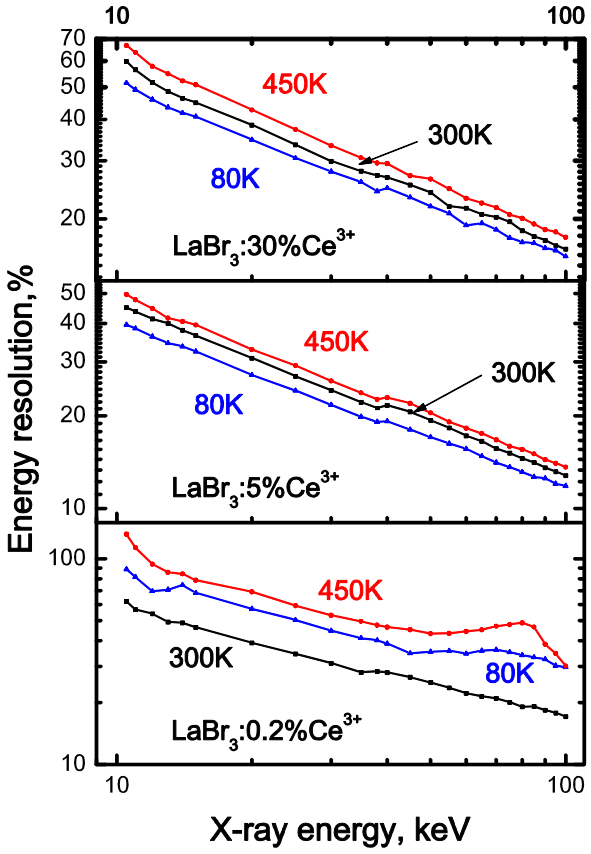


**Fig. 6.2** Energy resolution of $LaBr_3$ doped with 0.2%, 5% and 30% $Ce^{3+}$ as a function of X-ray energy at 80K, 300K, and 450K.

The energy resolution *R(E)* of $LaBr_3$ doped with 0.2%, 5% and 30% $Ce^{3+}$ at 80K, 300K and 450K is presented in Fig. 6.2. The overall pattern is consistent with the pattern of $\sigma_{ph}$. At a given energy for both $LaBr_3$ doped with 5% and 30% $Ce^{3+}$ the best energy resolution is obtained at 80K and the worst at 450K. $LaBr_3$:0.2%Ce shows the best resolution at 300K where $\sigma_{ph}$ is minimal. Figure 6.2 shows that at 80K, the already outstanding room temperature energy resolution of $LaBr_3$ doped with 5 and 30% $Ce^{3+}$ can be improved even further.

### *6.4.2 Energy resolution as a function of temperature at 662 keV*

To confirm the dependence of *R* on temperature and concentration, pulse height spectra were recorded using $^{137}Cs$ 662 keV gamma radiation. The energy resolution $\Delta E/E$ of a scintillator is determined by

$$\left(\frac{\Delta E}{E}\right)^2 = R^2 = R_M^2(T) + R_{sc}^2(T) = (2.35)^2 \frac{1+v(M)}{N_{phe}^{PMT}(T)} + R_{sc}^2(T), \qquad (6.3)$$

where $v(M)$ is the variance in the PMT gain, $N_{phe}^{PMT}$ is the number of photoelectrons that are produced by the interaction of scintillation photons with the PMT photocathode and are multiplied on the first dynode [13, 14], and $R_{sc}$ is given by

$$R_{sc}^2(T) = R_{nPR}^2(T) + R_{tr}^2(T) + R_{inh}^2(T), \qquad (6.4)$$

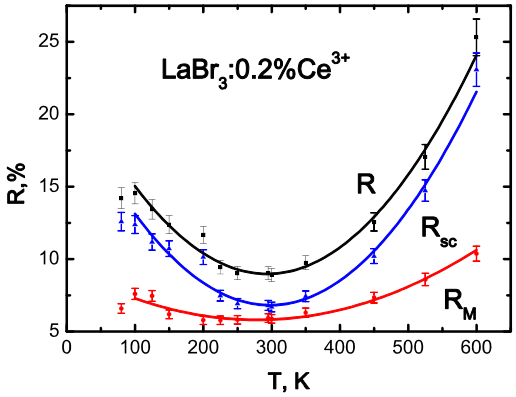


**Fig. 6.3** The separate contributions to the total energy resolution of $LaBr_3$:0.2% Ce at 662 keV as a function of temperature.

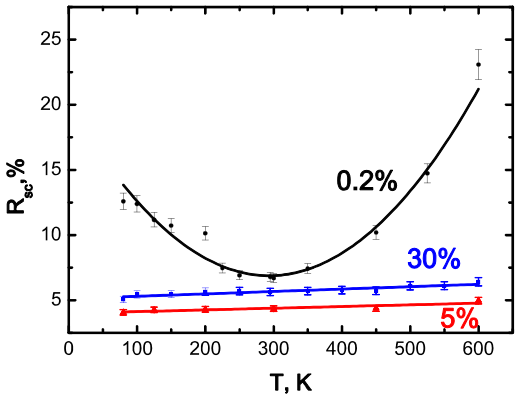


**Fig. 6.4** The $R_{sc}$ contribution to the energy resolution at 662 keV of 0.2%, 5% and 30% Ce-doped $LaBr_3$ as a function of temperature.

where $R_{nPR}(T)$ is a contribution from nonproportionality, $R_{tr}(T)$ is the so-called transport resolution, and $R_{inh}(T)$ is a contribution from inhomogeneity of the scintillation crystal. It is assumed that all contributions are independent from each other. To measure the temperature dependence of the $LaBr_3$:Ce energy resolution the parabolic-like cup covered with reflective Al foil was used. This configuration of the experimental set-up results in the collection of about 20% of the emitted scintillation photons, increasing importance of the statistical contribution $R_M(T)$.

Figure 6.3 shows the measured $R(T)$, $R_M(T)$ calculated from the measured $N_{phe}^{PMT}$, and $R_{sc}(T)$ obtained with Eq. (6.4) for $LaBr_3$:0.2%Ce. The parabolas through the data are drawn to guide the eye. $R_M(T)$ is small and $R(T)$ is almost entirely determined by $R_{sc}(T)$. The resolution is lowest at room temperature. This pattern is consistent with the pattern of $\sigma_{ph}$ in Table 6.1 where a larger $\sigma_{ph}$ results in poorer energy resolution which confirms a relationship between energy resolution and nonproportionality.

The contribution $R_{sc}(T)$ to the energy resolution at 662 keV is shown in Fig. 6.4 for 0.2%, 5% and 30% Ce-doped $LaBr_3$. $LaBr_3$:0.2%Ce shows a minimum at room temperature. In contrast, $LaBr_3$ with 5% and 30% $Ce^{3+}$ exhibits a linear decrease of the $R_{sc}(T)$ with decreasing temperature. Lower values of $R_{sc}(T)$ correlate with lower values of $\sigma_{ph}$.

## 6.5 Electron response

Using K-dip spectroscopy we derived the K-photoelectron-nPR curves $f_e(E)$ for $LaBr_3$ doped with 0.2%, 5% and 30% $Ce^{3+}$ at 80K, 300K and 450K which are shown in Fig. 6.5. The $f_e(E)$ data in Fig. 6.5 are quite scattered, especially below 1 keV [15]. To represent the data with a smoothly varying curve an approach similar to the algorithms used in [1, 16, 17] was employed. Using the nonrelativistic Bethe equation the rate of energy loss by the primary electron or stopping power [18] can be written as

$$-\frac{dE}{dx}=\frac{2\pi e^4\left(4\pi\varepsilon_0\right)\rho_e}{E}\ln\left\{1.164\left[E+0.81I\right]/I\right\}, \qquad (6.5)$$

where $e$ is the elementary charge, $\varepsilon_0$ is the vacuum dielectric permittivity, $\rho_e$ is the electron density in the scintillator, $E$ is the energy of the ionization track creating electron, and $I$ is the average ionization energy of the Hydrogen atom. Assuming cylindrical shape of high ionization density volume [19] along the track of the primary energetic electron as shown in Fig. 1.2, the concentration of the ionized charge carriers $n(x)$ is given by

$$n\left(x\right)=\frac{1}{\pi r^2 E_{e-h}}\left(-\frac{dE}{dx}\right), \qquad (6.6)$$

where $r$ is the radius of the high ionization density volume shown in Fig. 1.2 and $E_{e\text{-}h}$ is the average energy required to create a free electron- free hole pair in the scintillator [20, 21].

Finally, following the ideas in [1, 17] $f_e(E)$ can be represented by

$$f_e\left(E\right)=\left[A1+\frac{A2+A3\cdot n\left(x\right)}{A4+A5\cdot n\left(x\right)+A6\cdot n^2\left(x\right)}\right]\times 100\%, \qquad (6.7)$$

where A1 to A6 are independent fitting parameters. The results are shown by the solid curves in Figure 6.5, and will be used to calculate the degree of electron-nPR $\sigma_e$.

***Table 6.2*** *Degree (in %) of the $LaBr_3$:Ce electron-nPR $\sigma_e$ in the energy range from $E_{min}$ = 0.2 keV to $E_{max}$ = 662 keV.*

| $Ce^{3+}$ concentration (%) | Temperature, K | | |
|---|---|---|---|
| | 80 | 300 | 450 |
| 0.2 | 1.80 | 0.93 | 4.28 |
| 5 | 0.12 | 0.29 | 0.45 |
| 30 | 0.16 | 0.52 | 0.68 |

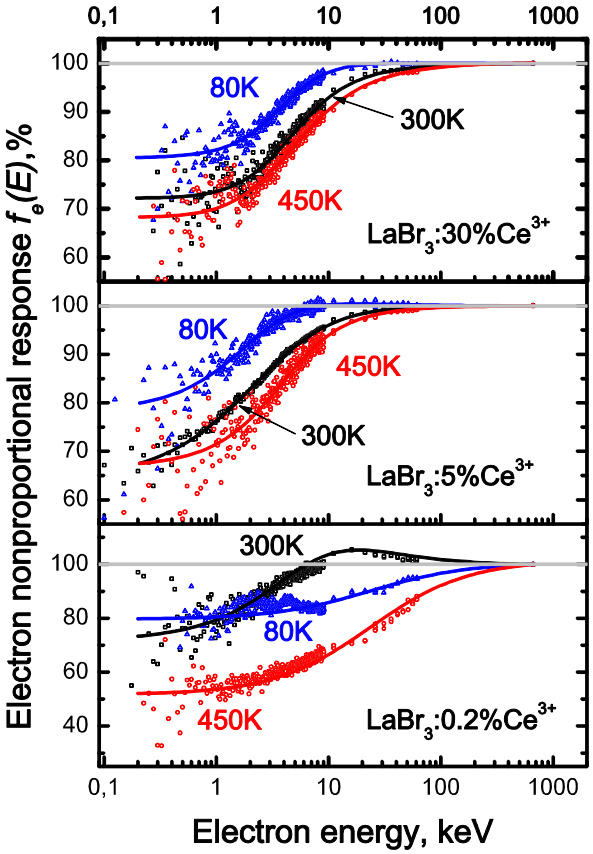


**Fig. 6.5** K-photoelectron nonproportional response of $LaBr_3$ doped with 0.2%, 5% and 30% $Ce^{3+}$ as a function of X-ray or gamma photon energy at 80K, 300K and 450K.

$\sigma_e$ is defined analogous to the degree of photon-nPR and is determined using Eq. (6.2) by integrating over the energy range from $E_{min}$ = 0.2 keV to $E_{max}$ = 662 keV. For a perfectly proportional scintillator the value of $\sigma_e$ is zero, and the scintillator with a lower value of $\sigma_e$ is considered to be more proportional.

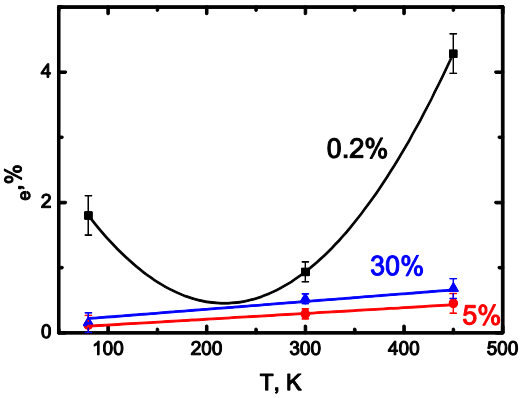


**Fig. 6.6** Degree of $LaBr_3$ electron-nPR $\sigma_e$ versus temperature and $Ce^{3+}$ concentration.

$\sigma_e$ versus $T$ and $Ce^{3+}$ concentration is shown in Fig. 6.6 and in Table 6.2. It behaves similar to $\sigma_{ph}$. The only difference is that $\sigma_e$ of $LaBr_3$:0.2%Ce at 300K shows a higher value of 0.93% compared to 0.29% for $LaBr_3$:5%Ce and 0.52% for $LaBr_3$:30%Ce. Linear extrapolation of $\sigma_e$ for $LaBr_3$:5%Ce and $LaBr_3$:30%Ce suggests that $\sigma_e$ for both concentrations reach zero at a temperature close to the absolute zero. This means, that an almost perfect proportional response would be obtained for 5% and for 30% Ce-doped $LaBr_3$ crystals.

## 6.6 Discussion

Using synchrotron irradiation the photon-nPR $f_{ph}(E)$ and energy resolution $R$ of $LaBr_3$:Ce scintillation crystals doped with 0.2%, 5% and 30% of $Ce^{3+}$ were studied at 80K, 300K and 450K. Results of these experiments were shown in Figs. 6.1 and 6.2, and in Table 6.1. $f_{ph}(E)$ and $\sigma_{ph}$ are characteristics of the gamma photon response of a scintillator, however, the response to energetic electrons is more fundamental. If $f_e(E)$ is known and when the process of ionization track creation can be simulated, the shape of $f_{ph}(E)$ over the entire energy range can be calculated [22, 23] by Monte-Carlo techniques. An example of such simulation for NaI:Tl was presented in Capter 2, section 2.3.5. The actual value of $f_{ph}(E)$ at energy $E$ is then a weighted average of several values of $f_e(E)$ at lower energies [24]. Using the electron-nPR function $f_e(E)$

then provides a better starting point to understand nonproportionality then using the photon-nPR function [24, 25]. Using the K-dip spectroscopy method $f_e(E)$ shown in Fig. 6.5 was derived from the $f_{ph}(E)$ and Table II was calculated using Eq. (6.2) and Eq. (6.7). Figure 6.6 shows $\sigma_e$ of $LaBr_3$ versus temperature and $Ce^{3+}$ concentration, and this figure is the most important outcome of the performed experiments and calculations. In the following discussion we will concentrate on better understanding of the results in Fig. 6.6 by using ideas on carrier mobility from semiconductor physics and apply them to the processes that occur inside the ionization track in scintillators.

### *6.6.1 Charge carrier diffusion and quenching*

There are several models proposed in the recent literature to explain the origin of nonproportionality [1-3, 11, 15, 26]. It is attributed to radiationless electron-hole pair recombination in the regions of a high concentration $n(x)$ of charge carriers along the ionization track as shown in Fig. 1.2. According to Eq. (6.5) and Eq. (6.6) $n(x)$ increases with smaller energy $E$ of the track creating primary electron [18]. This leads to a larger radiationless electron hole recombination rate which forms the basis of increasing nonproportionality with smaller gamma or X-ray photon or primary electron energy.

An overview of the current models on nonproportionality was presented by Moses *et al.* [6]. The basis of all those models is the competition between two opposing processes shown in Fig. 1.2: 1) quenching due to radiationless electron hole recombination inside the volume of high ionization density along the track, and 2) diffusion of the charge carriers from the point of creation towards a volume of lower ionization density. The faster the charge carriers escape the volume of high ionization density in which quenching occurs and reach luminescence centers, the higher the probability of converting the energy of the carriers into optical photons. An important factor determining the rate at which carriers leave this volume is the carrier diffusion coefficient [2, 3, 5]. Another very important parameter is concentration of luminescence or trapping centers inside the high ionization density volume. At high concentration of $Ce^{3+}$ in $LaBr_3$ essential part of the charge carriers can be promptly removed from the diffusion-quenching process. According to Bizarri and Dorenbos [27] carriers can be sequentially captured by $Ce^{3+}$ or form self-trapped excitons (STEs) which transfer their energy to $Ce^{3+}$ through thermally activated migration or directly. These effects can lead to a significant difference of quenching probability at low Ce concentration 0.2% and at high concentrations 5% and 30%.

First let us consider processes which apply to all concentrations of luminescence

centers. A high diffusion coefficient contributes to a more rapid transport of electrons, holes and excitons to regions away from the track where the radiationless recombination rate does not depend on concentration *n(x)*. Three different orders of radiationless recombination or quenching processes are distinguished in

$$\left.\frac{\partial n(r,t)}{\partial t}\right|_{quenching} = -k_i \cdot n^i(r,t), \qquad (6.8)$$

where $k_i(t)$ is the quenching rate and *i* is the order of the quenching process. First order quenching includes: radiationless decay of the excited luminescence centre due to emission of phonons and plasmons, radiationless recombination of free excitons and STEs [28]. Second order quenching includes bimolecular quenching due to dipole-dipole Förster transfer [29]. And third order quenching includes exciton-exciton annihilation due to Auger-like processes [2, 3]. These different quenching processes are also at the bases [1] of the phenomenological Eq. (6.7) that determines the shape of $f_e(E)$.

The diffusion equation [30] can be written as

$$\left.\frac{\partial n(r,t)}{\partial t}\right|_{diffusion} = \nabla\left[D(n)\nabla n(r,t)\right], \qquad (6.9)$$

where *n* is the concentration of charge carriers, *r* is the radial coordinate perpendicular to the ionization track as shown in Fig. 1.2, *t* is the time and *D* the diffusion coefficient. Assuming that in the high ionization density volume *D(n)* is constant [31], the Einstein relation

$$D = \mu(T)\cdot kT \qquad (6.10)$$

applies and one obtains

$$\left.\frac{\partial n(r,t)}{\partial t}\right|_{diffusion} = \mu(T)\cdot kT\cdot\nabla^2 n(r,t), \qquad (6.11)$$

where $\mu(T)$ is the mobility of the charge carriers, *k* is the Boltzmann constant and *T* is the effective temperature of the charge carriers. Based on Eq. (6.9), the transport of charge carriers becomes faster when carrier mobility and temperature increases.

### *6.6.2 Theory of electrical transport*

The minimum in $\sigma_e$ for $LaBr_3$:0.2% $Ce^{3+}$ in Fig. 6.6 at room temperature suggests a minimum in the loss processes at room temperature that within the above theory should correspond with a maximum in charge carrier mobility. According to theory of charge

carrier transport in wide band gap semiconductors, mobility indeed strongly depends on temperature [31, 32]. Here we will employ that theory in order to understand the results for $LaBr_3$:0.2% $Ce^{3+}$ in Fig. 6.6. The theory is for thermalized charge carriers and we therefore assume that all charge carriers are thermalized instantly [33, 34] after creation in the ionization track.

An increase of carrier mobility with temperature decrease is due to a reduced phonon interaction rate. Emission of optical phonons is the main mechanism responsible for carrier scattering by the lattice. $LaBr_3$ does not show any piezoelectric properties. That means that piezoelectric mode scattering caused by the electric field associated with acoustical phonons can also be ignored in our calculations. Lattice scattering due to optical phonons is independent on the carrier concentration [31].

The main lattice scattering mechanism is due to the interaction of carriers with the longitudinal-optical phonons. According to [31] the optical Hall lattice mobility can be calculated from

$$\mu_{L_{opt}} = \frac{e}{2\alpha\omega_0 m^*}\left(\exp\left(\frac{\hbar\omega_0}{kT}\right)-1\right) \qquad (6.12)$$

where $\alpha$ is the polaron coupling constant given by

$$\alpha = \left(\frac{1}{\varepsilon_\infty}-\frac{1}{\varepsilon}\right)\sqrt{\frac{m^* E_H}{m_e \hbar\omega_0}} \qquad (6.13)$$

For $LaBr_3$ the high frequency and the static dielectric constants are $\varepsilon_\infty \approx 5$ and $\varepsilon \approx 10$, respectively [35]; $E_H = 13.595\,eV$ is the first ionization energy of the hydrogen atom; $\frac{m^*}{m_e} = 1.323$ is the effective electron mass divided by the electron mass [11]; $\hbar\omega_0 = 23.7\,meV$ is the energy of the longitudinal-optical phonon in $LaBr_3$ [35].

An increase of carrier mobility with temperature *increase* can be caused only by the ionized impurity scattering, which according to Ziman [32] is given by

$$\mu_i = \frac{2^{7/2}\left(\varepsilon\varepsilon_0\right)^2\left(kT\right)^{3/2}}{\pi^{3/2} z^2 e^3 \left(m^*\right)^{1/2} N_i}\cdot F\left(3kT\right) \qquad (6.14)$$

where $z$ is the effective charge of the impurity with concentration $N_i$, $\varepsilon_0$ is the vacuum permittivity and $F\left(3kT\right)$ is the averaged Coulomb screening factor

$$F\left(3kT\right)=\ln\left(1+\frac{8m^{*}\cdot 3kT}{q^{2}\hbar^{2}}\right)-\left(1+\frac{q^{2}\hbar^{2}}{8m^{*}\cdot 3kT}\right)^{-1}, \qquad (6.15)$$

where

$$q^{2}=\frac{4\pi e^{2}}{\varepsilon\varepsilon_{0}kT}n\left(2-\frac{n}{N_{i}}\right). \qquad (6.16)$$

For our range of temperatures $F\left(3kT\right)\approx 1$.

The overall mobility $\mu(T)$ can be obtained from

$$\mu\left(T\right)=\left(\frac{1}{\mu_{L}\left(T\right)}+\frac{1}{\mu_{i}\left(T\right)}\right)^{-1}. \qquad (6.17)$$

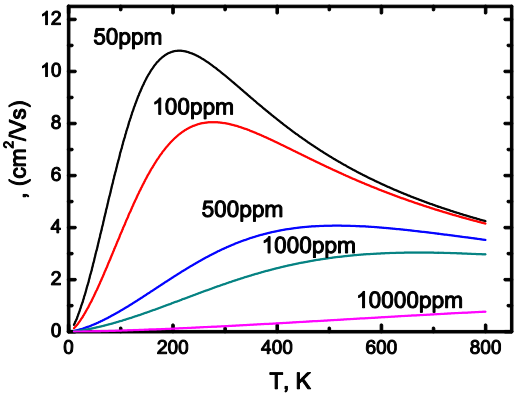


**Fig. 6.7** Calculated mobility of charge carriers in $LaBr_3$ versus temperature and ionized impurity concentration.

Figure 6.7 shows the mobility calculated with Eq. (6.17) for different concentrations of ionized impurity scattering centers with z = 1 in $LaBr_3$. At impurity concentration of 100ppm the maximum of the carrier mobility is slightly below room temperature. Therefore with our model an impurity concentration of 100ppm is needed to match well with the minimum of $R_{sc}(T)$ of $LaBr_3$:0.2%Ce at 300K in Fig. 6.3 and of $\sigma_e$ in Fig. 6.6.

Equations (6.12) to (6.16) pertain to a given density of carriers in the conduction or valence band. The calculations do not incorporate any carrier trapping [27] and also it was assumed that all charge carriers are thermalized instantly [33, 34] after creation in

the ionization track. However recent theoretical studies [15, 36] suggest that also non-thermalized carriers play an important role in carrier and phonon transport in scintillators. One should therefore interpret the results in Fig. 6.7 as qualitative.

Lattice and impurity scattering mechanisms are expected to be more important at low $Ce^{3+}$ concentration due to the longer distance carriers need to travel before they can reach $Ce^{3+}$ where they can recombine radiatively. The concentration of $Ce^{3+}$ in $LaBr_3$:0.2%Ce is $4.2 \cdot 10^{18}\, cm^{-3}$. At 5 and 30% $Ce^{3+}$ concentration the carrier density *n(x)* is $1.05 \cdot 10^{20} cm^{-3}$ and $6.3 \cdot 10^{20} cm^{-3}$ which is of the same order of magnitude as the concentration of recombination centers, and a high mobility of charge carriers needed to escape the dense ionization region becomes of less importance. Carriers can be trapped instantly after ionization and the trapping rate by $Ce^{3+}$ starts to dominate over the quenching rate and the escape rate. This can explain the better $\sigma_e$ shown in Fig. 6.6 for 5 and 30% Ce concentration. What then still needs to be explained is the temperature dependence of $\sigma_e$ for 5 and 30% of Ce.

### *6.6.3 Onsager mechanism*

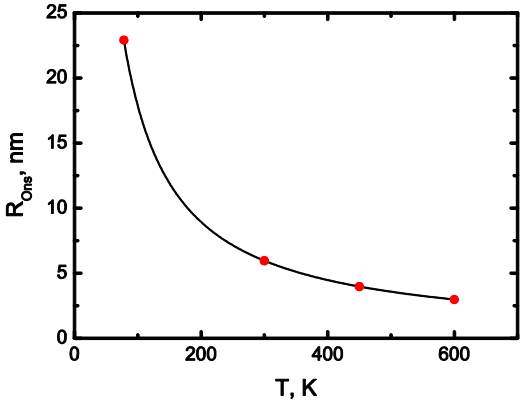


**Fig. 6.8** Onsager radius of charge carrier capture in $LaBr_3$ versus temperature.

According to the model of Bizarri [27] there are two routes for carriers to be trapped by $Ce^{3+}$ in $LaBr_3$. The first is the sequentially capture of first the hole by $Ce^{3+}$ with formation of $Ce^{4+}$ followed by capture of the electron, and the second through formation of STEs which transfer their energy to $Ce^{3+}$ though thermally activated migration or directly. Formation of STEs remains an important intermediate

mechanism even at high Ce concentration, and especially at low temperatures. It means that quenching inside the high ionization density volume around the track can be reduced by more efficient formation of STEs. Then according to the Onsager model [37] and following ideas by Payne *et al.* [38] one may express the Onsager radius ($R_{Ons}$) of exciton formation as

$$\frac{e^2}{4\pi\varepsilon\varepsilon_0 R_{Ons}} = kT \,. \qquad (6.18)$$

Figure 6.8 shows the temperature dependence of $R_{Ons}$ for $LaBr_3$. Rapid and efficient formation of STEs and transfer of their energy to the luminescence centers removes carriers from the diffusion-quenching process. Such mechanism will lower $\sigma_e$ and $R_{sc}(T)$ when temperature decreases, which then may explain the observations in Figs. 6.4 and 6.6.

## 6.7 Conclusion

The shape of the photon- and electron-nPR curves of $LaBr_3$:Ce depends on temperature. For 5% and 30% $Ce^{3+}$ concentration, $LaBr_3$ shows better proportionality and energy resolution when temperature decreases. This improvement means that at a low temperature even better energy resolution can be achieved with a $LaBr_3$ scintillation detector compared to the already outstanding 2.75% measured at room temperature.

The temperature dependence of the photon- and electron-nPRs of $LaBr_3$:0.2% Ce is different. The most proportional response was measured at 300K. At 80K and 450K the photon- and electron-nPR curves deviate strongly from the linear response. This leads to a significant deterioration of the energy resolution both at 80K and 450K.

Despite the limitations of the theoretical model that was used, the obtained results suggest that a significant factor determining the nonproportionality of $LaBr_3$:0.2%Ce is the mobility of charge carriers. The higher the carrier mobility and diffusion coefficient the lower the degree of electron-nPR, which leads to improved energy resolution. Semiconductor detectors based on HPGe with excellent energy resolution of 0.3% besides different statistics have a much higher mobility of charge carriers ~40000 $cm^2/Vs$ compared to ~8 $cm^2/Vs$ calculated for $LaBr_3$:0.2%Ce with 100ppm ionized impurity concentration. For 5% and 30% concentrations direct trapping by the recombination centers starts do dominate and a high mobility of charge carriers becomes of less importance.

Summarizing the results of the performed measurements and calculations and bearing in mind that carrier mobility in semiconductor detectors is high, we conclude that the

“ultimate energy resolution” should be sought in scintillation materials with high carrier mobility and high charge carrier capture efficiency.

**Acknowledgments**

The research leading to these results has received funding from the Netherlands Technology Foundation (STW), Saint Gobain, crystals and detectors division, Nemours, France, and by the European Community's Seventh Framework Programme (FP7/2007-2013) under grant agreement n° 226716. We thank the scientists and technicians of the X-1 beamline at the Hamburger Synhrotronstrahlungslabor (HASY-LAB) synchrotron radiation facilities for their assistance. The authors want to acknowledge Conny Hansson, Johannes van der Biezen and Alan Owens from the European Space Agency (ESTEC) for their assistance with the experiment and sharing some of the beam time at X-1.

## References

[1] G. Bizarri, W. W. Moses, J. Singh, A. N. Vasil’ev, and R. T. Williams, "An analytical model of nonproportional scintillator light yield in terms of recombination rates," *J. Appl. Phys.*, vol. 105, p. 044507, 2009.

[2] R. T. Williams, J. Q. Grim, Q. Li, K. B. Ucer, and W. W. Moses, "Excitation density, diffusion-drift, and proportionality in scintillators," *Phys. Status Solidi B*, vol. 248, pp. 426-438, 2011.

[3] Q. Li, J. Q. Grim, R. T. Williams, G. Bizarri, and W. W. Moses, "A transport-based model of material trends in nonproportionality of scintillators," *J. Appl. Phys.*, vol. 109, p. 123716, 2011.

[4] I. V. Khodyuk, M. S. Alekhin, J. T. M. de Haas, and P. Dorenbos, "Improved scintillation proportionality and energy resolution of $LaBr_3$:Ce at 80K," *Nucl. Instr. and Meth. A*, vol. 642, pp. 75-77, 2011.

[5] Q. Li, J. Q. Grim, R. T. Williams, G. Bizarri, and W. W. Moses, "The role of hole mobility in scintillator proportionality," *Nucl. Instr. and Meth. A*, vol. 652, pp. 288-291, 2010.

[6] W. W. Moses, G. Bizarri, R. T. Williams, and S. A. Payne, "The Origins of Scintillator Non-Proportionality," *IEEE Trans. Nucl. Sci.*, vol. 59, 2012.

[7] R. B. Murray and A. Meyer, "Scintillation Response of Activated Inorganic Crystals to Various Charged Particles," *Physical Review*, vol. 122, pp. 815-826, 1961.

[8] G. Bizarri, J. T. M. de Haas, P. Dorenbos, and C. W. E. van Eijk, "First time measurement of gamma-ray excited LaBr3:5% Ce3+ and LaCl3:10% Ce3+

temperature dependent properties," *physica status solidi (a),* vol. 203, pp. R41-R43, 2006.

[9] I. V. Khodyuk, J. T. M. de Haas, and P. Dorenbos, "Nonproportional Response Between 0.1-100 keV Energy by Means of Highly Monochromatic Synchrotron X-Rays," *IEEE Trans. Nucl. Sci.,* vol. 57, pp. 1175-1181, Jun 2010.

[10] P. Dorenbos, "Light output and energy resolution of $Ce^{3+}$-doped scintillators," *Nucl. Instr. and Meth. A,* vol. 486, pp. 208-213, 2002.

[11] W. Setyawan, R. M. Gaume, R. S. Feigelson, and S. Curtarolo, "Comparative Study of Nonproportionality and Electronic Band Structures Features in Scintillator Materials," *IEEE Trans. Nucl. Sci.,* vol. 56, pp. 2989-2996, 2009.

[12] I. V. Khodyuk and P. Dorenbos, "Trends and patterns of scintillator nonproportionality," *IEEE Trans. Nucl. Sci.,* 2012.

[13] J. T. M. de Haas and P. Dorenbos, "Methods for accurate measurement of the response of photomultiplier tubes and intensity of light pulses," *IEEE Trans. Nucl. Sci.,* vol. 58, pp. 1290-1296, 2011.

[14] J. T. M. de Haas, P. Dorenbos, and C. W. E. van Eijk, "Measuring the absolute light yield of scintillators," *Nucl. Instr. and Meth. A,* vol. 537, pp. 97-100, Jan 2005.

[15] A. Kozorezov, J. K. Wigmore, and A. Owens, "Picosecond dynamics of hot carriers and phonons and scintillator non-proportionality," *J. Appl. Phys.,* vol. 112, p. 053709, 2012.

[16] J. E. Jaffe, "Energy and length scales in scintillator nonproportionality," *Nucl.Instr.and Meth. A,* vol. 580, pp. 1378-1382, 2007.

[17] J. Singh, "Study of nonproportionality in the light yield of inorganic scintillators," *J. Appl. Phys.,* vol. 110, pp. 024503-8, 2011.

[18] G. F. Knoll, *Radiation Detection and Measurement*. the United States of America John Wiley & Sons, Inc., 1979.

[19] A. N. Vasil'ev, "From luminescence non-linearity to scintillation non-proportionality," *IEEE Trans. Nucl. Sci.,* vol. 55, pp. 1054-1061, Jun 2008.

[20] P. A. Rodnyi, *Physical Processes in Inorganic Scintillators*. NY: CRC Press, 1997.

[21] P. A. Rodnyi, P. Dorenbos, and C. W. E. van Eijk, "Energy Loss in Inorganic ScintiNators," *Phys. Statatus Solidi B,* vol. 187, pp. 15-29, 1995.

[22] B. D. Rooney and J. D. Valentine, "Scintillator light yield nonproportionality: calculating photon response using measured electron response," *IEEE Trans. Nucl. Sci.,* vol. 44, pp. 509-516, 1997.

[23] M. M. Terekhov, R. L. Aptekar, D. D. Frederiks, S. V. Golenetskii, V. N. Il'inskii, and E. P. Mazets, "The Konus-Wind and Konus-A instrument response functions and the spectral deconvolution procedure," in *Gamma-Ray Bursts, Pts 1 and 2* Melville: Amer Inst Physics, 1998, pp. 894-898.

[24] W. W. Moses, S. A. Payne, W. S. Choong, G. Hull, and B. W. Reutter, "Scintillator non-proportionality: Present understanding and future challenges," *IEEE Trans. Nucl. Sci.,* vol. 55, pp. 1049-1053, Jun 2008.

[25] E. V. D. van Loef, W. Mengesha, J. D. Valentine, P. Dorenbos, and C. W. E. van Eijk, "Nonproportionality and energy resolution of a $LaCl_3$:10% $Ce^{3+}$ scintillation crystal," *IEEE Trans. Nucl. Sci.,* vol. 50, pp. 155-158, 2003.

[26] S. A. Payne, W. W. Moses, S. Sheets, L. Ahle, N. J. Cherepy, B. Sturm, S. Dazeley, G. Bizarri, and C. Woon-Seng, "Nonproportionality of Scintillator Detectors: Theory and Experiment. II," *IEEE Trans. Nucl. Sci.,* vol. 58, pp. 3392-3402, 2011.

[27] G. Bizarri and P. Dorenbos, "Charge carrier and exciton dynamics in $LaBr_3$:$Ce^{3+}$ scintillators: Experiment and model," *Phys. Rev. B,* vol. 75, p. 184302, 2007.

[28] K. S. Song and R. T. Williams, *Self-Trapped Excitons*: Springer-Verlag, 1993.

[29] M. Kirm, V. Nagirnyi, E. Feldbach, M. De Grazia, B. Carre, H. Merdji, S. Guizard, G. Geoffroy, J. Gaudin, N. Fedorov, P. Martin, A. Vasil'ev, and A. Belsky, "Exciton-exciton interactions in $CdWO_4$ irradiated by intense femtosecond vacuum ultraviolet pulses," *Physical Review B,* vol. 79, p. 4, Jun 2009.

[30] J. Crank, *The Mathematics of Diffusion*. Oxford: Clarendon Press, 1956.

[31] K. Ellmer, A. Klein, and B. Rech, *Transparent Conductive Zinc Oxide*. Berlin: Springer, 2008.

[32] J. M. Ziman, *Electrons and phonons*. Oxford: The Clarendon Press, 1960.

[33] A. N. Belsky, R. A. Glukhov, I. A. Kamenskikh, P. Martin, V. V. Mikhailin, I. H. Munro, C. Pedrini, D. A. Shaw, I. N. Shpinkov, and A. N. Vasilev, "Luminescence quenching as a probe for the local density of electronic excitations in insulators," *Journal of Electron Spectroscopy and Related Phenomena,* vol. 79, pp. 147-150, May 1996.

[34] Q. Li, J. Q. Grim, K. B. Ucer, A. Burger, G. Bizarri, W. W. Moses, and R. T. Williams, "Host structure dependence of light yield proportionality in scintillators in terms of hot and thermalized carrier transport," *Phys. Status Solidi RRL,* vol. 6, pp. 346-348, 2012.

[35] B. Liu, M. Gu, Z. Qi, X. Liu, S. Huang, and C. Ni, "First-principles study of lattice dynamics and thermodynamic properties of $LaCl_3$ and $LaBr_3$," *Physical Review B*, vol. 76, p. 064307, 2007.

[36] R. Kirkin, V. V. Mikhailin, and A. N. Vasil'ev, "Recombination of Correlated Electron-Hole Pairs With Account of Hot Capture With Emission of Optical Phonons," *Nuclear Science, IEEE Transactions on*, vol. PP, pp. 1-1, 2012.

[37] L. Onsager, "Initial Recombination of Ions," *Phys. Rev.*, vol. 54, pp. 554-557, 15 October 1938.

[38] S. A. Payne, N. J. Cherepy, G. Hull, J. D. Valentine, W. W. Moses, and C. Woon-Seng, "Nonproportionality of Scintillator Detectors: Theory and Experiment," *IEEE Trans. Nucl. Sci.*, vol. 56, pp. 2506-2512, 2009.

# Summary

The main research objectives of this thesis stated in section 1.4 of the first chapter were:

- To develop a new experimental method that allows to measure nonproportional response at low energies (100 eV – 10 keV).
- To elucidate the true origin of nonproportionality.

In Chapters 2, 3 and 4 new methods, developed in this thesis, which can be used to measure photon or electron nonproportional response in the low energy range (below 10 keV) were introduced. Among these methods were the photopeak and escape peak analysis and K-dip spectroscopy. The essence of all the methods is the characterization of inorganic scintillators by means of highly monochromatic synchrotron X-ray photons in the energy range 9 – 100 keV at the X-1 beamline at HASYLAB. By utilizing the photopeak, the $K_\alpha$ escape peaks, and the $K_\beta$ escape peaks that appear in pulse height spectra three different types of strongly related nonproportionality curves were introduced. Together they provided good data for the photon nonproportionality curve down to energies of few keV. By paying special emphasis to the scintillator response near the K-shell electron binding energy of the heaviest element in the scintillator, the electron nonproportional response curve was derived. This new method for the first time introduced in this thesis was named K-dip spectroscopy, and it provides information on the electron response down to tens of eV.

The methods utilizing escape peaks and K-dip spectroscopy have the advantage that the nonproportionality curve can be extended to lower energies than possible with other methods like Compton Coincidence Technique or technique using radioactive sources.

In Chapter 2 the nonproportionality curve of NaI:Tl to X-ray photons was measured down to energies as low as 1 keV by utilizing escape peaks. Information that could not be obtained utilizing a 1 keV X-ray source because of unavoidable surface-effects of the scintillator. The nonproportional response curve of NaI:Tl to photoelectrons was measured in the energy range 0.03 – 65 keV by K-dip spectroscopy. Comparison of the experimental photon-nPR with data simulated with an MC code using as input the electron-nPR confirmed that electron-nPR derived using K-dip spectroscopy method is reliable. That also evidenced that the K-dip spectroscopy method can be used to determine the electron-nPR down to energies as low as tens of eV.

The photon- and electron-nPRs of LuAG:Ce, GSO:Ce, LSO:Ce, and LPS:Ce were studied in Chapter 3. The electron response curves of these scintillators were measured in the energy range 0.1 – 30 keV. From 30 keV to 1 keV, scintillation yield for all samples appears to drop by 50 to 75%. Below 500 eV the response becomes proportional again.

Chapter 4 was about the nonproportional scintillation response of the commercially important $LaBr_3$:Ce and $LaCl_3$:Ce scintillators. Special attention was paid to the X-ray fluorescence escape peaks as they provide us with information about photon response in the range 1.2 - 14.5 keV for $LaBr_3$:Ce and 2.0 - 11.6 keV for $LaCl_3$:Ce. In the X-ray energy range from 9 – 100 keV the results are in a good agreement with the data of other research groups for both scintillators. A rapid variation of the photon response curve is observed near the Lanthanum K- electron binding energy for both scintillators. No relation was seen between the magnitude of the drop at the Lanthanum K-edge and the magnitude of the photon-nPR drop over the entire range for $LaBr_3$:Ce and $LaCl_3$:Ce. We observed so-called *S-shape* structures in the energy resolution versus $N_{phe}^{PMT}$ curves which makes $LaBr_3$:Ce and $LaCl_3$:Ce not suitable for X-ray spectroscopy use in the energy ranges 38.5-39.5 keV and 38.0-40.0 keV respectively. In these ranges there is no unique relationship between $N_{phe}^{PMT}$ and $E_X$. Using K-dip spectroscopy the electron response curve was extended down to 70 eV for $LaBr_3$:Ce and down to 100 eV for $LaCl_3$:Ce.

Chapters 5 and 6 addressed more fundamental aspects of nonproportionality. By utilizing theory of charge carrier transport in wide band gap semiconductors, nonproportionality of various inorganic scintillators was studied versus index of refraction, dielectric permittivity, charge carrier mobility and binding energy of electrons.

In total data on the photon nonproportional response of 35 inorganic scintillation materials were measured during this thesis work. The results were systemized and analyzed in Chapter 5. Among main trends and patterns highlighted in Chapter 5 are:

- Complex oxides showed a decrease in the degree of photon-nPR in the sequence $RE_2Si_2O_7$:Ce – $REPO_4$:Ce – $RE_2SiO_5$:Ce – $RE_3Al_5O_{12}$:Ce – $REAlO_3$:Ce, where RE is Y or Lu. The decrease of the photon-nPR degree was correlated with an increase in the refractive index of the compounds. Refractive index was related to dielectric constant, carrier mobility and bonding energy of electrons.

- A decrease in the degree of photon-nPR similar to the complex oxides was observed for the halide scintillators with the anion replacement: fluoride to chloride to bromide and to iodide. An important factor in the halides nonproportionality is the width of the valence band. As the width of the valence band increases from fluorides to chlorides, to bromides and to iodides, a higher value for the photon-nPR at 10 keV was observed.
- In some materials the dopant had influence on the shape and degree of the photon-nPR. For LuAG and YSO hosts a decrease in the degree of photon-nPR was observed after doping with $Pr^{3+}$ compared to doping with $Ce^{3+}$.
- Full or partial replacement of the RE-cation in the complex oxides did not lead to a significant decrease in the degree of photon-nPR. In most cases oxides with a mixed type of RE-cation, e.g. LYSO:Ce, LGSO:Ce or LuYAP:Ce showed a higher degree of photon-nPR.

The nonproportional response and related energy resolution for gamma-photon detection with $LaBr_3$:Ce scintillation crystals doped with different concentrations of cerium were studied between 80K and 450K in Chapter 6. For 5% and 30% $Ce^{3+}$ concentrations, $LaBr_3$ showed better proportionality and energy resolution at low temperatures. For both concentrations improvement of the intrinsic energy resolution and decrease in the degree of photon- and electron-nPR were observed in 80K - 600K temperature range. From this improvement we predict that at a low temperature even better energy resolution can be achieved with a $LaBr_3$ scintillation detector compared to the already outstanding 2.75% measured at room temperature nowadays. The temperature dependence of the photon- and electron-nPRs of $LaBr_3$:0.2% Ce was different. The most proportional response was measured at 300K. At low (80K) and high (450K) temperatures the photon- and electron-nPR curves deviated strongly from the linear response. This gave a significant deterioration of the energy resolution at both 80K and 450K. A significant factor determining the nonproportionality of $LaBr_3$:0.2%Ce studied in this thesis is the mobility of charge carriers. The higher the carrier mobility and diffusion coefficient the lower the degree of electron-nPR, which leads to improved energy resolution. Semiconductor detectors based on HPGe with excellent energy resolution of 0.3% besides different statistics have a much higher mobility of charge carriers ~40000 $cm^2/Vs$ compared to ~8 $cm^2/Vs$ calculated for $LaBr_3$:0.2%Ce with 100 ppm ionized impurity concentration. For 5% and 30% $Ce^{3+}$ concentration the charge carrier capture rate starts to dominate the non-radiative electron-hole pair recombination rate and at low temperatures better proportionality was observed.

Summarizing the results of the performed measurements and calculations and bearing in mind that carrier mobility in semiconductor detectors is high, we can conclude that the “ultimate energy resolution” can be achieved for scintillation materials with higher carrier mobility and charge carrier capture efficiency.

The most important finding of this thesis is that nonproportionality of inorganic scintillator can be changed. We showed that it can be changed by host or cation substitution, temperature, concentration and type of luminescent centers. That opens new possibilities for materials engineering and finally scintillators with superior energy resolution that is limited by counting statistics and not by nonproportionality.

# Samenvatting

De belangrijkste onderzoeksdoelstellingen van dit proefschrift, zoals beschreven in paragraaf 1.4 van het eerste hoofdstuk, zijn:

- Het ontwikkelen van een nieuwe experimentele methode die het mogelijk maakt de niet-proportionele respons bij lage energie (100 eV – 10 keV) te meten.
- Het ophelderen van de daadwerkelijke oorzaak van de niet-proportionaliteit.

In hoofdstukken 2, 3 en 4 zijn nieuwe, in dit proefschrift ontwikkelde methodes geïntroduceerd, waarmee de niet-proportionele respons van fotonen of elektronen in het lage energiebereik (onder de 10 keV) kan worden gemeten. De ontwikkelde methodes zijn de fotopiek- en ontsnappingspiekanalyse en de K-dip-spectroscopie. De essentie van al deze methodes is de karakterisering van anorganische scintillatoren met behulp van zeer monochromatische röntgenfotonen in het 9 – 100 keV energiebereik van de X-1 lichtbundel van het HASYLAB-synchrotron. Door gebruik te maken van de fotopiek, de $K_\alpha$-ontsnappingspieken en de $K_\beta$-ontsnappingspieken die in de pulshoogtespectra verschijnen, werden drie verschillende soorten sterk gerelateerde niet-proportionaliteitskrommen geïntroduceerd. Samen leveren zij de juiste informatie om de foton-niet-proportionaliteitskromme aan de lage energiekant tot enkele keV te bepalen. Door speciale nadruk te leggen op de scintillatorrespons nabij de elektronbindingsenergie van het elektron in de K-schil van het zwaarste element van de scintillator, is de elektron-niet-proportionaliteitskromme afgeleid. Deze nieuwe methode werd voor het eerst geïntroduceerd in dit proefschrift onder de naam K-dip-spectroscopie en levert informatie over de elektronrespons tot een minimale energie van enkele tientallen eV.
De methodes die gebruik maken van ontsnappingspieken en de K-dip-spectroscopie hebben het voordeel dat de niet-proportionaliteitskromme uitgebreid kan worden tot een lagere energie dan wat bereikt kan worden met andere methodes zoals de Compton-coïncidentietechniek of een techniek waarbij gebruik wordt gemaakt van radioactieve bronnen.
In hoofdstuk 2 werd de niet-proportionaliteitskromme van NaI:Tl voor röntgenfotonen bepaald tot een minimale energie van 1 keV door gebruik te maken van de ontsnappingspieken. Deze informatie kan niet verkregen worden met een 1 keV röntgenbron vanwege onvermijdelijke oppervlakte-effecten van de scintillator. De niet-

proportionele responskromme van NaI:Tl voor foto-elektronen werd gemeten in het 0,03 – 65 keV energiebereik met K-dip-spectroscopie. Een vergelijking tussen de experimentele foton-niet-proportionaliteitsrespons en de via Monte Carlo-code verkregen gesimuleerde data waarbij de elektron-niet-proportionaliteitsrespons als invoer is gebruikt, bevestigde dat elektron-niet-proportionaliteitsrespons die via K-dip-spectroscopie werd verkregen, betrouwbaar is. Dit toonde ook aan dat de K-dip-spectroscopie gebruikt kan worden om de elektron-niet-proportionaliteitsrespons te bepalen tot een minimale energie van enkele tientallen eV.

In hoofdstuk 3 zijn de foton- en elektron-niet-proportionaliteitsresponsen van LuAG:Ce, GSO:Ce, LSO:Ce en LPS:Ce bestudeerd. De elektronresponskrommen van deze scintillatoren werden gemeten in het 0,1 – 30 keV energiebereik. Bij al deze scintillatoren lijkt het scintillatierendement tussen de 30 keV en 1 keV met 50 tot 75% te dalen. Onder de 500 eV wordt de respons weer proportioneel.

Hoofdstuk 4 behandelde de niet-proportionele scintillatierespons van de commercieel belangrijke scintillatoren $LaBr_3$:Ce en $LaCl_3$:Ce. Er werd speciale aandacht besteed aan de röntgenfluorescentie-ontnappingspieken, aangezien deze ons van informatie voorzien over de fotonrespons in het 1,2 – 14,5 keV energiebereik bij $LaBr_3$:Ce en het 2,0 – 11,6 keV energiebereik bij $LaCl_3$:Ce. Voor beide scintillatoren zijn de resultaten in het röntgenenergiebereik van 9 – 100 keV in goede overeenstemming met de gegevens van andere onderzoeksgroepen. Ook werd voor beide scintillatoren een snelle variatie van de fotonresponskromme waargenomen nabij de bindingsenergie van een elektron in de K-schil van lanthaan. Er werd geen relatie gevonden tussen de grootte van de K-rand van lanthaan en de grootte van de afname van de foton-niet-proportionaliteitsrespons over het gehele bereik voor zowel $LaBr_3$:Ce als $LaCl_3$:Ce. We namen zogenaamde S-vormige structuren waar wanneer de energieresolutie uitgezet werd tegen de $N_{phe}^{PMT}$. Dit maakt $LaBr_3$:Ce niet geschikt voor het doen van röntgenspectroscopie in het 38,5 – 39,5 keV energiebereik en $LaCl_3$:Ce niet geschikt in het 38,0 – 40,0 keV energiebereik. In deze gebieden is er geen unieke relatie tussen de $N_{phe}^{PMT}$ en $E_x$. Met K-dip-spectroscopie werd de elektronresponskromme uitgebreid tot 70 eV voor $LaBr_3$:Ce en tot 100 eV voor $LaCl_3$:Ce.

Hoofstukken 5 en 6 stellen fundamentelere aspecten van de niet-proportionaliteit aan de orde. Door gebruik te maken van de theorie van het ladingsdragerstransport in halfgeleiders met een grote bandkloof, werd de niet-proportionaliteit van verschillende anorganische scintillatoren bestudeerd als functie van de brekingsindex, de permittiviteit, de mobiliteit van de ladingsdragers en de bindingsenergie van de elektronen.

In totaal werd voor het werk dat beschreven staat in dit proefschrift de foton-niet-proportionaliteit van 35 anorganische scintillatiematerialen gemeten. De resultaten werden gesystematiseerd en geanalyseerd in hoofdstuk 5. Belangrijke tendensen en patronen die in hoofdstuk 5 aangestipt werden, zijn:

- Complexe oxiden lieten een afname in de mate van de foton-niet-proportionaliteitsrespons zien in de volgorde $RE_2Si_2O_7$:Ce – $REPO_4$:Ce – $RE_2SiO_5$:Ce – $RE_3Al_5O_{12}$:Ce – $REAlO_3$:Ce, waarbij RE staat voor Y of Lu. De afname in de mate van de foton-niet-proportionaliteitsrespons werd gecorreleerd aan een toename van de brekingsindex van de verbindingen. De brekingsindex werd gerelateerd aan de diëlektrische constante, de mobiliteit van de ladingsdragers en de bindingsenergie van de elektronen.
- Een afname van de mate van foton-niet-proportionaliteitsrespons vergelijkbaar met die voor de complexe oxiden werd waargenomen voor de halogenidescintillatoren met de anionsubstitutie: fluoride voor chloride, voor bromide, voor jodide. Een belangrijke factor in de niet-proportionaliteit bij de halogeniden is de breedte van de valentieband. Wanneer de breedte van de valentieband toeneemt van fluoriden, naar chloriden, naar bromiden en naar jodiden, werd er een hogere waarde voor de foton-niet-proportionaliteitsrespons bij 10 keV waargenomen.
- In sommige materialen had de doteerstof invloed op de vorm en mate van foton-niet-proportionaliteitsrespons. Bij de LuAG- en YSO-gatroosters werd er een afname in de mate van foton-niet-proportionaliteitsrespons waargenomen wanneer de dotering met $Ce^{3+}$ werd vervangen door dotering met $Pr^{3+}$.
- Volledige of gedeeltelijke vervanging van het zeldzame aardkation in de complexe oxiden leidde niet tot een significante afname in de mate van foton-niet-proportionaliteitsrespons. In de meeste gevallen lieten de oxiden met een gemengd type zeldzame aardkation, zoals LYSO:Ce, LGSO:Ce en LuYAP:Ce, een hogere mate van foton-niet-proportionaliteitsrespons zien.

In hoofdstuk 6 werden de niet-proportionele respons en de daaraan gerelateerde energieresolutie voor gammafotondetectie bestudeerd van $LaBr_3$:Ce-scintillatiekristallen gedoteerd met verschillende ceriumconcentraties, bij temperaturen tussen de 80 K en 450 K. Bij 5% en 30% $Ce^{3+}$-concentraties vertoont $LaBr_3$ bij lage temperaturen een betere proportionaliteit en energieresolutie. Bij beide concentraties werd een verbetering van de intrinsieke energieresolutie en een afname in de mate van foton- en elektron-niet-proportionaliteitsrespons waargenomen in het 80 K – 600 K

temperatuurbereik. Vanwege deze verbetering verwachten we dat bij een lage temperatuur een nog betere energieresolutie bereikt kan worden met een $LaBr_3$-scintillatiedetector ten opzichte van de al uitstekende 2,75% die heden ten dage bij kamertemperatuur wordt gemeten. De temperatuurafhankelijkheid van de foton- en elektron-niet-proportionaliteitsrespons van $LaBr_3$:0.2%Ce vertoonde een ander gedrag. De proportioneelste respons werd gemeten bij 300 K. Bij lage (80K) en hoge (450K) temperaturen weken de foton- en elektron-niet-proporitionaliteitsresponskrommen sterk af van de lineaire respons. Dit zorgde voor een significatie verslechtering van de energieresolutie bij zowel 80 K als 450 K. Een belangrijke factor die de niet-proportionaliteit van $LaBr_3$:0.2%Ce bepaalt en die bestudeerd is in dit proefschrift, is de mobiliteit van de ladingsdragers. Hoe hoger de mobiliteit en diffusiecoëfficiënt van de dragers is, des te lager is de mate van elektron-niet-proportionaliteitsrespons, wat resulteert in een verbeterde energieresolutie. Halfgeleiderdetectoren gebaseerd op HPGe met een uitstekende energieresolutie van 0,3% hebben een veel hogere ladingsdragersmobiliteit van ~40000 $cm^2/Vs$ vergeleken met de ~8 $cm^2/Vs$ die berekend is voor $LaBr_3$:0.2%Ce met een 100 ppm geïoniseerde onzuiverheidsconcentratie. Bij 5% en 30% $Ce^{3+}$-concentraties begint de invangstsnelheid van de ladingsdragers te domineren boven de niet-stralende elektron-gat-recombinatie en wordt bij lage temperaturen een betere proportionaliteit waargenomen.

De resultaten van de uitgevoerde metingen en berekeningen samenvattend en in gedachte houdend dat de mobiliteit van de ladingsdragers in halfgeleiderdetectoren hoog is, kunnen we concluderen dat de “ultieme energieresolutie” bereikt kan worden voor scintillatiematerialen met een hogere mobiliteit en invangstefficiëntie van de ladingsdragers.

De belangrijkste bevinding van dit proefschrift is dat de niet-proportionaliteit van anorganische scintillatoren veranderd kan worden. We lieten zien dat het gevarieerd kan worden door middel van gastrooster- of kationsubstitutie, temperatuur en concentratie en aard van de luminescerende centra. Dat opent nieuwe mogelijkheden voor het ontwerpen van materialen en uiteindelijk scintillatoren met een superieure energieresolutie die gelimiteerd wordt door telstatistiek en niet door niet-proportionaliteit.

# Acknowledgements

I want to express my gratitude to all my colleagues from Radiation Detection and Medical Imaging research group Delft University of Technology where this thesis research was completed. Especially, I want to thank my promoter and supervisor Prof. Dr. Pieter Dorenbos for fruitful discussions, critical scientific way of thinking, sense of humor and patience he had during countless reviews of the scientific publications this thesis is based on. Without his support, expertise and trust this thesis would not have been written. Also I want to thank Mikhail Alekhin, Francesco Quarati and Johan de Haas as well as colleagues from European Space Agency (ESTEC) Conny Hansson, Johannes van der Biezen and Alan Owens for sharing long night shifts at X1-beamline at DESY synchrotron facility in Hamburg. They helped me to gain not only scientific experience, but also to develop my beer drinking skills.

This thesis would not have happened without Prof. Dr. Piotr Rodnyi from the Ionic Crystals research group at Saint Petersburg State Politechnical University. He showed me the beauty and magic of the scientific research and opened for me opportunities to go to Delft.

Also I want to thank our industrial partners first Eric Mattman and later Vladimir Ouspenski from Saint-Gobain Crystals for custom made samples and interesting questions they asked during our bi-annual meetings in Delft and Paris.

Support from my family was also very helpful and can not be overestimated. I want to thank my wife Marina and my new born son Timofey for giving me an opportunity to finish this thesis on time. Also I want to thank my mother Tatiana for her faith in me and moral support especially during my early days in Delft.

# Curriculum Vitae

Ivan Vyacheslavovich Khodyuk was born in Leningrad, the USSR in 1985. The city and the country do not exist anymore. Ivan grew up in the North-East part of Saint Petersburg, where he first attended primary school 562 and later gymnasium 196. In 2002 Ivan started Bachelor's program at Experimental Nuclear Physics Department, Faculty of Physics and Mechanics of Saint Petersburg State Politechnical University. After completing this program and defending Bachelor thesis "Scintillating properties of ZnO:Zn optical ceramics" in 2006, Ivan continued his education at Experimental Nuclear Physics Department and in 2008 Master thesis "Fast and effective scintillators for medical tomography" was successfully defended. Significant part of the experimental data used in this thesis was measured at the Radiation Detection and Matter research group in Delft, where Ivan spent three months as a master student in the beginning of 2008.

Ivan started his career in the field of inorganic scintillators and luminescence materials research and development in 2005 as a part of Physics of the Ionic Crystals research group lead by Prof. Dr. Piotr Rodnyi. Being a part of this group Ivan was sent to the Radiation Detection and Matter research group at Delft University of Technology to conduct experiments in the course of his Master's thesis. During the time in Delft Ivan was offered to continue research on inorganic scintillators as a *promovendus* in Delft. In October 2008 he began working on his PhD research at Luminescence Materials research Group at Faculty of Applied Sciences, Delft University of Technology lead by Prof. Dr. Pieter Dorenbos. This thesis is the result of this work.

# List of publications

Publications related to this thesis:


[1]. I.V. Khodyuk, F.G.A. Quarati, M.S. Alekhin, P. Dorenbos. Charge carrier mobility and nonproportionality of $LaBr_3$:Ce scintillators. Submitted for publication at *Physical Review B.*

[2]. I.V. Khodyuk, P. Dorenbos. Trends and patterns of scintillator nonproportionality. Accepted for publication at *IEEE Trans. Nucl. Sci.* December 2012.

[3]. I. V. Khodyuk, P. A. Rodnyi, and P. Dorenbos, "Energy dependence of the relative light output of $YAlO_3$:Ce, $Y_2SiO_5$:Ce and $YPO_4$:Ce scintillators," *Instruments and Experimental Techniques*, vol. 55, pp. 187-197, 2012.

[4]. M. S. Alekhin, I. V. Khodyuk, J. T. M. De Haas, and P. Dorenbos, "Non-proportional response and energy resolution of pure $SrI_2$ and $SrI_2$:5%Eu scintillators," *IEEE Trans. Nucl. Sci.*, vol. 59, pp. 665-670, 2012.

[5]. I. V. Khodyuk, M. S. Alekhin, J. T. M. de Haas, and P. Dorenbos, "Improved scintillation proportionality and energy resolution of $LaBr_3$:Ce at 80K," *Nucl. Instr. and Meth. A*, vol. 642, pp. 75-77, 2011.

[6]. I. V. Khodyuk and P. Dorenbos, "Nonproportional response of $LaBr_3$:Ce and $LaCl_3$:Ce scintillators to synchrotron x-ray irradiation," *J. Phys. Condens. Matter*, vol. 22, p. 485402, Dec 2010.

[7]. I. V. Khodyuk, J. T. M. de Haas, and P. Dorenbos, "Nonproportional Response Between 0.1-100 keV Energy by Means of Highly Monochromatic Synchrotron X-Rays," *IEEE Trans. Nucl. Sci.*, vol. 57, pp. 1175-1181, Jun 2010.

[8]. I. V. Khodyuk, P. A. Rodnyi, and P. Dorenbos, "Nonproportional scintillation response of NaI:Tl to low energy x-ray photons and electrons," *J. Appl. Phys.*, vol. 107, p. 113513, Jun 2010.


Other publications:


[9]. F. G. A. Quarati, I. V. Khodyuk, C. W. E. Van Eijk, P. Quarati, and P. Dorenbos, "A study of $^{138}$La Radioactive-Decays using $LaBr_3$ Scintillators," *Nucl. Instr. and Meth. A*, vol. 683, pp. 46-52, 2012.

[10]. P. A. Rodnyi, K. A. Chernenko, E. I. Gorokhova, S. S. Kozlovskii, V. M. Khanin, I. V. Khodyuk, "Novel Scintillation Material – ZnO Transparent Ceramics," Accepted for publication at *IEEE Trans. Nucl. Sci.* October 2012.

[11]. M. S. Alekhin, J. T. M. de Haas, K. W. Kramer, I. V. Khodyuk, L. de Vries, and P. Dorenbos, "Scintillation properties and self absorption in $SrI_2$:$Eu^{2+}$," in *Nuclear Science Symposium Conference Record (NSS/MIC), 2010 IEEE*, 2011, pp. 1589-1599.

[12]. P. Rodnyi and I. Khodyuk, "Optical and luminescence properties of zinc oxide (Review)," *Optics and Spectroscopy*, vol. 111, pp. 776-785, 2011.
[13]. E. I. Gorokhova, G. V. Ananieva, S. B. Eron'ko, E. A. Oreschenko, P. A. Rodnyi, K. A. Chernenko, I. V. Khodyuk, E. P. Lokshin, G. B. Kunshina, O. G. Gromov, and K. P. Loot, "Structural, optical, and scintillation characteristics of ZnO ceramics," *Journal of Optical Technology*, vol. 78, pp. 753-760, Nov 2011.
[14]. P. A. Rodnyi, I. V. Khodyuk, and E. I. Gorokhova, "Integral, Absolute, and Relative Light Yield of ZnO-Based Ceramics," *Tech. Phys. Lett.*, vol. 36, pp. 714-716, 2010.
[15]. I. V. Khodyuk, P. A. Rodnyi, and E. I. Gorokhova, "Scintillation properties of Zinc oxide based optical ceramics," *NAUCH TEKHN VED SPBG*, vol. 109, pp. 28-38, 2010.
[16]. J. P. Zhong, H. B. Liang, Q. Su, J. Y. Zhou, I. V. Khodyuk, and P. Dorenbos, "Radioluminescence properties of $Ce^{3+}$-activated $MGd(PO_3)_4$ (M = Li, Na, K, Cs)," *Optical Materials*, vol. 32, pp. 378-381, Dec 2009.
[17]. C. W. E. van Eijk, J. T. M. de Haas, P. A. Rodnyi, I. V. Khodyuk, K. Shibuya, F. Nishikido, and M. Koshimizu, "Scintillation Properties of a Crystal of $(C_6H_5(CH_2)_2NH_3)_2PbBr_4$," *2008 IEEE Nuclear Science Symposium Conference Record*, vol. 1-9 pp. 3525-3528, 2009.
[18]. P. A. Rodnyi, I. V. Khodyuk, E. I. Gorokhova, S. B. Mikhrin, and P. Dorenbos, "Emission and excitation spectra of ZnO:Ga and ZnO:Ga,N ceramics," *Optics and Spectroscopy*, vol. 105, pp. 908-912, Dec 2008.
[19]. P. A. Rodnyi, I. V. Khodyuk, and G. B. Stryganyuk, "Location of the energy levels of the rare-earth ions in BaF2 and CdF2," *Physics of the Solid State*, vol. 50, pp. 1639-1643, Sep 2008.
[20]. P. A. Rodnyi, G. B. Stryganyuk, and I. V. Khodyuk, "Luminescence of a ZnO : Ga crystal upon excitation in vacuum UV region," *Optics and Spectroscopy*, vol. 104, pp. 210-212, Feb 2008.
[21]. E. I. Gorokhova, G. V. Anan'eva, V. A. Demidenko, P. A. Rodnyi, I. V. Khodyuk, and E. D. Bourret-Courchesne, "Optical, luminescence, and scintillation properties of ZnO and ZnO:Ga ceramics," *Journal of Optical Technology*, vol. 75, pp. 741-746, Nov 2008.
[22]. V. A. Demidenko, E. I. Gorokhova, I. V. Khodyuk, O. A. Khristicha, S. B. Mikhrin, and P. A. Rodnyi, "Scintillation properties of ceramics based on zinc oxide," *Radiation Measurements*, vol. 42, pp. 549-552, Apr-May 2007.